Evolution and development of the Archosaurian axial column

Hoai-Nam Bui

Department of Biology
McGill University, Montreal

August 2024
A thesis submitted to McGill University in partial fulfillment of the degree of Doctor of Philosophy

Table of Contents

List of Tables and Figures

List of Abbreviations

Abbreviation	Definition
SPHARM	Spherical harmonics
PDM	Point distribution model
HOX	Homeobox
CT	Computed tomography
DACs	Discrete anatomical characters
GMM	Geometric morphometrics
PCA	Principal Component Analysis
ANCOVA	Analysis of covariance
LDA	Linear discriminant analysis
AIC	Akaike Information Criterion
2B-PLS	Two-block partial least squares

Abstract

The production of phenotypic variation, and the mechanisms underlying it, are of fundamental importance to evolutionary processes, as natural selection acts only upon existing variation. Therefore, understanding the processes and mechanisms that give rise to morphological diversity is critical to evolutionary biology. The study of morphological variation also serves as a gateway to understanding the evolution of biological complexity. In the context of vertebrate animals, the evolution of a complex axial column provides a compelling case study in the development and evolution of biological complexity. The transition from a relatively simple, undifferentiated vertebral column to a complex structure capable of supporting diverse locomotor strategies and ecological niches exemplifies the evolutionary trajectory toward increased complexity. This thesis takes an interdisciplinary approach to shed light on the evolution and development of the axial column while also illuminating broader patterns of morphological evolution within Archosauria. In Chapter 2, we utilize the domestic chicken, *Gallus gallus*, as a model to map axial ossification and reveal patterns of fusion and ossification during development. Chapter 3 introduces spherical harmonics analysis (SPHARM) to quantify shape variation and regionalization in the axial column of *Caiman crocodilus*. Extending this novel, objective methodology to Crocodylia, Chapter 4 delves into the regionalization, integration, and modularity across specific taxa. Overall, the combined studies demonstrate the value of advanced analytical techniques in revealing the evolutionary significance and developmental intricacies of vertebral morphology. By tracing the history, development, and variation of the archosaurian axial column, we gain insight into processes driving the emergence of biological complexity in vertebrates. At its core, this study addresses the central question of how morphological complexity develops, how it can be quantified, and how we may approach questions regarding evolutionary time scales.

Résumé

La production de variations phénotypiques et les mécanismes qui les sous-tendent sont d'une importance fondamentale pour les processus évolutifs, car la sélection naturelle n'agit que sur les variations existantes. Par conséquent, la compréhension des processus et des mécanismes à l'origine de la diversité morphologique est essentielle pour la biologie évolutive. L'étude de la variation morphologique permet également de comprendre l'évolution de la complexité biologique. Dans le contexte des vertébrés, l'évolution d'une colonne axiale complexe fournit une étude de cas convaincante sur le développement et l'évolution de la complexité biologique. Le passage d'une colonne vertébrale relativement simple et indifférenciée à une structure complexe capable de supporter diverses stratégies locomotrices et niches écologiques illustre la trajectoire évolutive vers une complexité accrue. Cette thèse adopte une approche interdisciplinaire pour mettre en lumière l'évolution et le développement de la colonne axiale tout en éclairant des modèles plus larges d'évolution morphologique au sein de l'Archosauria. Dans le chapitre 2, nous utilisons le poulet domestique, *Gallus gallus,* comme modèle pour cartographier l'ossification axiale et révéler les schémas de fusion et d'ossification au cours du développement. Le chapitre 3 présente l'analyse des harmoniques sphériques (SPHARM) pour quantifier la variation de forme et la régionalisation dans la colonne axiale de *Caiman crocodilus*. En étendant cette nouvelle méthodologie objective aux Crocodylia, le chapitre 4 étudie la régionalisation, l'intégration et la modularité dans des taxons spécifiques. Dans l'ensemble, les études combinées démontrent la valeur des techniques analytiques avancées pour révéler la signification évolutive et les complexités du développement de la morphologie vertébrale. En retraçant l'histoire, le développement et les variations de la colonne axiale archosaurienne, nous comprenons mieux les processus à l'origine de l'émergence de la complexité biologique chez les vertébrés. Au fond, cette étude aborde la question centrale de savoir comment la complexité morphologique se développe, comment elle peut être quantifiée et comment nous pouvons aborder les questions relatives aux échelles de temps de l'évolution.

Acknowledgements

Thank you to my family for the unwavering support, for pushing me always, for reminding me to finish my PhD.

Thank you to my chosen family, my community, for being my biggest fans and always building me up.

Thanks to Nat and Cornelia, for being my rocks, my companions, my bestest of friends.

Thanks to Sarah and Simon, for making Montreal always feel like home, for providing constant laughs, and for making sure we always had the best meals ever.

Thanks to my supervisor, Hans Larsson, for the most colorful PhD experience I could have had.

Thanks to my committee members, Lauren Chapman and Ehab Abouheif, for their guidance and their support.

Thanks to the Larsson Lab members old and new, especially Trina, Jose, Christine, Tony, Alex, Dirley, Anthony, Louis-Philippe, Andre, for helping through the confusion, and for the laughs too.

Thank you to my fellow graduate school folk who have provided guidance, advice, listening ears, and a shared moment over Thomson House potato wedges.

I am forever grateful for you all and more.

Contributions

Contribution of authors

Chapter 2 is co-authored with Hans Larsson and is published in the Zoological Journal of the Linnean Society . The idea of the manuscript was conceived together. I gathered all of the data related to chick incubation, clearing and staining of the embryos, photography, and coding of characters. Hans and I prepared the discussion and figures together.

I am the sole author for Chapters 1, 3, 4 and 5. The data used in these analyses was collected with help from Anthony Smith for the *Caiman crocodilus* vertebrae, as well as data from Morphosource from the University of Florida repository. I segmented and created all the 3D models, planned and conducted all morphometric and statistical analyses, the text, and figures. Discussions and shared ideas with Hans heavily influenced the chapters and their conclusions.

Statement of original knowledge and scholarship

The work found in Chapter 2 is the first to establish a high resolution character matrix of the development of the avian axial column. Using well established clearing and staining techniques, this study provides an original contribution to the record of knowledge of the development and evolution of the avian axial column.

Chapter 3 utilizes existing software in a novel approach to quantify axial column variation. This method establishes a method in which all vertebrae can be compared sequentially, directly, and objectively. Without the need for homologous characters, shape variation was measured directly by surface variation and provided a first time analysis of an entire vertebral column.

Chapter 4 extends the methodology of Chapter 3 to multiple taxa within Crocodylia. This is the first attempt of characterizing vertebral morphology including post-sacral elements, utilizing entire surfaces.

Chapter 1
Introduction

Background

At the heart of macroevolutionary inquiry lies a fundamental question: what drives the origin of evolutionary novelties? Central to addressing this question is an understanding of morphological variation, which encompasses differences in form and structure among organisms. The production of phenotypic variation, and the mechanisms underlying it, are of fundamental importance to evolutionary processes, as natural selection only acts upon existing variation. Therefore, in order to understand evolutionary trends over time, we must understand the processes and mechanisms – whether genetic, developmental, functional, or phylogenetic – that give rise to morphological diversity (Carroll, 2005; Harmon et al., 2003; Lauder, 1990; Losos, 2008;Wagner & Altenberg 1996; Wainwright, 2007).

The study of morphological variation not only provides insights into the mechanisms driving phenotypic diversity, but also as a gateway to understanding the evolution of biological complexity. The evolution of complexity involves transitions from simple to more elaborate forms, driven by mechanisms such as gene duplication, regulatory innovation, and network rewiring (Carroll, 2005; Wagner & Altenberg, 1996). In the context of archosaurs, the evolution of a complex axial column provides a compelling case study in the development and evolution of biological complexity. Crocodylia with Aves form the crown group of Archosauria. Extant crocodilians display relatively conserved body plans, with regionalization traditionally defined by rib morphology (Claessens, 2009; Hoffstetter & Gasc, 1969). In contrast, the axial columns of birds become highly specialized, with fusions occurring along the spine, a reduction of their tail, as well as variable vertebral counts. The appearance of such a complex structure capable of

supporting diverse locomotor strategies and ecological niches exemplifies the evolutionary trajectory toward increased complexity (Figueirido et al., 2021; Soul & Benson, 2017).

This thesis takes an interdisciplinary approach to shed light on the evolution and development of a key anatomical innovation– the axial column– while also illuminating broader patterns of morphological evolution within Archosauria. By tracing the history, development, and variation of the archosaurian axial column, we gain insight into processes driving the emergence of biological complexity in vertebrates. At its core, this study addresses the central question of how morphological complexity develops, how it can be quantified, and how it has evolved over evolutionary time scales. The next three chapters of this work will explore different facets of axial column variation using a variety of methods.

Overview

Development and evolution of regionalization within the avian axial column (Chapter 2)

This work provides the first high resolution description of development within the avian axial column. By mapping chondrification and ossification sequences throughout development, we find that the pattern and sequence of fusion and ossification may reflect the development and presence of independent modules, and further evidence of downstream patterning by *Hox* expression. This chapter is heavily character-based, as I examine the timing of development of the morphological traits that determine vertebral identity.

Morphological variation in the axial column of *Caiman crocodilus* (Chapter 3)

The axial column, a structurally complex yet serially homologous anatomical feature, has traditionally presented challenges in studies of morphological variation due to its intricate nature.

This chapter uses a new approach to studying morphological variation using spherical harmonics and point distribution models (SPHARM-PDM). This work stands as the first of its kind to objectively quantify surface variation in vertebral morphology, and approach studies of regionalization and modularity in this way. Regionalization is typically determined by the relative positions of the appendicular and sternal skeletons in relation to the vertebrae. This work is an attempt at quantifying morphological regionalization through solely the shape of vertebral elements themselves.

Axial column regionalization in Crocodylia (Chapter 4)

Axial column variation, regionalization, and modularity across Crocodylia has yet to be studied. Building on the methodology established in Chapter 3, this chapter employs an innovative approach to studying axial column variation across distinct Crocodylian taxa. By juxtaposing morphological data with molecular insights, this study challenges the conventional assumptions of simplicity regarding axial column morphology in Crocodylia.

Literature Review

The axial column

The axial column, a defining characteristic of Vertebrates, is arguably one of the main evolutionary novelties of the clade (Janvier, 1996). The axial column is composed of a series of repeating ossified, cartilaginous, and ligamentous elements surrounding the spinal cord and notochord as well as provides attachment points for musculature (Gadow, 1933, Schultze & Arratia, 1988; Ward & Mehta, 2014). Each of these elements are patterned during early embryological development, with the number and regional identity of vertebrae acting as

subjects of major importance in the development and evolution of vertebrates (Böhmer, 2015). The axial column plays a critical cole in body support, with varying degrees of torsion, flexion-extension, and bending capacity playing different roles in body deformation, movement, and maneuvers (Long et al., 1997; Macpherson & Ye, 1998; Molnar et al., 2014; Pridmore, 1992; Randau et al., 2016; Schilling, 2011; Smit, 2002). Regionalization and variation along the axial columns provides insight into the influence of size, locomotion, prey-size specialization, and the form-function relationships that underlie vertebrate behavior and ecology (Buchholtz, 1998; Jones et al., 2020; Marchesi et al., 2021; Randau et al. 2016). The axial column is often utilized to study integration and modularity (Buccholtz, 2007; Polly et al., 2001; Randau & Goswami, 2017), providing a window into the underlying systems that shape vertebral morphology. Through the exploration of morphological variation, regionalisation and modularity, we can gain a greater understanding of potential drivers that have shaped vertebrate evolution (Arratia et al., 2001; Berio, 2022; Buccholtz, 2007; Jones et al., 2018; Martìn Serra et al., 2021; Sallan, 2012).

Development

The axial column originates from the paraxial mesoderm, with the vertebral column arising from sequentially added posterior somites (Christ et al., 2000). Somites undergo subdivision into myotomes, dermatomes, sclerotomes, with the latter giving rise to intersegmental vertebrae. Each vertebrae form from half of the posterior part of one pair of somites, and the other half from the anterior part of the succeeding pair. The identity of individual vertebrae along the anterior-posterior axis is determined by a subset of homeobox-containing genes: the *Hox* genes (Carroll, 1995; Kessel & Gruss, 1990; Liang et al., 2011**;** Mallo et al., 2010; McGinnis & Krumlauf, 1992). *Hox* genes are highly conserved,

encoding transcription factors that regulate the downstream expression of genes that pattern an organism's body plan (Foronda et al., 2009; Kessel & Gruss, 1990). The combination of *Hox* genes in somites is a requirement to establish such different vertebral morphologies (Casaca et al 2014; Wellik, 2007).

Vertebrae arise from mesenchymal condensations that chondrify and later ossify. Following chondrogenesis, in which chondrocytes proliferate, differentiate, and die, ossification of the axial column occurs through endochondral ossification, a process characterized by the gradual replacement of cartilage by bone (Mackie et al., 2008). The timing of ossification and the development of region-specific characteristics provide insight into heterochronic shifts, morphological diversification, and evolutionary transformations (Gould, 1977; Harrington et al 2013; McNamara, 2012; Weisbecker & Mitgutsch, 2010).

Regionalization

Vertebral columns across vertebrates vary in degree of regionalization (Ward & Brainerd, 2007). Fish axial columns are generally divided into two, separated by precaudal and caudal regions. Tetrapod axial columns typically exhibit four main regions: cervical, dorsal, sacral, and caudal. Derived axial columns of mammals and crocodylians include an additional lumbar region between the ribbed thoracic and sacral vertebrae (Bohmer, 2015). In birds, the lumbar region fuses with the sacrals forming a structure called the synsacrum. Each region within the axial column is adapted to perform specific functions. For example, the cervical region provides flexibility for movements in the head and neck. The thoracic region, bearing rib attachments, protects vital organs and plays a role in breathing through lung expansion. Regionalization and

consequent vertebral anatomy is closely related to the locomotory kinematics of an animal (Johnson & Shapiro, 1998).

Historically, axial skeleton evolution is typically portrayed as a linear trajectory from low regionalization in fish to a highly regionalized and modular state in mammals and birds, with varying degrees of regionalization in other vertebrates (Jones et al., 2018; Schilling, 2011). However, various studies have more recently highlighted greater complexity in the evolution of the axial skeleton in fish and snakes suggesting this anatomy has been evolving throughout vertebrate history (Criswell et al., 2021; Head & Polly, 2015; Sallan, 2012). These studies found general conservatism in the number of regions found along the axial columns, with boundaries associated with *Hox* expression boundaries, while displaying general lower shape variance among and between vertebrae. The conclusions of these works, however, all call for the reevaluation of regionalization amongst various taxa to assess evolutionary trends.

Modularity/Integration

The hierarchical nature of the axial column, with its distinct morphological regions and their relationship to *Hox* gene expression, exemplifies the concepts of modularity and integration in vertebrate morphology. Modularity is defined as discrete anatomical units capable of changing independently without affecting other structures (Gass & Bolker 2003; Raff, 1996; Ward & Brainerd, 2007). Modules possess the capacity for both developmental and evolutionary transformation (Bolker, 2000), as they can appear in multiple levels and provide insight into the coordinated or independent evolutionary trajectory of a structure at the population and species levels (Cheverud, 1996). Morphological integration refers to the strength of correlation among

traits, whereas modularity describes the degree in which tightly integrated traits form semi-independent subunits (Olson & Miller, 1999).

By studying patterns of integration and modularity among phenotypic traits, one can investigate the underlying developmental and genetic systems generating those traits in question (Felice et al., 2019; Goswami et al., 2006; Hallgrimsson et al 2009; Klingenberg, 2008; Wagner & Altenberg, 1996; Wagner & Zhang, 2011). Axial modularity has been studied in cetaceans (Buchholtz, 2007), mammals (Randau & Goswami, 2017) and snakes (Polly et al., 2001), whereas studies within Archosauria are generally lacking. This work is therefore an investigation into the quantification and pattern identification of phenotypic modularity within Archosauria, allowing for insight into the systems generating variation and the evolution of the Archosaurian axial column.

Select methods of studying variation in the axial column

Discrete anatomical characters

Discrete anatomical characters are specific traits or features that can be easily distinguished and categorized. These characters are typically binary or multi-state (Wiley, 1981). Discrete characters are commonly used in phylogenetic analyses to reconstruct evolutionary relationships among organisms (Felsenstein, 2014). When exploring morphological variation, the use of discrete characters typically utilizes cladistic data sets as a source of data on trait variation (Gerber, 2019; Lloyd, 2016; Wills et al., 1994). This approach involves analyzing character-taxon matrices where morphologies are scored using character states, the numbers of certain elements, the relationships between, or orientation of, elements and even general features relating to size and shape (Schaeffer et al., 2020).

Generally, the utilization of discrete characters provides a straightforward way to compare anatomical features across different taxa, as well as acts as an alternative to geometric morphometrics when it is not possible to do so. This is typically seen when there is a lack of homologous points, high complexity of the morphology, or the lack of completely preserved specimens (Schaeffer et al., 2020). However, their utility may be limited by subjectivity in character definition and scoring, as well as the potential for homoplasy, where similar traits evolve independently in different lineages (Wagner, 2000). Furthermore, discrete characters associated with the axial skeleton are heavily skewed towards the skull, with few focusing on the axial column itself as well as inconsistent landmarks across all regions. Moreover, discrete anatomical characters often do not capture the variation that ranges across several vertebrae.

Genetic patterning

Studies of Homeobox (*Hox*) gene expression patterns have the potential to elucidate homologies between vertebrate body plans and serve as a distinct set of characters to homologize segments across organisms (Mallo et al., 2010). Hox genes play a critical role in determining the identity and regionalization of vertebrae along the axial column (Müller & Wagner, 1996). Since their discovery, researchers have invested over three decades in uncovering the role of these genes. They have found that the specific temporal and spatial expression pattern orchestrates the anteroposterior organization and segmentation of all metazoans, including chordates (Böhmer et al., 2015; Carroll, 1995; Krumlauf, 1994). Consequently, investigating morphological variation in vertebrae offers an opportunity to establish the homologies of different body sections in related taxa with varying vertebral counts, using expression patterns of a proxy to vertebral identity (Bohmer et al., 2015). Axial regionalization of the vertebrae is determined by *Hox* gene

expression (Burke et al., 1995). The combination of active *Hox* genes specifies the region and identity of the vertebral elements, with changes in expression patterns leading to homeotic transformations or changes in segment identity (Kessel & Gruss, 1991). For example, there is a consistent association of the expression of *Hoxc-5* and *Hoxc-6* with the cervical-thoracic transition, *Hoxa-9, Hoxb-9,* and *Hoxc-9* with the thoracic-lumbar transition, and so on. The expression of *Hox13* paralogs posteriorly acts to terminate tail elongation (Economides et al., 2003). Studies of these highly conserved expression patterns across vertebrates provides insight into the evolutionary mechanisms responsible for the variability and adaptability of the vertebrate axial column (Böhmer et al., 2015).

Ossification sequences

Ossification sequences refer to the chronological order in which bones begin to ossify during embryonic and postnatal growth (Hall, 2005). Ossification sequences have been used to describe axial development across a wide breadth of vertebrates and differences used to infer evolutionary changes in their development (Hautier et al., 2011; Mitgutsch et al., 2011; Verriére et al., 2021). Ossification sequences are species-specific patterns of bone formation, with a general degree of conservation between species (Sheil, 2003). Comparative analyses of ossification sequences across species can shed light into evolutionary changes in developmental timing and patterning, providing information on the origins of morphological diversity in vertebrate history and the support of phylogenetic hypotheses (Maisano, 2002; Maxwell, 2008). Additionally, ossification sequences may reflect on modularity as modules are expected to have more organized developmental sequences within them than between other modules. In amniotes, the ossification patterns within the vertebral column are generally well understood, however the

timing and spatial progression along the vertebral column for many model taxa remain understudied (Verrière et al.. 2021)

Traditional and Geometric Morphometrics

Morphometrics is the study of shape variation and covariation and has played a foundational role in biological research (Bookstein, 1997). Throughout history, comparing anatomical features and biological shape has been essential for understanding the diversity of life and for taxonomic classification. In the 1970s, "traditional morphometrics" emerged when morphological measurements of lengths, angles, and ratios were combined with multivariate statistical techniques (Blackith & Reyment, 1971; Marcus, 1990). These measurements quantified covariation and patterns of variation within and among samples, utilizing statistical analyses such as Principal Components Analysis, factor analysis, Canonical Variates Analysis, and Discriminant Function Analysis (Adams et al., 2009). These techniques created space for traditional morphometrics to play a role within the biological 'quantification revolution' (Bookstein, 1997).

However, traditional morphometrics faced challenges such as a lack of an agreed-upon method for size correction, as well as difficulties in assessing homology of linear distances. Additionally, representing shape from linear distances was incomplete as geometric relationships among variables were not preserved (Adams et al., 2009). In response to this, geometric morphometrics emerged in the late 1980s as a method to analyze shape variation while preserving original geometry (Bookstein, 1997). This approach involves capturing variation using Cartesian coordinates, either in two or three dimensions, of anatomical landmarks placed on the structure of interest (Adams et al., 2013; Gunz et al., 2005; Rohlf & Marcus, 1993;

Zelditch et al., 2012). These landmarks, chosen based on biological significance and repeatability in their identification, are then analyzed using statistical techniques like Principal Components Analysis after Procrustes superimposition, a method to align all specimens to a common coordinate system (Slice, 2007).

Geometric morphometrics has been extensively used in biological research, providing insights into evolutionary patterns, functional morphology, and developmental processes across diverse organisms (Zelditch et al., 2012). While these methods are a powerful tool for comparative analyses, they still pose a few challenges. Landmark selection by users describing features of perceived importance, may influence predictions of form-function relationships, and ensuring replicable points across structures can be difficult for certain shapes or structures with extreme topographies (Ege et al., 2020; Wimberly et al., 2022). Spherical harmonics (SPHARM) offers an alternative method of shape analysis that sidesteps difficulties associated with geometric morphometrics (Shen et al., 2009).

Spherical Harmonics and Point Distribution Models

Landmark selection in geometric morphometrics can be relatively subjective in terms of placement across different users. The utilization of spherical harmonics (SPHARM) may be a solution to objectively quantify biological shape and the variation that is fundamental to evolutionary biology. Spherical harmonics is an extension of elliptical Fourier analysis to three-dimensional surfaces. Elliptical fourier analysis typically is used to describe the outline of a 2D object as a function, mapping the distance from a specified origin to each point on the outline as a function of the angle in the polar coordinate system (Brechbühler et al., 1995; Ritchie & Kemp, 1999; Rohlf & Archie, 1984; Shen et al., 2009). This function is then expressed in terms

of harmonic functions with Fourier coefficients that can be used in standard multivariate statistical analyses (Harper et al 2021; Shen et al 2009).

When applied to a three dimensional system, we can utilize SPHARM to compute point distribution models (PDMs). This involves acquiring spherical topology, followed by surface mesh computation to achieve spherical parameterization using area-preserving and distortion-minimizing spherical mapping. Using icosahedron subdivision on the output SPHARM description, a set number of points is sampled to generate corresponding PDMs (Vicory et al., 2018). These points can then be utilized similarly to homologous landmarks in geometric morphometric analyses. The advantage of this approach is its initial requirement of only a small set of homologous landmarks and can accommodate the loss or gain of 'novel' structures (Polly, 2008). Spherical harmonics also produces an orthogonal basis for mathematically representing shape among a large class of objects, providing a basis for reconstructing the tempo of evolutionary change among the structures themselves (Shen et al., 2009).

Previously used by neuroscientists to compare brain shapes (Gerig et al., 2001; Goldberg-Zimring et al., 2005), the utilization of SPHARM has expanded to include studies of complex morphologies such as fruit fly genitalia (Shen et al., 2009), carnivoran calcanea (Wimberly et al., 2022), carnivoran frontal sinuses (Curtis & Van Valkenburgh, 2014), and mammalian cervical vertebrae (Vander Linden et al., 2019).

With recent advances in imaging, microscopy, laser scanning, and computed tomography (CT), the acquisition of high resolution three dimensional data has become faster and more accessible. These technological advancements have revolutionized our ability to study morphological variation, necessitating the development of analytical techniques that go beyond

traditional methods like linear or landmark-based geometric morphometrics. In this thesis, the exploration of morphological variation and its manifestations in development and evolution is a central theme. Specifically, the focus lies on novel approaches to studying morphological variation and their implications for advancing our understanding of the development and evolution of structures and systems.

References

Adams, D., Rohlf, F. J., & Slice, D. (2013). A field comes of age: geometric morphometrics in the 21st century.

Adams, D. C., & Collyer, M. L. (2009). A general framework for the analysis of phenotypic trajectories in evolutionary studies. *Evolution*, 63(5), 1143-1154.

Arratia, G., Schultze, H. P., & Casciotta, J. (2001). Vertebral column and associated elements in dipnoans and comparison with other fishes: development and homology. *Journal of morphology*, 250(2), 101-172.

Berio, F., Bayle, Y., Riley, C., Larouche, O., & Cloutier, R. (2022). Phenotypic regionalization of the vertebral column in the thorny skate Amblyraja radiata: Stability and variation. *Journal of Anatomy*, 240(2), 253-267.

Blackith, R. E., & Reyment, R. A. (1971). Multivariate morphometrics.

Böhmer, C., Rauhut, O. W., & Wörheide, G. (2015). Correlation between Hox code and vertebral morphology in archosaurs. *Proceedings of the Royal Society B: Biological Sciences*, 282(1810), 20150077.

Böhmer, C., Rauhut, O. W., & Wörheide, G. (2015). New insights into the vertebral Hox code of archosaurs. *Evolution & development*, 17(5), 258-269.

Bolker, J. A. (2000). Modularity in development and why it matters to evo-devo. *American Zoologist*, 40(5), 770-776.

Bookstein, F. L. (1997). Morphometric tools for landmark data.

Brechbühler, C., Gerig, G., & Kübler, O. (1995). Parametrization of closed surfaces for 3-D shape description. *Computer vision and image understanding*, 61(2), 154-170.

Buchholtz, E. A. (2007). Modular evolution of the cetacean vertebral column. *Evolution & development*, 9(3), 278-289.

Burke, A. C., Nelson, C. E., Morgan, B. A., & Tabin, C. (1995). Hox genes and the evolution of vertebrate axial morphology. *Development*, 121(2), 333-346.

Carroll, S. B. (1995). Homeotic genes and the evolution of arthropods and chordates. *Nature*, 376(6540), 479-485.

Carroll, S. B. (2005). Evolution at two levels: on genes and form. *PLoS biology*, 3(7), e245.

Casaca, A., Santos, A. C., & Mallo, M. (2014). Controlling Hox gene expression and activity to build the vertebrate axial skeleton. *Developmental Dynamics*, 243(1), 24-36.

Cheverud, J. M. (1996). Developmental integration and the evolution of pleiotropy. *American Zoologist*, 36(1), 44-50.

Christ, B., Huang, R., & Wilting, J. (2000). The development of the avian vertebral column. *Anatomy and embryology*, 202, 179-194.

Claessens, L. P. (2009). A cineradiographic study of lung ventilation in Alligator mississippiensis. *Journal of Experimental Zoology Part A: Ecological Genetics and Physiology*, *311*(8), 563-585.

Criswell, K. E., Roberts, L. E., Koo, E. T., Head, J. J., & Gillis, J. A. (2021). hox gene expression predicts tetrapod-like axial regionalization in the skate, Leucoraja erinacea. *Proceedings of the National Academy of Sciences,* 118(51), e2114563118.

Curtis, A. A., & Van Valkenburgh, B. (2014). Beyond the sniffer: frontal sinuses in Carnivora. *The Anatomical Record*, 297(11), 2047-2064.

Economides, K. D., Zeltser, L., & Capecchi, M. R. (2003). Hoxb13 mutations cause overgrowth of caudal spinal cordand tail vertebrae. *Developmental biology*, 256(2), 317-330.

Ege, Y. C., Foth, C., Baum, D., Wirkner, C. S., & Richter, S. (2020). Adapting spherical-harmonics-based geometric morphometrics (SPHARM) for 3D images containing large cavity openings using ambient occlusion: a study with hermit crab claw shape variability. *Zoomorphology*, 139, 421-432.

Felice, R. N., Watanabe, A., Cuff, A. R., Noirault, E., Pol, D., Witmer, L. M., . . . Goswami, A. (2019). Evolutionary integration and modularity in the archosaur cranium. *Integrative and comparative biology*, 59(2), 371-382.

Felsenstein, J. (2012). A comparative method for both discrete and continuous characters using the threshold model. *The american naturalist*, 179(2), 145-156.

Figueirido, B., Martín-Serra, A., Pérez-Ramos, A., Velasco, D., Pastor, F. J., & Benson, R. J. (2021). Serial disparity in the carnivoran backbone unveils a complex adaptive role in metameric evolution. *Communications Biology,* 4(1), 863.

Foronda, D., Navas, L. F. d., Garaulet, D. L., & Sánchez-Herrero, E. (2009). Function and specificity of Hox genes.

Gadow, H. F. (2014). The evolution of the vertebral column: *Cambridge University Press.*

Gass, G., & Bolker, J. (2003). Modularity: 260–267. Keywords & Concepts in Evolutionary Developmental Biology. *Harvard University Press,* Cambridge.

Gerber, S. (2019). Use and misuse of discrete character data for morphospace and disparity analyses. *Palaeontology,* 62(2), 305-319.

Gerig, G., Styner, M., Jones, D., Weinberger, D., & Lieberman, J. (2001). Shape analysis of brain ventricles using spharm. Paper presented at the Proceedings IEEE workshop on mathematical methods in biomedical image analysis (MMBIA 2001).

Goldberg-Zimring, D., Talos, I.-F., Bhagwat, J. G., Haker, S. J., Black, P. M., & Zou, K. H. (2005). Statistical validation of brain tumor shape approximation via spherical harmonics for image-guided neurosurgery. *Academic radiology,* 12(4), 459-466.

Goswami, A. (2006). Morphological integration in the carnivoran skull. *Evolution,* 60(1), 169-183.

Gould, S. (1977). Ontogeny and phylogeny. In: Cambridge. MA: *Harvard University Press*.

Gunz, P., Mitteroecker, P., & Bookstein, F. L. (2005). Semilandmarks in three dimensions. *Modern morphometrics in physical anthropology*, 73-98.

Hall, B. K. (2005). Bones and cartilage: developmental and evolutionary skeletal biology: *Elsevier*.

Hallgrímsson, B., Jamniczky, H., Young, N. M., Rolian, C., Parsons, T. E., Boughner, J. C., & Marcucio, R. S. (2009). Deciphering the palimpsest: studying the relationship between morphological integration and phenotypic covariation. *Evolutionary biology,* 36, 355-376.

Harmon, L. J., Schulte, J. A., Larson, A., & Losos, J. B. (2003). Tempo and mode of evolutionary radiation in iguanian lizards. *Science*, 301(5635), 961-964.

Harper, C. M., Goldstein, D. M., & Sylvester, A. D. (2022). Comparing and combining sliding semilandmarks and weighted spherical harmonics for shape analysis. *Journal of Anatomy,* 240(4), 678-687.

Harrington, S. M., Harrison, L. B., & Sheil, C. A. (2013). Ossification sequence heterochrony among amphibians. *Evolution & development*, 15(5), 344-364.

Hautier, L., Weisbecker, V., Goswami, A., Knight, F., Kardjilov, N., & Asher, R. J. (2011). Skeletal ossification and sequence heterochrony in xenarthran evolution. *Evolution & development*, 13(5), 460-476.

Head, J. J., & Polly, P. D. (2015). Evolution of the snake body form reveals homoplasy in amniote Hox gene function. *Nature*, 520(7545), 86-89.

Hoffstetter, R., & Gasc, J. P. (1969). Vertebrae and ribs of modern reptiles. *Biology of the Reptilia*, *1*(5), 201-310.

Janvier, P. (1996). Early vertebrates: *Oxford University Press*.

Johnson, S. E., & Shapiro, L. J. (1998). Positional behavior and vertebral morphology in atelines and cebines. *American Journal of Physical Anthropology: The Official Publication of the American Association of Physical Anthropologists*, 105(3), 333-354.

Jones, K. E., Angielczyk, K. D., Polly, P. D., Head, J. J., Fernandez, V., Lungmus, J. K., . . .

Pierce, S. E. (2018). Fossils reveal the complex evolutionary history of the mammalian regionalized spine. *Science*, 361(6408), 1249-1252.

Jones, K. E., Gonzalez, S., Angielczyk, K. D., & Pierce, S. E. (2020). Regionalization of the axial skeleton predates functional adaptation in the forerunners of mammals. *Nature ecology & evolution*, 4(3), 470-478.

Kessel, M., & Gruss, P. (1991). Homeotic transformations of murine vertebrae and concomitant alteration of Hox codes induced by retinoic acid. *Cell*, 67(1), 89-104.

Klingenberg, C. P. (2008). Morphological integration and developmental modularity. *Annual review of ecology, evolution, and systematics*, 39, 115-132.

Krumlauf, R. (1994). Analysis of gene expression by northern blot. *Molecular biotechnology*, 2, 227-242.

Lauder, G. V. (1990). Functional morphology and systematics: studying functional patterns in an historical context. *Annual Review of Ecology and Systematics*, 21(1), 317-340.

Liang, D., Wu, R., Geng, J., Wang, C., & Zhang, P. (2011). A general scenario of Hox gene inventory variation among major sarcopterygian lineages. *BMC Evolutionary Biology*, 11, 1-13.

Lloyd, G. T. (2016). Estimating morphological diversity and tempo with discrete character-taxon matrices: implementation, challenges, progress, and future directions. *Biological Journal of the Linnean Society*, 118(1), 131-151.

Long JR, J. H., Pabst, D. A., Shepherd, W. R., & Mclellan, W. A. (1997). Locomotor design of dolphin vertebral columns: bending mechanics and morphology of Delphinus delphis. *Journal of Experimental Biology*, 200(1), 65-81.

Losos, J. B. (2008). Phylogenetic niche conservatism, phylogenetic signal and the relationship between phylogenetic relatedness and ecological similarity among species. *Ecology letters*, 11(10), 995-1003.

Mackie, E., Ahmed, Y., Tatarczuch, L., Chen, K.-S., & Mirams, M. (2008). Endochondral ossification: how cartilage is converted into bone in the developing skeleton. *The international journal of biochemistry & cell biology*, 40(1), 46-62.

Macpherson, J., & Ye, Y. (1998). The cat vertebral column: stance configuration and range of motion. *Experimental brain research*, 119, 324-332.

Maisano, J. A. (2002). The potential utility of postnatal skeletal developmental patterns in squamate phylogenetics. *Zoological Journal of the Linnean Society*, 136(2), 277-313.

Mallo, M., Wellik, D. M., & Deschamps, J. (2010). Hox genes and regional patterning of the vertebrate body plan. *Developmental biology*, 344(1), 7-15.

Marchesi, M. C., Mora, M. S., Dans, S. L., & González-José, R. (2021). Allometry and ontogeny in the vertebral column of southern hemisphere dolphins: a 3D morphofunctional approach. *Journal of Mammalian Evolution*, 28(1), 125-134.

Marcus, L. F. (1990). Traditional morphometrics. Paper presented at the Proceedings of the Michigan morphometrics workshop.

Martín-Serra, A., Figueirido, B., & Palmqvist, P. (2014). A three-dimensional analysis of morphological evolution and locomotor performance of the carnivoran forelimb. *PLoS One,* 9(1), e85574.

Martín-Serra, A., Pérez-Ramos, A., Pastor, F. J., Velasco, D., & Figueirido, B. (2021). Phenotypic integration in the carnivoran backbone and the evolution of functional differentiation in metameric structures. *Evolution Letters*, 5(3), 251-264.

Maxwell, E. E. (2008). Ossification sequence of the avian order Anseriformes, with comparison to other precocial birds. *Journal of morphology*, 269(9), 1095-1113.

McGinnis, W., & Krumlauf, R. (1992). Homeobox genes and axial patterning. *Cell*, 68(2), 283-302.

McNamara, K. J. (2012). Heterochrony: the evolution of development. *Evolution: Education and Outreach,* 5, 203-218.

Mitgutsch, C., Wimmer, C., Sánchez-Villagra, M. R., Hahnloser, R., & Schneider, R. A. (2011). Timing of ossification in duck, quail, and zebra finch: intraspecific variation,

heterochronies, and life history evolution. *Zoological science*, 28(7), 491.

Molnar, J. L., Pierce, S. E., & Hutchinson, J. R. (2014). An experimental and morphometric test of the relationship between vertebral morphology and joint stiffness in Nile crocodiles (Crocodylus niloticus). *Journal of Experimental Biology*, 217(5), 758-768.

Müller, G. B., & Wagner, G. P. (1996). Homology, Hox genes, and developmental integration. *American Zoologist*, 36(1), 4-13.

Olson, E. C., & Miller, R. L. (1999). Morphological integration: *University of Chicago Press*.

Polly, P. D. (2008). Adaptive zones and the pinniped ankle: a three-dimensional quantitative analysis of carnivoran tarsal evolution. *In Mammalian evolutionary morphology*: A tribute to Frederick S. Szalay (pp. 167-196): Springer.

Polly, P. D., Head, J. J., & Cohn, M. J. (2001). Testing modularity and dissociation: the evolution of regional proportions in snakes. *Beyond heterochrony: the evolution of development*, 307-335.

Pridmore, P. A. (1992). Trunk movements during locomotion in the marsupial Monodelphis domestica (Didelphidae). *Journal of morphology*, 211(2), 137-146.

Raff, R. A. (2012). The shape of life: genes, development, and the evolution of animal form: *University of Chicago Press.*

Randau, M., Cuff, A. R., Hutchinson, J. R., Pierce, S. E., & Goswami, A. (2017). Regional differentiation of felid vertebral column evolution: a study of 3D shape trajectories. *Organisms Diversity & Evolution*, 17, 305-319.

Randau, M., & Goswami, A. (2017). Morphological modularity in the vertebral column of Felidae (Mammalia, Carnivora). *BMC Evolutionary Biology*, 17, 1-12.

Randau, M., Goswami, A., Hutchinson, J. R., Cuff, A. R., & Pierce, S. E. (2016). Cryptic complexity in felid vertebral evolution: shape differentiation and allometry of the axial skeleton. *Zoological Journal of the Linnean Society*, 178(1), 183-202.

Ritchie, D. W., & Kemp, G. J. (1999). Fast computation, rotation, and comparison of low resolution spherical harmonic molecular surfaces. *Journal of Computational Chemistry,* 20(4), 383-395.

Rohlf, F. J., & Archie, J. W. (1984). A comparison of Fourier methods for the description of wing shape in mosquitoes (Diptera: Culicidae). *Systematic Zoology*, 33(3), 302-317.

Rohlf, F. J., & Marcus, L. F. (1993). A revolution morphometrics. *Trends in ecology &*

evolution, 8(4), 129-132.

Sallan, L. C. (2012). Tetrapod-like axial regionalization in an early ray-finned fish. *Proceedings of the Royal Society B: Biological Sciences,* 279(1741), 3264-3271.

Schaeffer, J., Benton, M. J., Rayfield, E. J., & Stubbs, T. L. (2020). Morphological disparity in theropod jaws: comparing discrete characters and geometric morphometrics. *Palaeontology,* 63(2), 283-299.

Schilling, N. (2011). Evolution of the axial system in craniates: morphology and function of the perivertebral musculature. *Frontiers in zoology,* 8, 1-19.

Schultze, H. P., & Arratia, G. (1988). Reevaluation of the caudal skeleton of some actinopterygian fishes: II. Hiodon, Elops, and Albula. *Journal of morphology,* 195(3), 257-303.

Sheil, C. A. (2003). Skeletal development in turtles: patterns of ossification through ontogeny in Apalone spinifera, Chelydra serpentina, Macrochelys temminckii, and Eretmochelys imbricata (Reptilia: Testudinata): University of Kansas.

Shen, L., Farid, H., & McPeek, M. A. (2009). Modeling three-dimensional morphological structures using spherical harmonics. *Evolution,* 63(4), 1003-1016.

Slice, D. E. (2007). Geometric morphometrics. *Annu. Rev. Anthropol.*, 36, 261-281.

Smit, T. H. (2002). The use of a quadruped as an in vivo model for the study of the spine–biomechanical considerations. *European spine journal,* 11(2), 137-144.

Soul, L. C., & Benson, R. B. (2017). Developmental mechanisms of macroevolutionary change in the tetrapod axis: a case study of Sauropterygia. *Evolution*, 71(5), 1164-1177.

Vander Linden, A., Campbell, K. M., Bryar, E. K., & Santana, S. E. (2019). Head-turning morphologies: Evolution of shape diversity in the mammalian atlas–axis complex. *Evolution*(73(10)), 2060-2071.

Verrière, A., Fröbisch, N. B., & Fröbisch, J. (2022). Regionalization, constraints, and the ancestral ossification patterns in the vertebral column of amniotes. *Scientific Reports*, 12(1), 22257.

Vicory, J., Pascal, L., Hernandez, P., Fishbaugh, J., Prieto, J., Mostapha, M., . . . Liu, Z. (2018). Slicersalt: Shape analysis toolbox. Paper presented at the Shape in Medical Imaging: International Workshop, ShapeMI 2018, Held in Conjunction with MICCAI 2018, Granada, Spain, September 20, 2018, Proceedings.

Wagner, G. P. (2000). The character concept in evolutionary biology. Elsevier.

Wagner, G. P., & Altenberg, L. (1996). Perspective: complex adaptations and the evolution of evolvability. *Evolution,* 50(3), 967-976.

Wagner, G. P., & Zhang, J. (2011). The pleiotropic structure of the genotype–phenotype map: the evolvability of complex organisms. *Nature Reviews Genetics,* 12(3), 204-213.

Wainwright, P. C. (2007). Functional versus morphological diversity in macroevolution. *Annu. Rev. Ecol. Evol. Syst.,* 38, 381-401.

Ward, A. B., & Brainerd, E. L. (2007). Evolution of axial patterning in elongate fishes. *Biological Journal of the Linnean Society*, 90(1), 97-116.

Ward, A. B., & Mehta, R. S. (2014). Differential occupation of axial morphospace. *Zoology*, 117(1), 70-76.

Weisbecker, V., & Mitgutsch, C. (2010). A large‐scale survey of heterochrony in anuran cranial ossification patterns. *Journal of Zoological Systematics and Evolutionary Research,* 48(4), 332-347.

Wellik, D. M. (2007). Hox patterning of the vertebrate axial skeleton. *Developmental dynamics: an official publication of the American Association of Anatomists*, 236(9), 2454-2463.

Wiley, E. O. (1981). Phylogenetics: theory and practice of phylogenetic systematics: *John Wiley & Sons.*

Wills, M. A., Briggs, D. E., & Fortey, R. A. (1994). Disparity as an evolutionary index: a comparison of Cambrian and Recent arthropods. *Paleobiology,* 20(2), 93-130.

Wimberly, A. N., Natale, R., Higgins, R., & Slater, G. J. (2022). Choice of 3D morphometric method leads to diverging interpretations of form–function relationships in the carnivoran calcaneus. *bioRxiv*, 2022.2005. 2016.492149.

Wolpert, L., Tickle, C., & Arias, A. M. (2015). Principles of development: *Oxford University Press,* USA.

Zelditch, M., Swiderski, D. L., & Sheets, H. D. (2012). Geometric morphometrics for biologists: a primer: academic press.

Chapter 2
Development and evolution of regionalization within the avian axial column

Published as:

Bui, H.-N. N., & Larsson, H. C. (2021). Development and evolution of regionalization within the avian axial column. *Zoological Journal of the Linnean Society, 191*(1), 302-321.

Abstract

The origin of birds from their terrestrial antecedents was accompanied by a wholesale transformation of their skeleton as they transitioned from a terrestrial to aerial realm. Part of this dramatic transformation is the reduction of separate vertebral elements into regional fusions to limit axial flexibility. This is partially mirrored within the development of the axial column, with regions of the axial column experiencing increasing morphological modularity and the loss of skeletal elements through vertebral fusions. Using a detailed description of the morphological development of the axial column in the model domestic chicken, *Gallus gallus*, we present a map of axial ossification based on discrete characters. Delays in ossification are found to occur in conjunction with the formation of fusions. Our study shows that the pattern and sequence of fusion and ossification during development may reflect the presence of independent modules as subsets within the typical regions of the avian axial column. Interestingly, few of these fusion modules correspond to the initial axial *Hox* expression patterns, suggesting another patterning mechanism is driving axial fusion regionalization. Additionally, two regions of fusion are

discovered in the synsacrum. The anterior region of seven fused synsacrals may correspond to the non-ornithuran pygostylian synsacrum of the same number of vertebrae.

Introduction

The study of ossification patterns, the sequence of bone formation during development, has provided insight into the mechanisms responsible for the origin of evolutionary variation and the support of phylogenetic hypotheses (Maisano, 2002; Maxwell, 2008). Variability in the timing of ossification has led to insights in the adaptation and development of morphological changes in size and shape (Maxwell, 2009; Prochel, 2006; Sánchez-Villagra, 2002; Sánchez-Villagra et al., 2008). Numerous studies have addressed the patterns of ossification in the chicken, however few have focused specifically on the axial column in detail. Crocodylian skeletal element ossification has been studied by Bellairs and Kamal (1981), Muller (1967), Deraniyagla (1939), and Rieppel (1993). More recent work of ossification sequences has been done for the skeletons of palaeognathous birds (Maxwell, 2008), quail (Nakamura et al., 2019), and frog (Arenas-Rodríguez et al., 2018).

The axial column is a series of repeating ossified, cartilaginous, and ligamentous elements surrounding the spinal cord and notochord (Schultze & Arratia, 1988; Ward & Mehta 2014). As one of the major defining characteristics of Vertebrata, the axial column protects the spinal cord and dorsal aorta, provides attachment points for the axial musculature, and is linked to body shape variation and a diverse suite of locomotory repertoires (Bergmann & Irschick, 2012; Ward & Brainerd, 2007; Ward & Mehta, 2014).

Axial skeleton formation in early embryo development has been extensively studied and well described for several species, but mainly through a mouse and chicken model (Christ &

Wilting, 1992; Hautier et al., 2014; Shapiro, 1992; Verbout, 1985; Wallin et al., 1994). Axial patterning and development has also been described in zebrafish (Fisher & Halpern, 1999; Morin-Kensicki et al., 2002), alligator (Mansfield & Abzhanov, 2010), crocodile (Böhmer et al., 2015), turtle (Ohya et al., 2005) and snakes (Cohn & Tickle, 1999). The vertebral column and ribs originate from somites, with the relationship between them being the subject of 150 years of investigation (Christ et al., 2000). Somites are formed from the paraxial mesoderm. Somites are added sequentially from anterior to posterior in pairs at regular intervals along the axis and are divided into myotomes, dermatomes, and sclerotomes (Christ et al., 2000). The sclerotome give rise to intersegmental vertebrae, with each vertebrae forming from the posterior half of one pair of somites and the anterior half of the succeeding pair of somites. Remnants of the notochord form intervertebral discs, with their condensation determining the boundaries of the vertebral bodies to be established (Christ et al., 2000). Lateral components of the sclerotome contribute to the rib, pediculus, lamina of the neural arch, the dorsal components give rise to the dorsal-most parts of the neural arch and spinous process, and the ventral components form the vertebral bodies (Christ et al., 2000). Each vertebra is composed of a ventral centrum and dorsal vertebral arches. Various processes project from the centra and their arches and the number, shape, and sizes of these processes vary based on vertebral identity and function. Within Archosauria, these structural processes are highly disparate, with such structures and vertebral count significantly varying between birds, crocodylians, and dinosaurs (Böhmer et al., 2015; Scheyer et al., 2019). These processes, or apophyses, may form interlocking structures between vertebrae, muscle attachment sites, or may articulate with ribs in the thoracic region of the axial column, depending on their location within the axial column and their general function.

The axial column develops from a series of repeating mesenchymal condensations that chondrify and later ossify. The early cartilaginous elements are relatively similar to one another and subsequently develop the characteristics unique to regions within the axial column and individual vertebrae. Vertebrae vary both between adjacent pairs and regionally throughout the axial column. In fish, the axial column is typically divided into precaudal and caudal regions with little differentiation within each of these two regions. Tetrapod axial columns however, are generally composed of four regions: cervical, dorsal, sacral, and caudal. All but the caudal vertebrae have ribs. The derived axial columns of mammals, crocodylians, and birds have an additional lumbar region lacking ribs between the ribbed thoracic and sacral vertebrae. These regional boundaries generally follow Hox axial expression with overlapping expressions in fish associated with undifferentiated columns and non-overlapping expressions associated with more complex axial columns (Figure 2.1).

Axial regionalization of the vertebrae is initially determined by Homeobox (*Hox)* gene expression (Burke et al., 1995). Homeobox genes are a family of regulatory genes expressed along the anterior-posterior axis, encoding transcription regulators involved in pattern formation. The combination of active *Hox* genes specifies the region and identity of the vertebral elements, with alterations within the code leading to homeotic transformations and changes in segment identity (Kessel & Gruss, 1991). For example, there is a consistent association of the expression of *Hoxc-5* and *Hoxc-6* with the cervical-thoracic transition, *Hoxa-9, Hoxb-9,* and *Hoxc-9* with the thoracic-lumbar transition, and so on (Figure 2.1). The expression of *Hox13* paralogs posteriorly acts to terminate tail elongation as well as neuronal proliferation (Economides et al., 2003). Vertebral identity is determined at the somite level within the segmental plate mesenchyme, whereas muscle rudiments do not possess such axial identity. Instead, region

specific development of muscles is determined by the derivatives of the sclerotome and lateral plate mesoderm (Christ et al., 2000).

The vertebral regionalization and anatomy of these vertebrae within a specific region is often related to the locomotory kinematics of an animal (Johnson & Shapiro, 1998). The varying degree of regionalization within the axial columns of vertebrates reflects the hierarchical organization of a serially homologous structure. These regions and their relationship to Hox gene expression is a reflection of the concept of modularity.

Modularity is formally described as the division of an organism into units that are products of a shared developmental origin, have hierarchical organization, interactions with similar units (Raff, 1996), and the ability to undergo developmental and evolutionary transformation (Bolker, 2000). Morphological modularity and its implications for evolution has been studied in cetaceans (Buchholtz, 2007), mammals (Randau & Goswami, 2017), and even snakes (Polly et al., 2001). The identification of morphological modules provides insight into evolutionary modules and their ability to evolve independently in response to selective pressures (Polly et al., 2001; Ward and Brainerd, 2007; Woltering, 2012). Mammal axial columns are highly regionalized and modular, having been mostly studied due to their conserved vertebral count. However, birds also have a highly derived axial column that has undergone many changes through evolution, such as (extensive vertebral number loss and, extensive fusions throughout the axial column) (James, 2009; Rashid et al., 2014). The development of regionalization and modularity within the avian axial column has not yet been looked at in detail.

The axial column of birds varies significantly in number of individual vertebrae and anatomy across all taxa. Although vertebral counts vary, each region of the axial column among birds maintains a similar function and structure. The avian axial column consists of a highly

flexible neck with varying cervical counts, fused lumbosacral vertebrae forming a synsacrum, several free caudals and a pygostyle. Several birds also experience several fused thoracic vertebrae, leading to the formation of a notarium (James, 2009). Notaria are not universal among birds, but the fusion itself reduces flexibility to that part of the vertebral column reducing the likelihood of dislocation during jarring movement (Storer, 1982). Fused sacral vertebrae in tetrapods develop for body support and rigidity, and fused caudals in birds and oviraptorid dinosaurs have been hypothesized as an anchor for tail retrices (Abitbol, 1987; Hildebrand & Goslow, 2001; Persons et al., 2014). In birds, the adjacent bones of the pelvic girdle fuse into the os coxae, which fuses with the synsacrum, a fusion of multiple lumbosacral vertebrae. These fusions result in regionally fused sections of the axial column that act to modularize the column into sturdy units able to support the body. The variation found within the avian axial column is directly related to the kinematics and biomechanics of the animal with increased or decreased mobility for flexibility and strength respectively (James, 2009; Storer, 1982). Fusions along the axial column significantly reduce the mobility and increase stability within certain areas of the vertebral column allowing for a various number of functional, behavioral, and ecological implications (James, 2009; Mulder, 2001). Vertebral fusions and their function in extant birds have been associated with biomechanical implications in relation to flight and landing, bipedal posture, and breathing (James, 2009). These fusions create individual functional units, or modules, within specific regions of the avian axial column.

A detailed description of the anatomical development of these skeletal characters within the axial skeleton is lacking. Therefore, prior to understanding the evolutionary implications of the structure of the avian axial skeleton, we here describe and track its development in detail in order to assess anatomical evolution and the development of modularity. By examining the

development of the regionalization of the axial column, we hope to gain a greater understanding of its anatomical evolution. Using the domestic chicken as a model system, this paper describes the normal development of the chicken axial skeleton to track the timing of discrete anatomical character ossification and vertebral fusions that lead to the complex axial regionalization of birds. Our goal is to provide information on the developmental timing and origin of axial skeletal elements and describe the ontogeny of axial regionalization in a model bird.

Materials and Methods

Gallus gallus domesticus eggs were purchased from Steve Paquette Farm, (Roch De L'Achigan, QC, Canada) and artificially incubated under normal conditions (approximately 37° C). Embyos were staged according to Hamburger & Hamilton (1951). Three embryos per stage from stages 27 to 45 were collected. All embryos were fixed in 4% paraformaldehyde (PFA) prior to clearing and staining. Embryos of stage 40 and above were skinned and eviscerated prior to staining. These specimens were cleared and stained for bone and cartilage according to the Dingerkus and Uhler procedure (1977). Specimens older than stage 40 were macerated in Trypsin while stages 39 and younger were not. This was done in order to remove greater muscle, subcutaneous and intermuscular fat deposits, prior to staining. These efforts resulted in a sample size of $N = 44$. All embryos were then photographed in 100% glycerol with a Sony Rx1000. All embryos are accessioned in the Redpath Museum under lot number RM 084337.

The degree of ossification for each element of each vertebral segment was scored and presented in Supplementary Table 1. Codings are absent (0), present and cartilaginous (1), present and ossified less than 50% (2), present and ossified more than 50% (3). Averages for

each vertebral segment were calculated to represent a degree of ossification for each individual vertebral segment.

Vertebral counts of fossil birds and 1 modern bird were collected for *Confuciusornis sanctus* (Chiappe et al., 1999)*, Ichthyornis dispar* (Clarke, 2004), *Apsaravis ukhaana* (Clark & Norell, 2002), *Archaeopterygidae* (Elzanowski, 2002), *Microraptor gui* (Hwang et al., 2002; Pei et al., 2014; Xu et al., 2002), *Dromaius novaehollandiae* (Kumar & Singh, 2014), *Orientantius ritteri* (Liu et al., 2019), *Hesperornis regalis* (Marsh, 1880), *Baptornis advenus* (Martin & Tate, 1976), *Calciavis grandei* (Nesbitt & Clarke, 2016), *Parapengornis eurycaudatus* (Hu et al., 2015), *Protopteryx fengningensis* (Zhang & Zhou 2000), *Longipteryx chaoyangensis* (Zhang & Zhou, 2001), *Sapeornis chaoyangensis* (Zhou & Zhang, 2003), *Jeholornis prima* (Zhou & Zhang, 2003), and *Piscivoravis lii* (Zhou et al., 2014).

Results

Stage 27: Embryos of this stage were studied and compared, however are too small and fragile to photograph well. These embryos all lack clear or fully chondrified vertebrae. Axial columns consist of small chondrifications in ring-like formations. Cartilage is a dense collection of ‘points’ where each centra would be, with small outgrowths laterally.

Stage 28 (Figure 2.2A-C)*:* The atlas and axis are cartilaginous and relatively unspecialized relative to the rest of the vertebrae within the axial column. The atlas centrum is approximately half the length of the centrum of the axis and the rest of the vertebrae. Both vertebrae are composed of cartilaginous centra, neural arches, and spinous processes. No trace of ossification is present. Cervical vertebrae are uniform throughout the series with cartilaginous centra of equal length and width, neural arches, and spinous

processes angled caudally. Near the end of the series, small protrusions from the ventral side of the vertebral bodies appear as rib facets. The thoracic vertebrae are indistinguishable from cervical vertebrae morphologically except for the attachment of rudimentary cartilaginous ribs. Sacral vertebrae are also fully cartilaginous, however their centra are slightly wider laterally with more pronounced transverse processes than the rest of the axial column. There is also less intervertebral space between vertebrae. Caudals are all unfused and decreasing in size throughout the series. Hints of spinous processes on the bigger vertebrae, as well as clear transverse processes are present early in the series.

Stage 29 (Figure 2.2D-F): Tiny cartilaginous costal processes are present within the cervical series.

Stage 30 (Figure 2.2G-I)*:* Atlas is present as an anteriorly-posteriorly compressed vertebra containing a centrum and caudally angled spinous process. Axis is cartilaginous with centrum and tall and thin spinous process that does not significantly extend caudally. No pygostyle present, all cartilaginous free caudals with weak spinous processes and transverse processes.

Stage 31 (Figure 2.3A-C): Vertebral arches of cervicals increase in width throughout the series and transverse processes laterally expand while centra remain the same length. Transverse processes and pre- and post-zygapophyses are present. The spinous processes are more defined and angled caudally, becoming more dorsally angled later in the series. Small costal processes present increasing in length at the end of the series. Lumbosacrals are comprised of cartilaginous centra and spinous processes, all unfused to each other but closer together in space compared to thoracic series. Arches are longer and wider than the

thoracic series, as well as retain caudally angled spinous processes that remain faint in presence.

Stage 32 (Figure 2.3D-F): Cervical vertebrae are cartilaginous and decrease in length throughout the series. Nearing the end of the series, the dorsal view of the vertebrae become more X-shaped with an increase in length of the transverse processes and a widening of the arch.

Stage 33 (Figure 2.3G-I): Atlas and axis are both cartilaginous. Atlas is ring-shaped. Transverse processes of the axis are more accentuated, and neural arch and spinous process flare to be wider and longer. The first two non-specialized cervicals form a cartilaginous connection between their pre-zygapophyses and post-zygapophyses. Spinous processes of the thoracic series remain unfused but are more square sail-shaped and prominent dorsally. Post-zygapophyses lie caudally to the articulation between vertebra and rib. Ribs are completely cartilaginous and uncinate processes are small but present. Vertebral arches of the lumbosacral series expand laterally and transverse processes elongate to articulate with the pelvic girdle. Transverse processes rostral to the acetabulum angle more rostrally and those caudal to the acetabulum within the sacral series angle more caudally. The beginnings of a crista spinosa synsacri appears as cartilage. Caudal neural arches form in thin structures connecting the left and right sides. Spinous processes are present on the left and right sides, present through the end of the series.

Stage 34 (Figure 2.4A-C): Costal processes increase in length until the 12th cervical then diminish prior to the ribs of the thoracic series. The first two non-specialized cervicals form their accessory foramina. Crista spinosa synsacri forms through fused spinous

processes from the 1st to 7th lumbosacrals. Transverse processes of 9th and 10th lumbosacrals begin to fuse.

Stage 35 (Figure 2.4D-F): Cervical transverse processes increase in length. Arches increase in length, as intervertebral space increases prior to the thoracic series. The transverse processes elongate where the rib articulations are present. Spinous processes thicken but remain unfused to one another. Post-zygapophyses lie caudally to the articulation between vertebrae and rib and more medial compared to the pre-zygapophyses. Vertebral arches of the lumbosacrals thicken to create bars across the pelvic girdle but have not fully fused yet. Transverse processes cranial to the acetabulum thicken and angle cranially, caudally to the acetabulum, the processes begin to angle caudally. 9th and 10th caudals may be weakly fused.

Stage 36 (Figure 2.4G-I)*:* Fusions of the spinous processes forming the crista spinosa synsacri and transverse processes of 8th and 9th lumbosacral vertebrae.

Stage 37 (Figure 2.5A-C)*:* Atlas ring is thinner ventrally and thicker dorsally. Dorsal spines of thoracic vertebrae significantly increase in prominence and height on the arch. The most dorsal portion of the spines from the 2nd to 5th thoracic fuse. The ribs are cartilaginous with the center of the ribs articulating with 2nd and 3rd thoracics begin to ossify. Both capitulum and tuberculum on the ribs are present and articulate with vertebrae. Uncinate processes are present and all remain cartilaginous. The dorsal spinous processes of the lumbosacrals decrease in prominence caudally to the acetabulum. Transverse processes of 8th through 11th lumbosacrals are fused.

Stage 38 (Figure 2.5D-F): 3rd to 6th thoracic ribs begin to ossify from the center of the rib.

Elongate transverse processes caudal to the acetabulum connect the ala postacetabularis to the axial column. Transverse processes of 8th to 12th lumbosacrals fuse. 8th through 10th caudals are somewhat fused.

Stage 39 (Figure 2.5G-I): Lateral portion of atlas and lateral and ventral region of axis begin to ossify. The dorsal most tip of the spinous process of the axis as well as the ventral most portion of the axis centrum begin to ossify. 3rd cervical centra is almost completely ossified with the vertebral arch and spinous process remaining cartilaginous. The dorsal most tip of the spinous processes begins to ossify. Ossification occurs through the series within the centra, however most are not complete. Greater amount of ossification through 1st to 5th cervical vertebra. The centers of the centra remain cartilaginous with the dorsal and ventral edges ossifying from the edges. Bases of the arches beginning to ossify. Centra within the lumbosacrals/synsacrum begin to ossify ventrally.

Stage 40 (Figure 2.6A-C): Lateral regions of atlas and lateral and ventral region of axis completely ossified. Vertebral centra of the series are almost completely ossified. Ossification has spread up the base of the vertebral arches, but the majority remain cartilaginous. Neural arches and spinous processes of each vertebra are not fully ossified, but are present and identifiable as darker cartilaginous features. Ossification in the later series of the cervical vertebrae seem to extend further up the arch compared to earlier vertebrae in the series. Costal processes are present as cartilaginous features throughout the entire series, as well as their attachment points to the centra. Thoracic centra appear to be fully ossified with vertebral arches almost completely ossified. The dorsal most part of the arch including the pre- and post-zygapophyses and spinous processes remain cartilaginous. Thoracic vertebrae 2-5 have fused cartilaginous spinous processes,

however full notarium is not present. The capitulum, uncinate process, and distal portion of the ribs remain cartilaginous, with the capitulum articulating with cartilage. The tuberculum is fully ossified, articulating with an ossified vertebral centra. Synsacrum centra have begun to ossify ventrally in vertebrae before the acetabulum, vertebral arches remain cartilaginous. The cartilaginous arches connecting the ala precetabularis have not fully fused but have thickened and a cartilaginous crisa spinosa synsacra has become more prominent. Caudally angled transverse processes remain cartilaginous and connect the thickened arches to the ala postacetabularis. Proximal caudals remain unfused with hint of fusion distally. Transverse processes and spinous processes present throughout the series. All cartilaginous.

Stage 41 (Figure 2.6D-F): Small ventral region of atlas is ossified. Axis centrum is completely ossified with the majority of the arch also ossified. Spinous process and post-zygapophyses remain cartilaginous. First two non-specialized cervical vertebrae are almost completely ossified except for the most caudal regions of the vertebrae. Vertebrae still remain separate by a thin cartilaginous region with attachments of costal processes. This cartilaginous band is more prominent later in the cervical series. Costal processes have begun to ossify distally in earlier vertebrae in the cervical series. Thoracic centra are fully ossified. Arches and dorsal processes remain cartilaginous, with ossification beginning in the dorsal most regions in vertebrae early in the thoracic series. Rib capitulum, uncinate processes, and distal regions remain cartilaginous. Ossification of ventral portions of the centra of the synsacrum has continued towards the acetabulum. Empty space between the arches decreases, and some fusion is present, hint at development of the synsacrum. 6 free caudals with transverse processes, bodies are in a

u-shaped arrangement. Fusion of the pygostyle is not complete, but space between centra is limited.

Stage 42 (Figure 2.6G-I): Cervical vertebral centra fully ossified. Arches mostly ossified except for dorsal most regions of spinous processes. Costal processes are elongate and ossified, articulation remains cartilaginous with vertebrae. Distal ribs remain cartilaginous but both tuberculum and capitulum of ribs are almost fully ossified. Capitulum remains proximally cartilaginous. Ossification of ventral centra in synsacrum continues caudally. Cartilage remains caudally from the acetabulum.

Stage 43 (Figure 2.7A-C): Atlas centrum ossified, articulation between centra and vertebral arch has not fully ossified. Medial dorsal aspect of vertebral arch also remains cartilaginous, creating an interrupted ring representing the whole atlas. Pre- and post- zygapophyses of cervical vertebrae are ossified except for their distalmost regions. Transverse processes also remain partially ossified.

Stage 44 (Figure 2.7D-F): Medial dorsal aspect of vertebral arch of the atlas remains cartilaginous, creating an interrupted ring representing the whole atlas. Axis is fully ossified except for the posterior portion of its spinous process. The post-zygapophyses are not highly defined from the arch but remain cartilaginous. Anterior portions of each centrum within the cervical series including the articulation point for the costal processes are partially ossified. Pre- and post- zygapophyses are ossified except for their distalmost regions. Transverse processes also remain partially ossified. Costal processes are elongate and ossified. Transverse processes extend to a greater lateral degree after the first two non-specialized cervicals and then shorten by the last three cervicals. The arches on the last three cervical vertebrae have lengthened and widened as the thoracic series

approaches. Thoracic centra fully ossified, spinous processes remain as cartilage. Vertebral arches of all thoracics are mostly ossified. Fusion of the spinous processes is more prominent with the dorsal regions of the 2nd through 5th thoracis fused. Distal areas of the ribs and their capitula remain cartilaginous. Vertebral arches of the lumbosacrals remain fully cartilaginous excluding the last two vertebrae within the series. Rostrally to the acetabulum, the arches have begun to fuse into bar-like struts with transverse processes articulating to the pelvis. Caudally to the acetabulum, the bars decrease in lateral extension, but display caudally angled transverse processes that connect to each other posteriorly and anteriorly. The transverse processes on the last few sacral vertebrae do not fuse together.

Stage 45 (Figure 2.7G-I): Atlas contains an ossified centrum with a ventral and anterior process along with a thin ring-shape arch. Post-zygapophyses are ossified and extend posteriorly over the axis. The axis is fully ossified with a centrum and its odontoid process as well as a ventral process that is anterior-posteriorly elongated. Cervical centra are elongate along the series until the 12th through 14th cervical. Neural arches are completely ossified, with pre- and post- zygapophyses creating a thin X-shape in dorsal view. Cartilage remains on the most distal ends of each zygapophysis. Arches thicken anterior-posteriorly nearing the thoracic series, with pre-zygapophyses flaring out in shape and extending more laterally, as post-zygapophyses thicken and shorten, migrating more medially. Spinous processes are all present and ossified with slight remnants of cartilage on the most dorsal ends of the 3rd through 5th, and 13th and 14th cervicals. All of them extend more dorsally than caudally. Costal processes are ossified and extend in length throughout the series, but never extend past the length of their respective centrum. Articular surfaces retain

hints of cartilage. Thoracic centra and neural arches are fully ossified while the spinous processes remain cartilaginous. The most dorsal regions of the cartilaginous spinous processes of the 2nd to 5th thoracics thoracics 2-5 are fused, with open spaces remaining underneath the fusions between the processes. Distal ends of the transverse processes as well as the proximal ends of the ribs remain cartilaginous. Distal ends of the ribs and their uncinate processes also remain cartilaginous. Centra and neural arches in synsacrum are ossified throughout the series as wide horizontal bars with rounded ends. Prior to the acetabulum, the arches are angled more rostrally with a crista spinosus forming medially. Past the acetabulum, the bars begin to decrease in lateral length and mostly cartilaginous, caudally angled transverse processes connect the main bodies of the vertebrae to the pelvis. The main bodies of the vertebrae through the series until halfway along the ischium are fused. Nearing the end of the series, intervertebral space between the arches increases and the transverse processes extend more laterally than caudally. Free caudals and pygostyle remains cartilaginous. Centra, arches, spinous processes, and ventrally angled transverse processes are all present. The spinous processes appear as two parasagittal, cartilaginous protrusions. Pygostyle does not appear fully fused.

Discussion

The axial column of chicken begins development as a simple, repetitive sequence of cartilaginous units that ossify and increases in anatomical complexity throughout development. From about 5 days after fertilization, we are able to discern the traces of a developing axial column, at stage 27. From the early stages of 28 to 32, vertebrae are relatively uniform, with specific regions determined only by the presence of ribs (thoracic), or their adjacency to the

pelvic girdle. Continuing through development, vertebrae become more specialized as cervical vertebrae begin to diverge with posteriorly angled spinous processes, prominent costal processes, and laterally expanding transverse processes. Thoracic vertebrae are first identified only through the presence of ribs and rib-bearing processes. Throughout development, their anatomy shifts and diverges from that of the cervicals with larger spinous processes. Lumbosacral vertebrae also diverge from early development as their neural arches and transverse arches begin to articulate to the pelvic girdle. Caudal vertebrae remain relatively simple and similar throughout development with the pygostyle only fusing during later stages.

At the resolution of developmental stages, the centra and neural arches chondrify together and throughout the entire axial column at stage 28. There is no trace of one region chondrifying before the other nor the centrum or neural arch before each other. However, at stage 39, the centra of the axis, cervical vertebrae 3 and 4, thoracics 2-7 have either partially or fully ossified whereas their neural arches have not. By stage 40, all vertebrae anterior to and including lumbosacral 7 have partially or fully ossified either centra and only all cervicals have ossified a portion of their neural arches. Only by stage 45 have all remaining lumbosacral vertebrae ossified their centra in an anterior to posterior trend. Caudal centra remain cartilaginous throughout the pre-hatchling series. Our results are consistent with the general description of vertebral development through whole-mount staining in previous work (Shapiro, 1992).

The first vertebral fusions occur by stage 33 within the spinous processes of the lumbosacral vertebrae, the beginnings of a crista spinosa synsacri. By stage 36, the 8th through 10th lumbosacral vertebrae have begun to fuse their transverse processes, and the last caudals have also begun to fuse. The spinous processes of the 2nd thoracic vertebrae through the 5th begin to fuse by stage 37. By stage 38, the 2nd to 5th thoracics have fused spinous processes and

the 1st through 7th lumbosacrals have fused spinous processes, and the 8th through 12th lumbosacrals 8 have fused transverse processes. The 8th through 10th caudals have also incompletely fused at this stage. From stages 41-45, the synsacrum begins to form more fully by fusing the 7th thoracic vertebrae into the lumbosacral complex, as the spinous processes are fully fused from Thoracic 7 to Lumbosacral 7, and the transverse processes of the 8th lumbosacral are fused to the 13th. The 6th through 10th caudals within these stages also fuse incompletely during these stages.

The majority of ossification occurs as expected in most archosaurs, rostrally to caudally. The timing of ossification occurs after the establishment of most vertebral fusions. Ossification only begins by stage 38 in the 2nd cervical. At stage 39, ossification has begun in 3 cervicals and the fused thoracics. By stage 40, the entire cervical and thoracic series has begun to ossify, as have the 1st through 7th lumbosacrals. After stage 41, the majority of each bone within the cervicals are ossified. By stage 45, ossification is still not fully complete as the synsacrum remains mostly cartilage with some elements fully ossified, and the caudals remaining mostly cartilaginous.

Some patterns emerge from the ontogeny of relative ossification throughout the axial column (Figure 2.8). Early, during stages 27 - 31, three major regions delay chondrification. These are an anterior section of the cervicals, the entire thoracic region, and the posterior seven lumbosacrals and caudals. The caudals advance to be fully chondrified in advance of the posterior lumbosacrals. The delay in chondrification of the thoracic and posterior lumbosacrals may be associated with the later fusion of vertebrae in these regions with respect to the early fusion of the anterior lumbosacrals. Interestingly, not only do the anterior and posterior

lumbosacrals initiate fusions separately, these two regions remain separate until stage 42 before coalescing.

The most advanced ossification occurs in the atlas and axis, several stages before any other vertebral segment. The next two cervicals are relatively delayed in ossification with respect to the rest of the cervicals, suggesting some degree of independence between the atlas/axis and cervicals 5-14. The relative delay of the third and fourth cervicals correlates with the anteriorly delayed chondrification region. The only ossification signal in advance of the cervical - thoracic and thoracic - lumbosacral boundaries are a delay in ossification of the first, sixth, and seventh thoracics from their adjacent vertebrae. Perhaps this delayed ossification aids to establish regionalization. The most delayed are the posterior two lumbosacral vertebrae. These maintain an only partially chondrified state until stage 44, separating the other fusing lumbosacral vertebrae from the caudals. The most advanced post-cervical regions are the middle thoracics, anterior lumbosacrals, and caudals. In the former two, the same vertebral segments that advance ossification also initiate fusions. The former two are also well preceded by fully chondrified segments prior to fusion, whereas the posterior lumbosacral fusion occurs only when those vertebrae chondrify.

The caudals appear to be the most uniform and most different from the other vertebrae. They are relatively delayed to chondrify and do not ossify even partially during embryogenesis. In spite of their relatively synchronized order of chondrification, the posterior caudals fuse, from posterior to anterior, into the pygostyle. The lack of advanced chondrification in only the posterior caudals make this fusion different than the other axial fusions.

The ontogeny of regionalization can be illustrated with the number of isolated vertebral segments. Figure 2.9 illustrates the number of segments throughout ontogeny and depicts two

main developmental times for this remarkable regionalization in birds. The first occurs between stages 32 and 33 when the 45 isolated segments fuse to 38. Lumbosacrals 1-7 fuse at this stage. At stage 35 the pygostyle begins to fuse the posterior two caudals. The pygostyle fuses three more caudals gradually throughout ontogeny. From stage 36 to 38, another drop to only 29 segments occurs as lumbosacrals 8-10 (stage 34), thoracics 2-4 (stage 37) and lumbosacrals 8-12 (stage 38). Finally to total segments reduce further as the lumbosacral fusions fuse together at stage 42. By the end of ossification, only 25 segments exist. Adult chickens have only 24 axial segments as a further posterior lumbosacral vertebrae is incorporated into the synsacrum.

Some patterns emerge between the Hox expression zones and axial development. The anterior boundary of Hox B5 expression lies at the axis, which is also the anterior boundary of the delayed chondrification region in the anterior cervicals. Anterior Hox A5 expression is present from cervicals 7-14, matching the posterior boundary of the anterior cervical delayed chondrification block and the advanced chondrification zone cervicals 7-14 that begins at stage 28. Hox A7 expression is along thoracics 2-7, which covers the zone of thoracic fusion (thoracics 2-5) into the notarium and the eventual fusion of thoracic 7 into the synsacrum.

Hox expression patterning occurs at much earlier stages, stages 22-26 (Burke et al. 1995), their downstream patterning may be influencing overall axial ossification and fusion. Although Hox C6 has long been associated with the cervical-thoracic boundary, the other expression associations we identify here may reflect more subtle axial regionalization and fusion zones worth exploring.

In general, the chicken axial column begins with 45 discrete vertebrae. During development, regions fuse to create single functional units, thus also reducing the number of axial segments. Graphing this reduction shows a steady trend in reduction from stage 33 through

to hatchling, with one additional vertebral fusion into the posterior lumbosacrals posthatching (Figure 2.9). The final adult axial segment number is only 24, as a result of the extensive fusions in the notarium, synsacrum, and pygostyle.

The developmental pattern of reducing the number of vertebral segments from 45 to 23 in the chicken is partially mirrored in early Avialae evolution. *Archaeopteryx* has a completely unfused vertebral column, with the exception of a fused sacrum of only five vertebrae, for a total of 46 segments (Elzanowski, 2002). *Jeholornis* is similar with 49, with a few more caudal vertebrae (Zhou & Zhang, 2003). The non-avialian paravian, *Microraptor*, has a total of 50 segments due to a slightly shortened tail (Hwang et al., 2002; Pei et al., 2014; Xu et al., 2003). However, with the origin of *Sapeornis* and the clade Pygostylia, birds with shortened tails and a pygostyle, the segment count drops dramatically to only 31 in *Sapeornis,* 28 in *Confuciusornis* (Chiappe et al. 1999, Zhou & Zhang, 2003), 29 in Protopteryx, 22 Longipteryx, 28, Parapengornis, 28, Orienantius, 28 Piscivoravis (Hu et al., 2015; Liu et al., 2019; Zhang & Zhou, 2000; Zhang & Zhou, 2001; Zhou et al., 2014). There are no evolutionary intermediates, suggesting a rapid evolution to this reduced state (Rashid et al. 2014). Only two additional vertebrae fuse into the sacrum of these non-neornithine birds that otherwise lack other regions of axial fusion.

Ornithurae actually increase their axial segments. The basal ornithuran Apsaravis has at least 12 cervicals and 7 thoracic vertebrae (Clarke & Norell, 2002). In addition to 10 synsacrals and five free caudals and a pygostyle, the axial segment count for Apsaravis is at least 26. *Baptornis* may have had 23 to 25 free presacral vertebrae, 10 vertebrae within the synsacrum, 5 free caudals and a pygostyle for a total of at least 30 free vertebral segments (Martin & Tate, 1976). *Hesperornis* also had 23 presacral vertebrae, with 14 vertebrae fused within the

synsacrum, and 12 vertebrae in the tail with the last 3 or 4 fused into a pygostyle, leading to at least 33 individual vertebral units (Marsh, 1880). Both these hesperornithiformes had 16 cervicals suggesting a trend in cervical expansion in Ornithurae. Complete counts of vertebrae for *Ichthyornis* are unknown, however it is estimated to have about 21 to 23 free presacral vertebrae, 10 fused vertebrae comprising the synsacrum, 5 free caudals, and a pygostyle for a total of 28 to 30 free vertebral segments (Clarke, 2004). Within Aves, notaria evolve independently at least 17 different times, occuring in Tinamiformes, Pelecaniformes, Threskiornithidae, Galliformes, Columbiformes, and most Falconidae (Storer, 1982) and at least 12 independent times in oscine passerines (James, 2009). The presence of a notarium brings the total vertebral unit count back down to 24 in the chicken, in spite of it having 14 cervical vertebrae.

Mapped phylogenetically, the evolution of vertebral units drops dramatically at Pygostylia with the origin of a pygostyle and extensive synsacrum (Figure 2.9). This number increases at Ornithurae with the advent of higher cervical counts before reducing again in many Aves with the origin of notaria. The developmental and phylogenetic trends in axial element reduction appear to generally parallel one other. In both cases, the expanded synsacrum and pygostyle appear first. Although both evolved together at Pygostylia, the expanded synsacrum leads in chicken development. Fusions are followed by the posterior expansion of the synsacrum, and finally the notarium. The bipartite fusion of the synsacrum in the chicken, with seven anterior synsacrals fusing first may reflect a homology with the seven synsacrals of non-ornithurine pygostylians. The addition of one synsacral anteriorly and seven posteriorly may represent yet unknown transitions in early Ornithurae evolution.

Conclusion

The avian axial column is of particular interest due to its evolutionary history. The transition from non-avialian theropods to highly derived birds is accompanied with the loss of an elongate tail, fusion of posterior caudals into a pygostyle, a broadly fused synsacra, and, sometimes, notaria. These fusions all appear independent from each other during the ontogeny of chicken. Moreover, they do not cross particular regional boundaries, such as the cervical-thoracic, thoracic-lumbosacral, and lumbosacral-caudal boundaries. Higher resolution of axial development was explored by creating a matrix of relative chondrification and ossification of discrete anatomical characters of each vertebrae. This method revealed more complex patterns of axial regionalization. For example, an additional sub-region is identified within the lumbosacral region, between the 7th and 8th lumbosacral that will be worthy of follow-up comparisons. The initial fusion of seven synsacrals may have homology to the seven fused synsacrals present in many non-ornithuran pygostylians of the Cretaceous. Some Hox axial expression patterns are correlated with the developmental regionalization identified here, such as regions of advanced and delayed chondrification and vertebral fusions. These patterns to not follow the coarse axial regionalizations examined in the past and are worthy of future investigations.

Figures

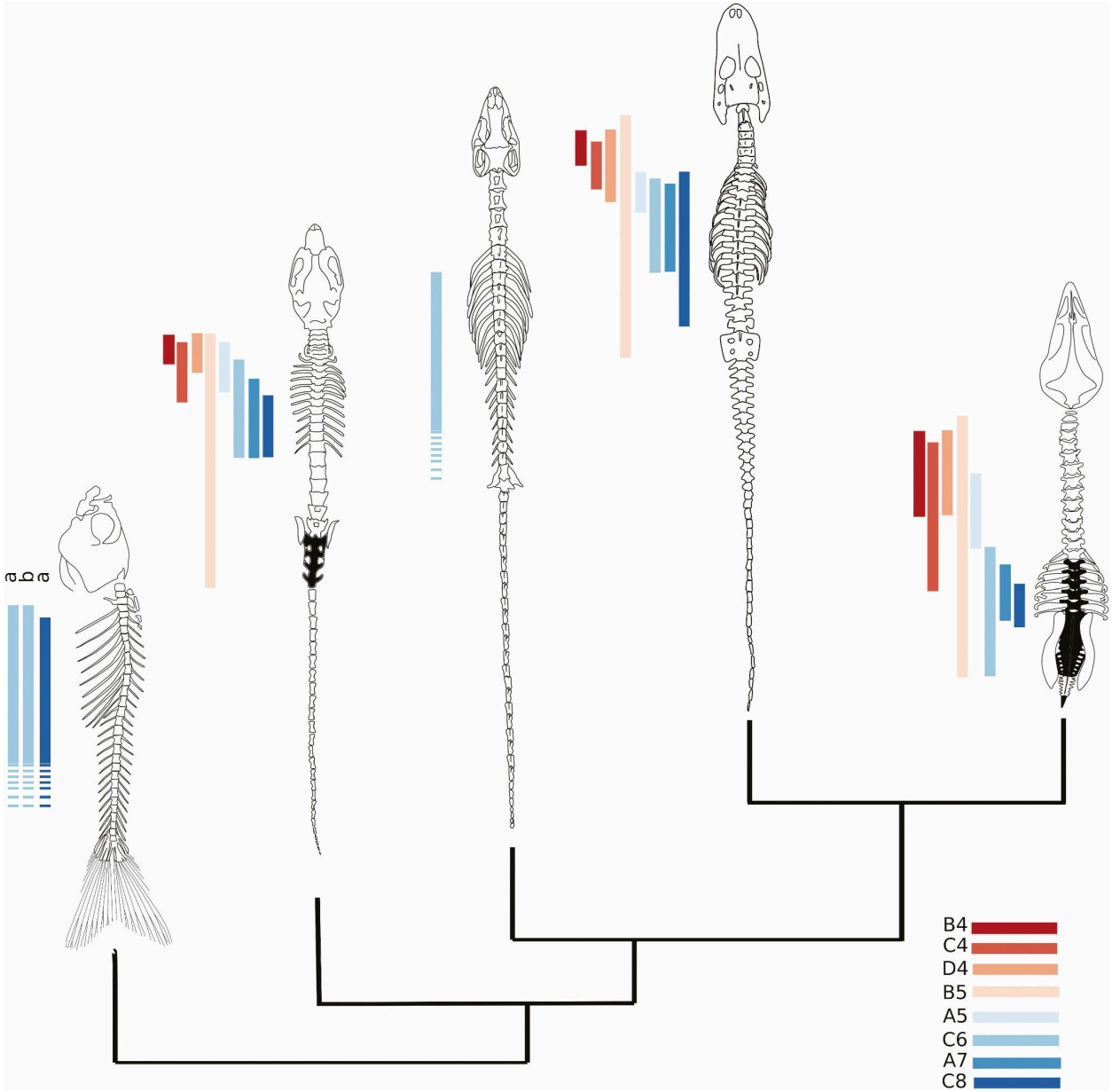

Figure 2.1. Simplified vertebrate phylogeny with selected published Hox expression boundaries within the somitic mesoderm. Axial skeletons are drawn in dorsal view, except for zebrafish drawn in left lateral view. Anterior-posterior Hox expression boundaries are represented by

colored bars. Fusions within the axial column are represented by black shading. Zebrafish expression patterns are reported by Morin-Kensicki et al. (2002), whiptail lizard by Woltering et al. (2009), alligator by Mansfield & Abzhanov (2010), in and chicken and mouse by Burke et al. (1995).

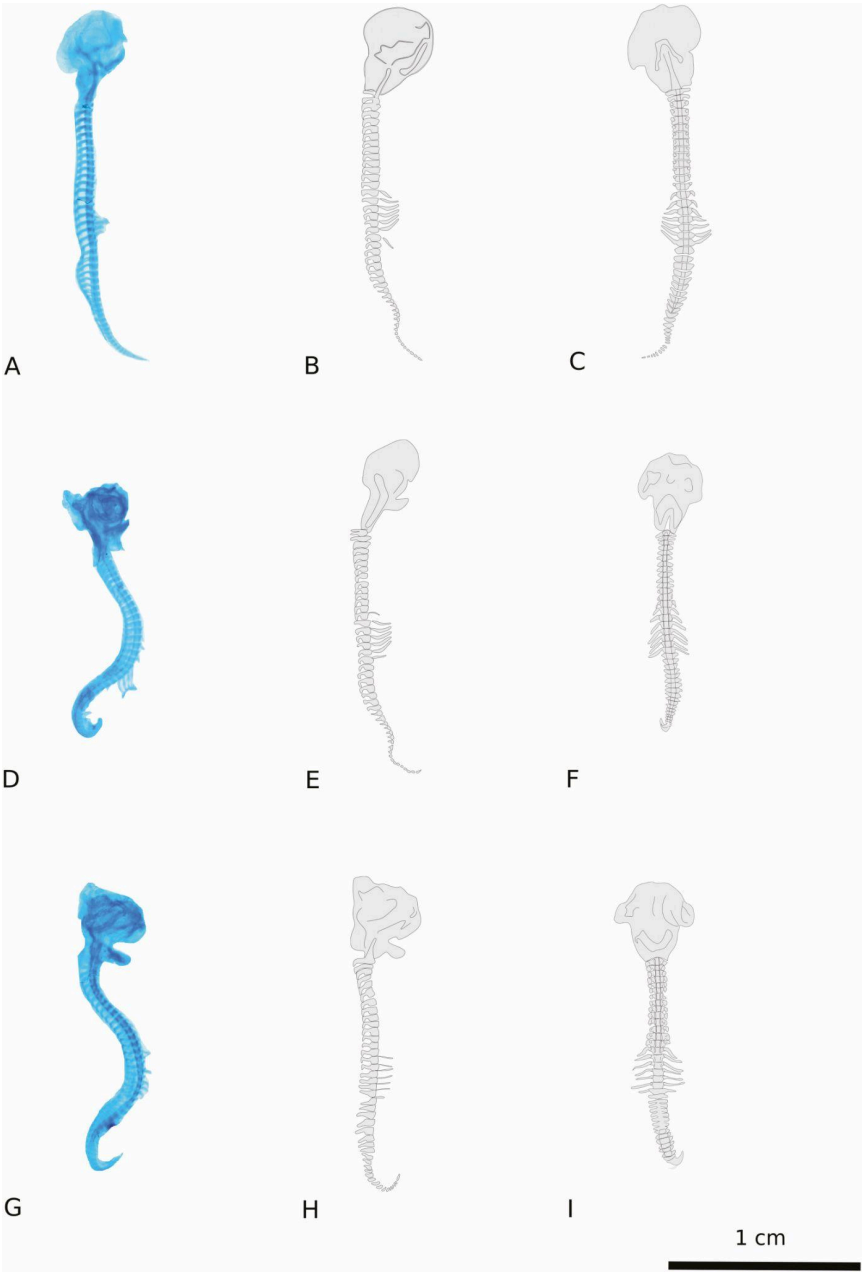

Figure 2.2. Images and associated schematic diagrams of cleared and stained axial skeletons of chicken (*Gallus gallus domesticus*) embryos from developmental stages 28 to 30. A, stage 28 (day 5 ½ of incubation) right lateral view; B, stage 28 right lateral schematic; C, stage 28 posterior schematic; D, stage 29 (day 6 of incubation) right lateral view; E, stage 29 right lateral

schematic; F, stage 29 posterior schematic; G, stage 30 (day 6 ½ of incubation) right lateral view; H, stage 30 right lateral schematic; I, stage 30 posterior schematic. Blue is cartilage and dark purple represents ossified tissue within the images. Light gray is cartilage and black represents ossified tissue within the diagrams. Scale bar, 1 cm.

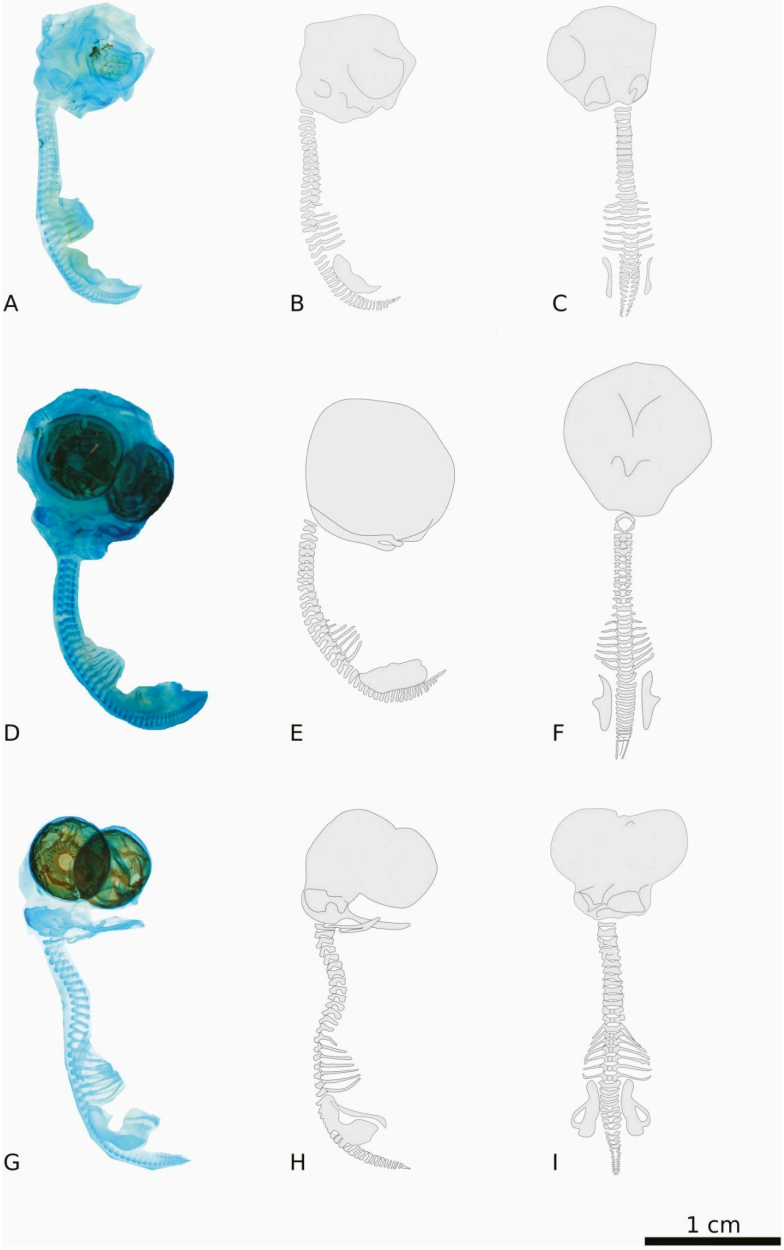

Figure 2.3. Images and associated schematic diagrams of cleared and stained axial skeletons of chicken (*Gallus gallus domesticus*) embryos from developmental stages 31 to 33. A, stage 31 (day 7 of incubation) right lateral view; B, stage 31 right lateral schematic; C, stage 31 posterior schematic; D, stage 32 (day 7 ½ of incubation) right lateral view; E, stage 32 right lateral

schematic; F, stage 32 posterior schematic; G, stage 33 (day 7 ½ - 8 of incubation) right lateral view; H, stage 33 right lateral schematic; I, stage 33 posterior schematic. Blue is cartilage and dark purple represents ossified tissue within the images. Light gray is cartilage and black represents ossified tissue in the diagrams. Scale bar, 1 cm.

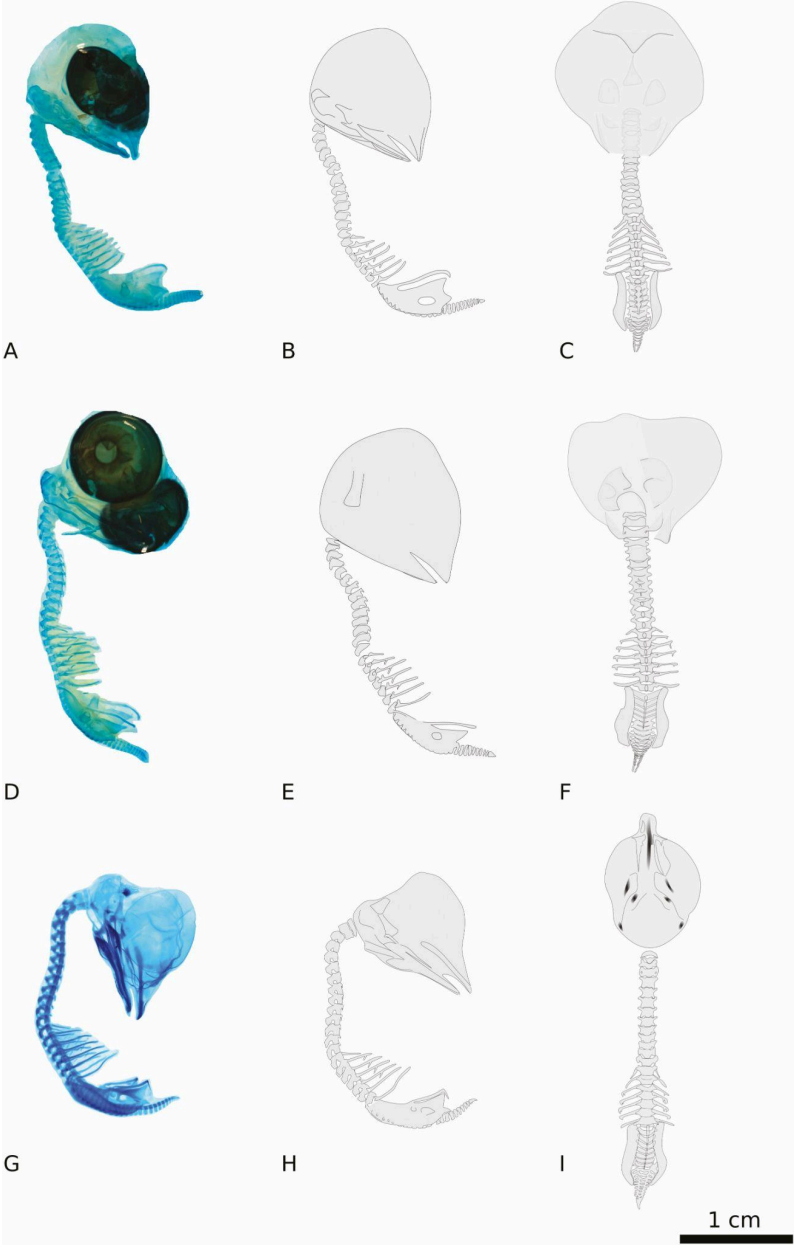

Figure 2.4. Images and associated schematic diagrams of cleared and stained axial skeletons of chicken (*Gallus gallus domesticus*) embryos from developmental stages 34 to 36. A, stage 34 (day 8 of incubation) right lateral view; B, stage 34 right lateral schematic; C, stage 34 posterior schematic; D, stage 35 (day 8-9 of incubation) right lateral view; E, stage 35 right lateral

schematic; F, stage 35 posterior schematic; G, stage 36 (day 10 of incubation) right lateral view; H, stage 35 right lateral schematic; I, stage 35 posterior schematic. Blue is cartilage and dark purple represents ossified tissue within the images. Light gray is cartilage and black represents ossified tissue in the diagrams. Scale bar, 1 cm.

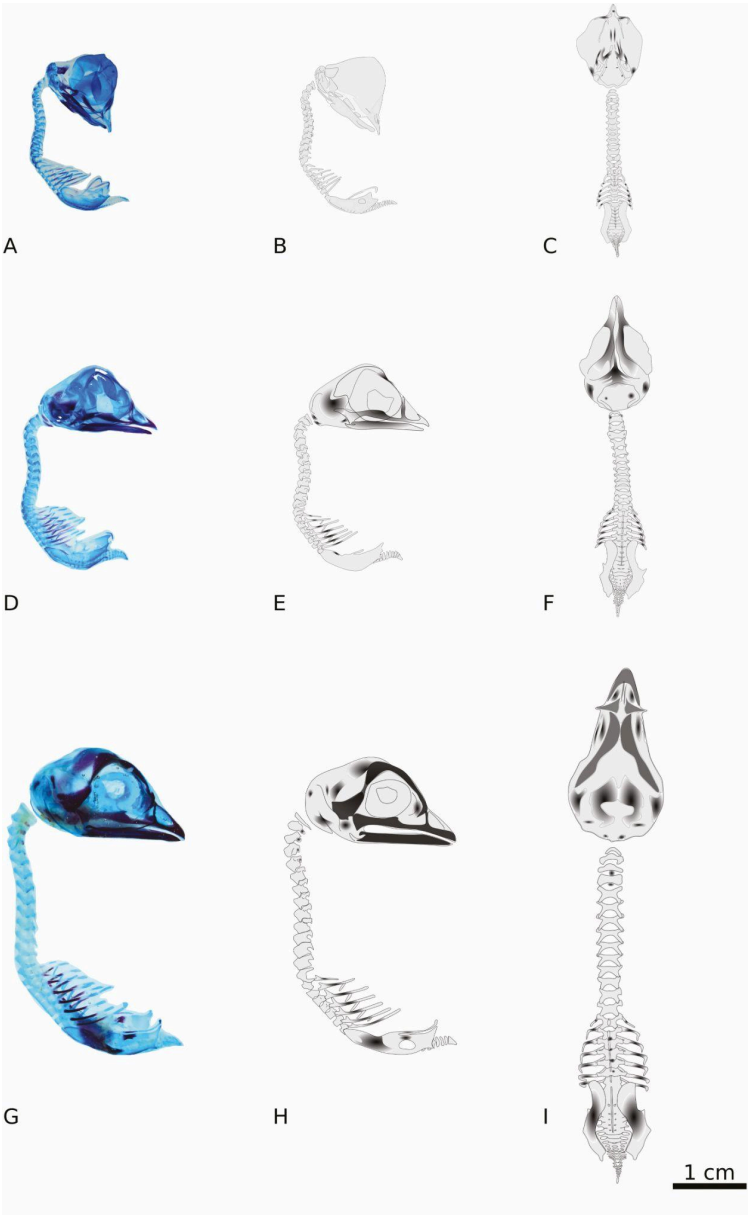

Figure 2.5. Images and associated schematic diagrams of cleared and stained axial skeletons of chicken (*Gallus gallus domesticus*) embryos from developmental stages 37 to 39. A, stage 37 (day 11 of incubation) right lateral view; B, stage 37 right lateral schematic; C, stage 37 posterior schematic; D, stage 38 (day 12 of incubation) right lateral view; E, stage 38 right lateral

schematic; F, stage 38 posterior schematic; G, stage 39 (day 13 of incubation) right lateral view; H, stage 39 right lateral schematic; I, stage 39 posterior schematic. Blue is cartilage and dark purple represents ossified tissue. Light gray is cartilage and black represents ossified tissue in the diagrams. Scale bar, 1 cm.

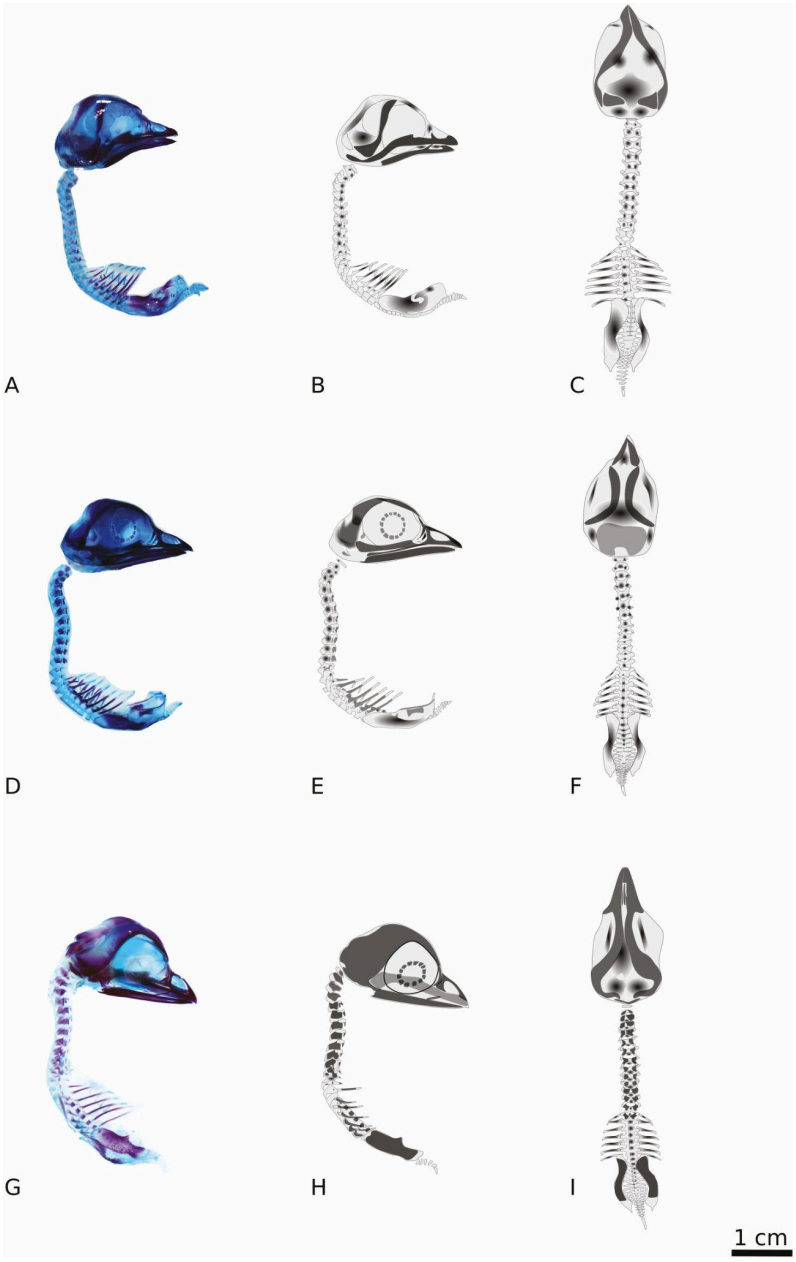

Figure 2.6. Images and associated schematic diagrams of cleared and stained axial skeletons of chicken (*Gallus gallus domesticus*) embryos from developmental stages 40 to 42. A, stage 40 (day 14 of incubation) right lateral view; B, stage 40 right lateral schematic; C, stage 40 posterior schematic; D, stage 41 (day 15 of incubation) right lateral view; E, stage 41 right lateral

schematic; F, stage 41 posterior schematic; G, stage 42 (day 16 of incubation) right lateral view; H, stage 42 right lateral schematic; I, stage 42 posterior schematic. Blue is cartilage and dark purple represents ossified tissue. Light gray is cartilage and black represents ossified tissue in the diagrams. Scale bar, 1 cm.

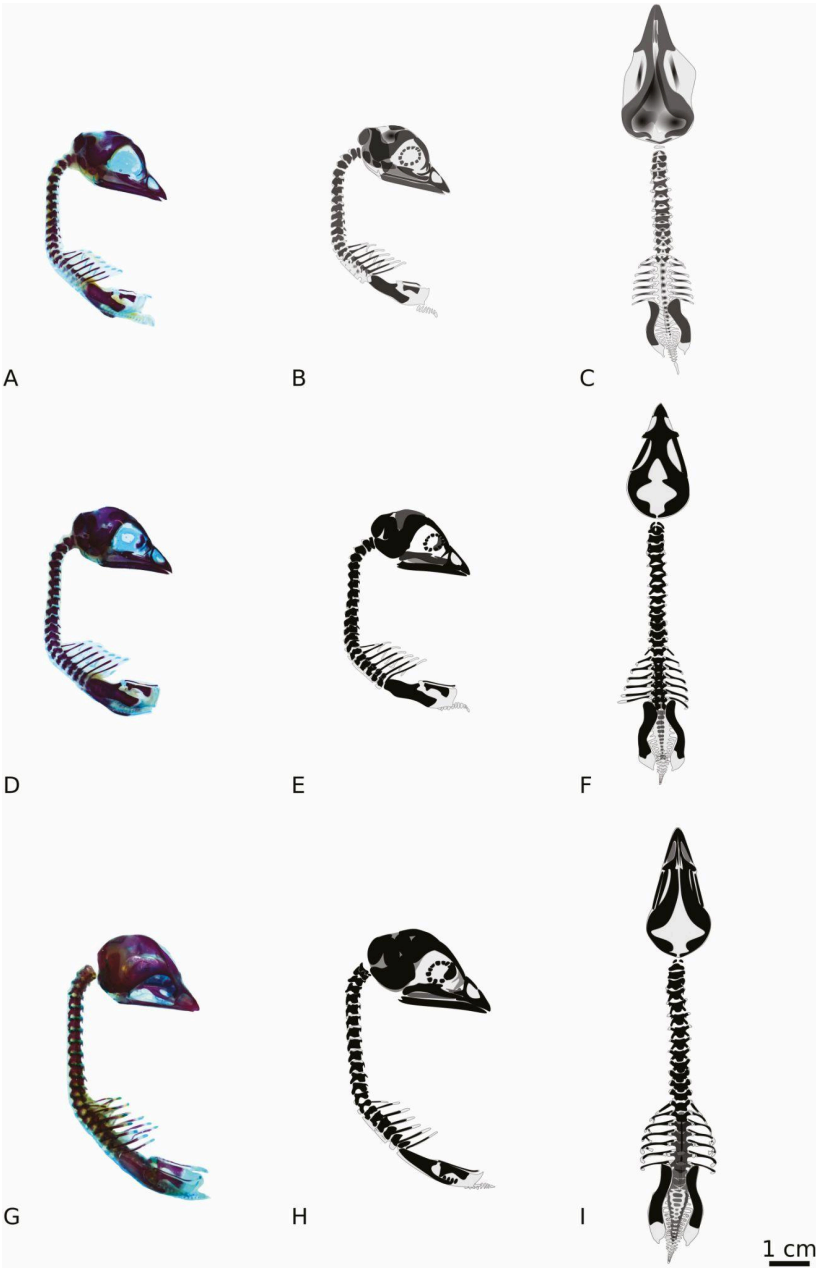

Figure 2.7. Images and associated schematic diagrams of cleared and stained axial skeletons of chicken (*Gallus gallus domesticus*) embryos from developmental stages 43 to 45. A, stage 43 (day 17 of incubation) right lateral view; B, stage 43 right lateral schematic; C, stage 43 posterior schematic; D, stage 44 (day 18 of incubation) right lateral view; E, stage 44 right lateral

schematic; F, stage 44 posterior schematic; G, stage 45 (day 19-20 of incubation) right lateral view; H, stage 45 right lateral schematic; I, stage 45 posterior schematic. Blue is cartilage and dark purple represents ossified tissue. Light gray is cartilage and black represents ossified tissue in the diagrams. Scale bar, 1 cm.

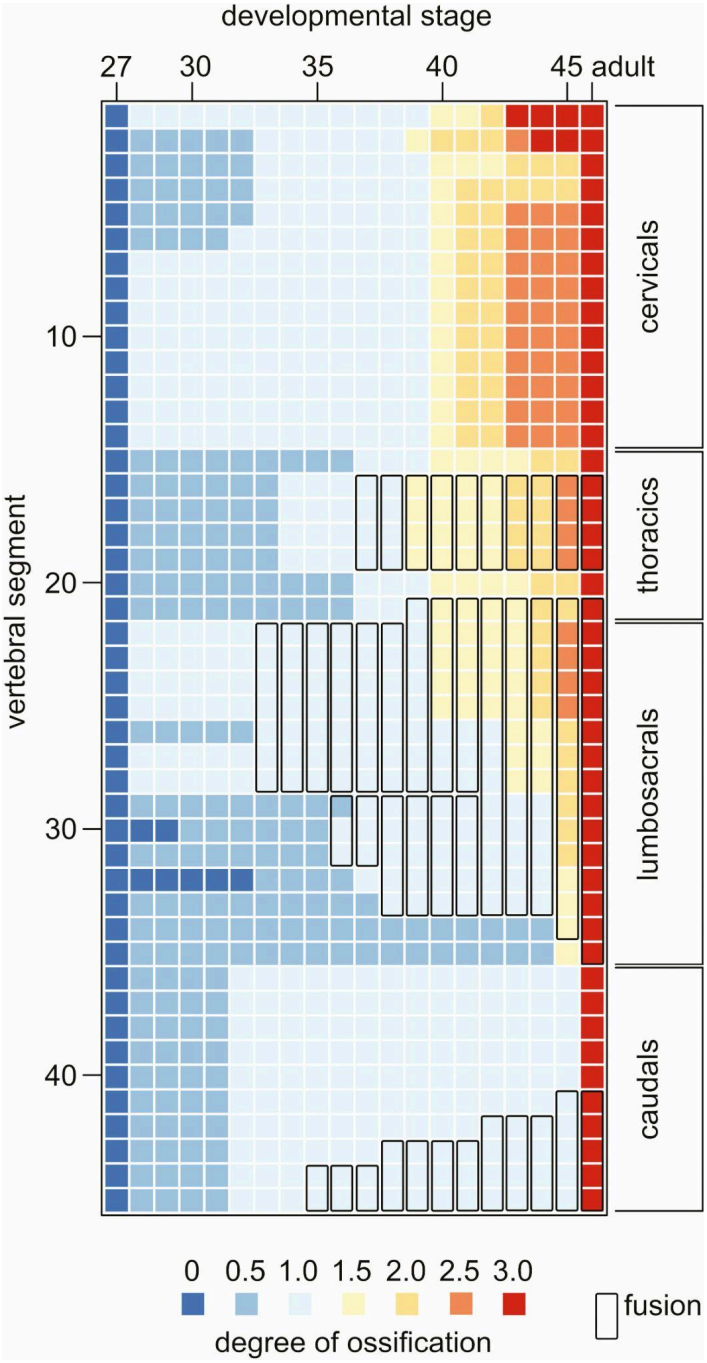

Figure 2.8. Schematic of ossification and fusion sequence of the developing chicken axial column. Shading indicates degree of ossification of all scored anatomies within each vertebral segment, given in Supplementary Table 1. Fusions between adjacent vertebrae are indicated with black outlines. Note that the lumbosacrals begin fusions from two regions that remain separate until stage 42.

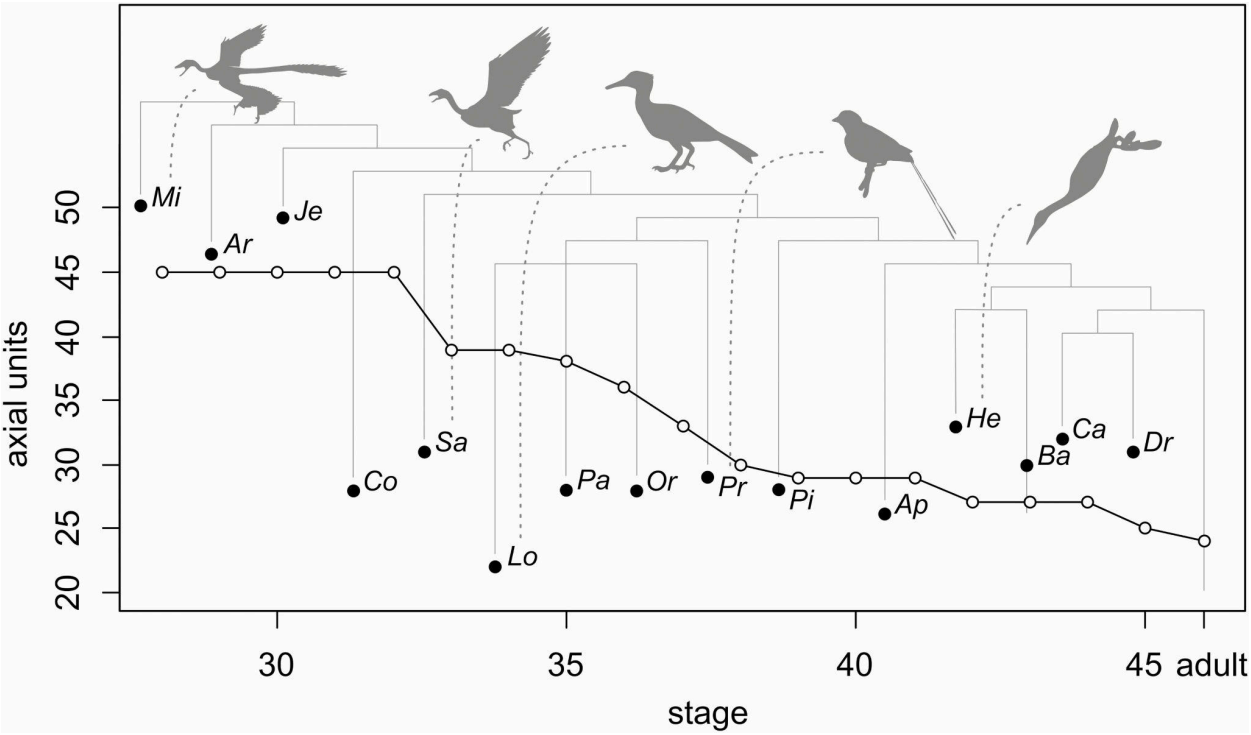

Figure 2.9. Plot of the number of vertebral units throughout chicken development and avialan evolution. As individual vertebrae fuse throughout ontogeny, the number of segments within the axial columns decreases. Starting with 45 individual segments at stage 28, adult chickens have a total of only 23 segments. Avialan evolution is plotted as a phylogeny with representative taxa plotted with their respective vertebral units. Included taxa are *Mi*, *Microraptor*; *Ar*, *Archeopteryx*; *Je*, *Jeholornis*; *Confuciusornis, Co; Sa*, *Sapeornis*; *Lo*, *Longipteryx*; *Pa*, *Parapengornis*; *Or*, *Orienantius*; *Pr*, *Protopteryx*; *Pi*, *Piscivoravis*; *Ap*, *Apsaravis*; *He*, *Hesperornis*; *Ba*. *Baptornis*; *Ca*, *Calciavis*; *Dr*, *Dromaius*. Silhouettes for *Microraptor* and *Archaeopteryx* are from Dececchi and Larsson (2013), *Piscivoravis* from phylopic.org, and *Longipteryx* and *Hesperornis* are new.

References

Abitbol MM. 1987. Evolution of the sacrum in hominoids. *American Journal of Physical Anthropology* 74: 65–81.

Arenas-Rodríguez A, Vargas JFR, Hoyos JM. 2018. Comparative description and ossification patterns of *Dendropsophus labialis* (Peters, 1863) and *Scinax ruber* (Laurenti, 1758) (Anura: Hylidae). *PeerJ* 6: e4525.

Bellairs ADA, Kamal, AM. 1981. The chondrocranium and the development of the skull in recent reptiles. *Biology of the Reptilia* 11:1-263.

Bergmann PJ, Irschick DJ. 2012. Vertebral evolution and the diversification of squamate reptiles. *Evolution* 66: 1044–1058.

Böhmer C, Rauhut OW, Wörheide G. 2015. New insights into the vertebral Hox code of archosaurs. *Evolution & development*. 17: 258-269.

Böhmer C, Rauhut OW, Wörheide G. 2015. Correlation between Hox code and vertebral morphology in archosaurs. *Proceedings of the Royal Society B: Biological Sciences*. 282: 20150077.

Bolker JA. 2000. Modularity in development and why it matters to evo-devo. *American Zoologist* 40: 770-776.

Buchholtz EA. 2007. Modular evolution of the cetacean vertebral column. *Evolution & Development* 9: 278-289.

Burke AC, Nelson CE, Morgan BA, Tabin C. 1995. Hox genes and the evolution of vertebrate axial morphology. *Development* 121: 333–346.

Chiappe LM, Ji SA, Ji Q, & Norell MA. 1999. Anatomy and systematics of the Confuciusornithidae (Theropoda, Aves) from the late Mesozoic of northeastern China. *Bulletin of the American Museum of Natural History*: no. 242.

Christ B, Huang R, Wilting J. 2000. The development of the avian vertebral column. *Anatomy and Embryology* 202: 179–194.

Christ B, Wilting J. 1992. From somites to vertebral column. *Annals of Anatomy – Anatomischer Anzeiger* 174: 23–32.

Clarke JA. 2004. Morphology, phylogenetic taxonomy, and systematics of *Ichthyornis* and *Apatornis* (Avialae: Ornithurae). *Bulletin of the American Museum of Natural history* 286: 1-179.

Clarke JA, Norell MA. 2002. The morphology and phylogenetic position of *Apsaravis ukhaana* from the Late Cretaceous of Mongolia. *American Museum Novitates* 3387: 1–47.

Cohn MJ, Tickle C. 1999. Developmental basis of limblessness and axial patterning in snakes. *Nature* 399: 474.

Dececchi TA, Larsson HCE. 2013. Body and limb size dissociation at the origin of birds: Uncoupling allometric constraints across a macroevolutionary transition. *Evolution* 67: 2741–2752.

Deraniyagala PEP. 1939. *The Tetrapod Reptiles of Ceylon: Volume 1 Testudinates and Crocodilians.* Colombo: Ceylon Government Press.

Dingerkus G, Uhler LD. 1977. Enzyme clearing of alcian blue stained whole small vertebrates for demonstration of cartilage. *Stain Technology* 52: 229-232.

Economides KD, Zeltser L, Capecchi MR. 2003. Hoxb13 mutations cause overgrowth of caudal spinal cord and tail vertebrae. *Developmental Biology* 256: 317-330.

Elzanowski AN. 2002. Archaeopterygidae (Upper Jurassic of Germany). In: Chiappe L, Witer L eds. *Mesozoic birds: above the heads of dinosaurs*. Berkeley: University of California Press, 129-159.

Fisher S, Halpern ME. 1999. Patterning the zebrafish axial skeleton requires early chordin function. *Nature Genetics* 23:442.

Hamburger V, Hamilton HL. 1992. A series of normal stages in the development of the chick embryo. *Developmental Dynamics* 195: 231–272.

Hildebrand MG, Goslow. 2001. Analysis of Vertebrate Structure. Wiley, New York.

Hwang SH, Norell MA, Qiang JI, Keqin GAO. 2002. New specimens of *Microraptor zhaoianus* (Theropoda: Dromaeosauridae) from northeastern China. *American Museum Novitates* 3381:1-44.

James HF. 2009. Repeated evolution of fused thoracic vertebrae in songbirds. *The Auk* 126: 862-872.

Johnson SE, Shapiro LF. 1998. Positional behavior and vertebral morphology in atelines and cebines. *American Journal of Physical Anthropology* 105: 333-354.

Kessel M, Gruss P. 1991. Homeotic transformations of murine vertebrae and concomitant alteration of Hox codes induced by retinoic acid. *Cell* 67: 89-104.

Kumar P, Singh G. 2014. Gross anatomy of axial skeleton in Emu (*Dromaius novaehollandiae*). *Indian Journal of Veterinary Anatomy* 26: 87-91.

Hautier L, Charles C, Asher RJ, Gaunt SJ. 2014. Ossification sequence and genetic patterning in the mouse axial skeleton. *Journal of Experimental Zoology Part B: Molecular and Developmental Evolution*. 322: 631-642.

Hu H, O'Connor JK, Zhou Z. 2015. A new species of Pengornithidae (Aves: Enantiornithes) from the Lower Cretaceous of China suggests a specialized scansorial habitat previously unknown in early birds. *PLoS One* 10: e0126791.

Liu D, Chiappe LM, Zhang Y, Serrano FJ, Meng Q. 2019. Soft tissue preservation in two new enantiornithine specimens (Aves) from the Lower Cretaceous Huajiying Formation of Hebei Province, China. *Cretaceous Research* 95: 191-207.

Mackie E, Ahmed YA, Tatarczuch L, Chen KS, Mirams M. 2008. Endochondral ossification: how cartilage is converted into bone in the developing skeleton. *The International Journal of Biochemistry & Cell Biology* 40: 46-62.

Maisano JA. 2002. The potential utility of postnatal skeletal developmental patterns in squamate phylogenetics. *Zoological Journal of the Linnean Society* 136: 277–313.

Mansfield JH, Abzhanov A. 2010. Hox expression in the American alligator and evolution of archosaurian axial patterning. *Journal of Experimental Zoology Part B: Molecular and Developmental Evolution* 314: 629-644.

Marsh OC. 1880. Odontornithes: a monograph on the extinct toothed birds of North America (Vol. 1). *Memoirs of the Peabody Museum of Natural History:* 1-201.

Martin LD, Tate J. 1976. The skeleton of *Baptornis advenus* (Aves: Hesperornithiformes). *Smithsonian Contributions to Paleobiology* 27: 35-66.

Maxwell EE. 2008. Ossification sequence of the avian order anseriformes, with comparison to other precocial birds. *Journal of Morphology* 269: 1095–1113.

Maxwell EE. 2009. Comparative ossification and development of the skull in palaeognathous birds (Aves: Palaeognathae). *Zoological Journal of the Linnean Society* 156: 184–200.

Morin-Kensicki EM, Melancon E, Eisen JS. 2002. Segmental relationship between somites and vertebral column in zebrafish. *Development* 129: 3851-3860.

Mulder EW. 2001. Co-ossified vertebrae of mosasaurs and cetaceans: implications for the mode of locomotion of extinct marine reptiles. *Paleobiology* 27: 724-734.

Müller F. 1967. On the embryonal development of the head in *Crocodylus cataphractus* CUV. *Revue Suisse de Zoologie; Annales de la Societe Zoologique Suisse et du Museum d'Histoire Naturelle de Geneve* 74: 189–294.

Nakamura Y, Nakane Y, Tsudzuki M. 2019. Skeletal development in blue‐breasted quail embryos. *Animal Science Journal* 90: 353-365.

Nesbitt SJ, Clarke JA. 2016. The anatomy and taxonomy of the exquisitely preserved Green River formation (early Eocene) Lithornithids (Aves) and the relationships of Lithornithidae. *Bulletin of the American Museum of Natural History* 406: 1-91.

Ohya YK, Kuraku S, Kuratani S. 2005. Hox code in embryos of Chinese soft‐shelled turtle *Pelodiscus sinensis* correlates with the evolutionary innovation in the turtle. *Journal of Experimental Zoology Part B: Molecular and Developmental Evolution*. 304: 107-118.

Pei R, Li Q, Meng Q, Gao KQ, Norell MA. 2014. A new specimen of *Microraptor* (Theropoda: Dromaeosauridae) from the Lower Cretaceous of western Liaoning, China. *American Museum Novitates* 3821: 1-28.

Persons WS, Currie PJ, Norell MA. 2013. Oviraptorosaur tail forms and functions. *Acta Palaeontologica Polonica* 59: 553-568.

Polly PD, Head JJ, Cohn MJ. 2001. Testing modularity and dissociation: the evolution of regional proportions in snakes. In: Zelditch ML ed. *Beyond heterochrony: the evolution of development*. New York: John Wiley and Sons, 307-335.

Prochel J. 2006. Early Skeletal Development in *Talpa europaea*, the Common European Mole. *Zoological Science* 23: 427–434.

Raff RA. 1996). *The Shape of Life: Genes, Development, and the Evolution of Animal Form*. Chicago: University of Chicago Press

Randau M, Goswami, A. 2017. Morphological modularity in the vertebral column of Felidae (Mammalia, Carnivora). *BMC Evolutionary Biology* 17:133.

Rashid DJ, Chapman SC, Larsson HC, Organ CL, Bebin AG, Merzdorf CS, Bradley R, Horner JR. 2014. From dinosaurs to birds: a tail of evolution. *EvoDevo* 5: 25.

Rieppel O. 1993. Studies on skeleton formation in reptiles. v. Patterns of ossification in the skeleton of *Alligator mississippiensis* DAUDIN (Reptilia, Crocodylia). *Zoological Journal of the Linnean Society* 109: 301–325.

Sánchez‐Villagra MR. 2002. Comparative patterns of postcranial ontogeny in therian Mammals: An analysis of relative timing of ossification events. *Journal of Experimental Zoology* 294: 264–273.

Sánchez‐Villagra MR, Goswami A, Weisbecker V, Mock O, Kuratani S. 2008. Conserved relative timing of cranial ossification patterns in early mammalian evolution. *Evolution & Development* 10: 519–530.

Scheyer TM, Hutchinson JR, Strauss O, Delfino M, Carrillo-Briceño JD, Sánchez R, Sánchez-Villagra MR. 2019. Giant extinct caiman breaks constraint on the axial skeleton of extant crocodylians. *eLife*. 8.

Schultze HP, Arratia G. 1988. Reevaluation of the caudal skeleton of some actinopterygian fishes: II. *Hiodon*, *Elops*, and *Albula*. *Journal of Morphology* 195: 257–303.

Shapiro F. 1992. Vertebral development of the chick embryo during days 3–19 of incubation. *Journal of Morphology* 213: 317-333.

Storer RW. 1982. Fused thoracic vertebrae in birds. *Journal of the Yamashina Institute for Ornithology* 14: 86-95.

VanBuren CS, Evans DC. 2017. Evolution and function of anterior cervical vertebral fusion in tetrapods. *Biological Reviews* 92: 608–626.

Verbout AJ. 1985. The development of the vertebral column. *Advances in Anatomy, Embryology, and Cell Biology* 90: 1–122.

Wallin J, Wilting J, Koseki H, Fritsch R, Christ B, Balling R. 1994. The role of Pax-1 in axial skeleton development. *Development* 120: 1109–1121.

Ward AB, Brainerd EL. 2007. Evolution of axial patterning in elongate fishes. *Biological Journal of the Linnean Society* 90: 97–116.

Ward AB, Mehta RS. 2014. Differential occupation of axial morphospace. *Zoology* 117: 70-76.

Woltering JM. 2012. From lizard to snake; behind the evolution of an extreme body plan. *Current Genomics* 13: 289-299.

Xu X, Zhou Z, Wang X, Kuang X, Zhang F, Du X. 2003. Four-winged dinosaurs from China. *Nature* 6921: 335-340.

Zhang F, Zhou Z. 2000. A primitive enantiornithine bird and the origin of feathers. *Science* 290: 1955-1959.

Zhang F, Zhou Z, Hou L, Gu, G. 2001. Early diversification of birds: evidence from a new opposite bird. *Chinese Science Bulletin* 46: 945-949.

Zhou Z, Zhang F. 2003. *Jeholornis* compared to *Archaeopteryx*, with a new understanding of the earliest avian evolution. *Naturwissenschaften* 90: 220-225.

Zhou Z, Zhang F. 2003. Anatomy of the primitive bird *Sapeornis chaoyangensis* from the Early Cretaceous of Liaoning, China. *Canadian Journal of Earth Sciences* 40: 731-747.

Zhou S, Zhou Z, O'Connor J. 2014. A new piscivorous ornithuromorph from the Jehol Biota. *Historical Biology* 26: 608-618.

Appendix A

Table A1. Ossification sequence of *Gallus gallus* axial column elements. Numbers 0 to 3 represent the degree of ossification. * represents an element that is fused to its posterior articulation.

	Stage																		
Element	**27**	**28**	**29**	**30**	**31**	**32**	**33**	**34**	**35**	**36**	**37**	**38**	**39**	**40**	**41**	**42**	**43**	**44**	**45**
Atlas																			
arcus dorsalis	0	1	1	1	1	1	1	1	1	1	1	1	1	1	1	1	3	3	3
arcus ventralis	0	1	1	1	1	1	1	1	1	1	1	1	1	2	2	3	3	3	3
Axis																			
corpus vertebrae	0	1	1	1	1	1	1	1	1	1	1	1	3	3	3	3	3	3	3
p. spinosus	0	1	1	1	1	1	1	1	1	1	1	1	1	1	1	1	2	3	3
c. ventralis	0	0	0	0	0	0	1	1	1	1	1	1	1	2	3	3	3	3	3
Cervical 3																			
corpus vertebrae	0	1	1	1	1	1	1	1	1	1	1	1	3	3	3	3	3	3	3
p. spinosus	0	1	1	1	1	1	1	1	1	1	1	1	1	1	1	1	2	3	3
p. transversus	0	1	1	1	1	1	1	1	1	1	1	1	1	2	3	3	3	3	3
foramen accessorium	0	0	0	0	0	0	1	1	1	1	1	1	1	1	1	1	1	1	1
p. costarius	0	0	0	0	0	0	1	1	1	1	1	1	1	2	3	3	3	3	3
p. articularis cranialis	0	1	1	1	1	1	1	1	1	1	1	1	1	1	1	1	2	2	2
p. articularis caudalis	0	1	1	1	1	1	1	1	1	1	1	1	1	1	1	1	2	2	2

Cervical 4

corpus vertebrae	0	1	1	1	1	1	1	1	1	1	1	1	3	3	3	3	3	3	3
p. spinosus	0	1	1	1	1	1	1	1	1	1	1	1	1	1	1	1	2	3	3
p. transversus	0	1	1	1	1	1	1	1	1	1	1	1	1	2	2	3	3	3	3
foramen accessorium	0	0	0	0	0	0	1	1	1	1	1	1	1	1	1	1	1	1	1
p. costarius	0	0	0	0	0	0	1	1	1	1	1	1	1	2	3	3	3	3	3
p. articularis cranialis	0	1	1	1	1	1	1	1	1	1	1	1	1	1	2	2	2	2	2
p. articularis caudalis	0	1	1	1	1	1	1	1	1	1	1	1	1	1	2	2	2	2	2

Cervical 5

corpus vertebrae	0	1	1	1	1	1	1	1	1	1	1	1	1	2	3	3	3	3	3
p. spinosus	0	1	1	1	1	1	1	1	1	1	1	1	1	1	1	1	3	3	3
p. transversus	0	1	1	1	1	1	1	1	1	1	1	1	1	2	3	3	3	3	3
p. costarius	0	0	0	0	0	0	1	1	1	1	1	1	1	2	3	3	3	3	3
p. articularis cranialis	0	1	1	1	1	1	1	1	1	1	1	1	1	1	2	2	2	2	2
p. articularis caudalis	0	1	1	1	1	1	1	1	1	1	1	1	1	1	2	2	2	2	2

Cervical 6

corpus vertebrae	0	1	1	1	1	1	1	1	1	1	1	1	1	2	3	3	3	3	3
p. spinosus	0	1	1	1	1	1	1	1	1	1	1	1	1	1	1	1	3	3	3
p. transversus	0	1	1	1	1	1	1	1	1	1	1	1	1	2	3	3	3	3	3

p. costarius	0	0	0	0	0	1	1	1	1	1	1	1	1	2	3	3	3	3	3
p. articularis cranialis	0	1	1	1	1	1	1	1	1	1	1	1	1	1	2	2	2	2	2
p. articularis caudalis	0	1	1	1	1	1	1	1	1	1	1	1	1	1	2	2	2	2	2

Cervical 7

corpus vertebrae	0	1	1	1	1	1	1	1	1	1	1	1	1	2	3	3	3	3	3
p. spinosus	0	1	1	1	1	1	1	1	1	1	1	1	1	1	1	1	3	3	3
p. transversus	0	1	1	1	1	1	1	1	1	1	1	1	1	2	3	3	3	3	3
p. costarius	0	1	1	1	1	1	1	1	1	1	1	1	1	2	3	3	3	3	3
p. articularis cranialis	0	1	1	1	1	1	1	1	1	1	1	1	1	1	2	2	2	2	2
p. articularis caudalis	0	1	1	1	1	1	1	1	1	1	1	1	1	1	2	2	2	2	2

Cervical 8

corpus vertebrae	0	1	1	1	1	1	1	1	1	1	1	1	1	2	3	3	3	3	3
p. spinosus	0	1	1	1	1	1	1	1	1	1	1	1	1	1	1	1	3	3	3
p. transversus	0	1	1	1	1	1	1	1	1	1	1	1	1	2	3	3	3	3	3
p. costarius	0	1	1	1	1	1	1	1	1	1	1	1	1	2	3	3	3	3	*2*
p. articularis cranialis	0	1	1	1	1	1	1	1	1	1	1	1	1	1	2	2	2	2	*2*
p. articularis caudalis	0	1	1	1	1	1	1	1	1	1	1	1	1	1	2	2	2	2	*2*

Cervical 9

corpus vertebrae	0	1	1	1	1	1	1	1	1	1	1	1	1	2	3	3	3	3	3
p. spinosus	0	1	1	1	1	1	1	1	1	1	1	1	1	1	1	1	3	3	3
p. transversus	0	1	1	1	1	1	1	1	1	1	1	1	1	2	3	3	3	3	3
p. costarius	0	1	1	1	1	1	1	1	1	1	1	1	1	2	3	3	3	3	3
p. articularis cranialis	0	1	1	1	1	1	1	1	1	1	1	1	1	1	2	2	2	2	2
p. articularis caudalis	0	1	1	1	1	1	1	1	1	1	1	1	1	1	2	2	2	2	2

Cervical 10

corpus vertebrae	0	1	1	1	1	1	1	1	1	1	1	1	1	2	3	3	3	3	3
p. spinosus	0	1	1	1	1	1	1	1	1	1	1	1	1	1	1	1	3	3	3
p. transversus	0	1	1	1	1	1	1	1	1	1	1	1	1	2	3	3	3	3	3
p. costarius	0	1	1	1	1	1	1	1	1	1	1	1	1	2	3	3	3	3	3
p. articularis cranialis	0	1	1	1	1	1	1	1	1	1	1	1	1	1	2	2	2	2	2
p. articularis caudalis	0	1	1	1	1	1	1	1	1	1	1	1	1	1	2	2	2	2	2

Cervical 11

corpus vertebrae	0	1	1	1	1	1	1	1	1	1	1	1	1	2	3	3	3	3	3
p. spinosus	0	1	1	1	1	1	1	1	1	1	1	1	1	1	1	1	2	3	3
p. transversus	0	1	1	1	1	1	1	1	1	1	1	1	1	2	3	3	3	3	3
p. costarius	0	1	1	1	1	1	1	1	1	1	1	1	1	2	3	3	3	3	3
p. articularis cranialis	0	1	1	1	1	1	1	1	1	1	1	1	1	1	2	2	2	2	2

p. articularis caudalis	0	1	1	1	1	1	1	1	1	1	1	1	1	2	2	2	2	2

Cervical 12

corpus vertebrae	0	1	1	1	1	1	1	1	1	1	1	1	1	2	3	3	3	3	3
p. spinosus	0	1	1	1	1	1	1	1	1	1	1	1	1	1	1	1	2	3	3
p. transversus	0	1	1	1	1	1	1	1	1	1	1	1	1	2	3	3	3	3	3
p. costarius	0	1	1	1	1	1	1	1	1	1	1	1	1	2	3	3	3	3	3
p. articularis cranialis	0	1	1	1	1	1	1	1	1	1	1	1	1	1	2	2	2	2	2
p. articularis caudalis	0	1	1	1	1	1	1	1	1	1	1	1	1	1	2	2	2	2	2

Cervical 13

corpus vertebrae	0	1	1	1	1	1	1	1	1	1	1	1	1	2	2	3	3	3	3
p. spinosus	0	1	1	1	1	1	1	1	1	1	1	1	1	1	1	1	2	3	3
p. transversus	0	1	1	1	1	1	1	1	1	1	1	1	1	2	2	3	3	3	3
p. costarius	0	1	1	1	1	1	1	1	1	1	1	1	1	2	3	3	3	3	3
p. articularis cranialis	0	1	1	1	1	1	1	1	1	1	1	1	1	1	2	2	2	2	2
p. articularis caudalis	0	1	1	1	1	1	1	1	1	1	1	1	1	1	2	2	2	2	2

Cervical 14

corpus vertebrae	0	1	1	1	1	1	1	1	1	1	1	1	1	2	2	3	3	3	3
p. spinosus	0	1	1	1	1	1	1	1	1	1	1	1	1	1	1	1	2	3	3
p. transversus	0	1	1	1	1	1	1	1	1	1	1	1	1	2	2	3	3	3	3

p. costarius	0	1	1	1	1	1	1	1	1	1	1	1	1	2	3	3	3	3	3
p. articularis cranialis	0	1	1	1	1	1	1	1	1	1	1	1	1	1	2	2	2	2	2
p. articularis caudalis	0	1	1	1	1	1	1	1	1	1	1	1	1	1	2	2	2	2	2
Thoracic 1																			
corpus vertebrae	0	1	1	1	1	1	1	1	1	1	1	1	1	3	3	3	3	3	3
p. spinosus	0	1	1	1	1	1	1	1	1	1	1	1	1	1	1	1	1	1	1
p. transversus	0	1	1	1	1	1	1	1	1	1	1	1	1	1	1	1	2	3	3
costa vertebralis	0	1	1	1	1	1	1	1	1	1	2	2	2	3	3	3	3	3	3
proc. uncinatus	0	0	0	0	0	0	0	0	0	0	0	0	0	0	0	0	0	0	0
Thoracic 2																			
corpus vertebrae	0	1	1	1	1	1	1	1	1	1	1	1	3	3	3	3	3	3	3
p. spinosus	0	1	1	1	1	1	1	1	1	1	1	1*	1*	1*	1*	1*	1*	1*	1*
p. transversus	0	1	1	1	1	1	1	1	1	1	1	1	1	1	1	1	2	3	3
costa vertebralis	0	1	1	1	1	1	1	1	1	1	2	2	3	3	3	3	3	3	3
proc. uncinatus	0	0	0	0	0	0	0	1	1	1	1	1	1	1	1	1	1	1	3
Thoracic 3																			
corpus vertebrae	0	1	1	1	1	1	1	1	1	1	1	1	3	3	3	3	3	3	3
p. spinosus	0	1	1	1	1	1	1	1	1	1	1	1*	1*	1*	1*	1*	1*	1*	1*
p. transversus	0	1	1	1	1	1	1	1	1	1	1	1	1	1	1	1	2	3	3

costa																			
vertebralis	0	1	1	1	1	1	1	1	1	1	2	2	3	3	3	3	3	3	3
proc. uncinatus	0	0	0	0	0	0	0	1	1	1	1	1	1	1	1	1	1	1	3

Thoracic 4

corpus																			
vertebrae	0	1	1	1	1	1	1	1	1	1	1	1	3	3	3	3	3	3	3
p. spinosus	0	1	1	1	1	1	1	1	1	1	1	1*	1*	1*	1*	1*	1*	1*	1*
p. transversus	0	1	1	1	1	1	1	1	1	1	1	1	1	1	1	1	2	3	3
costa																			
vertebralis	0	1	1	1	1	1	1	1	1	1	2	2	3	3	3	3	3	3	3
proc. uncinatus	0	0	0	0	0	0	0	1	1	1	1	1	1	1	1	1	1	1	3

Thoracic 5

corpus																			
vertebrae	0	1	1	1	1	1	1	1	1	1	1	1	3	3	3	3	3	3	3
p. spinosus	0	1	1	1	1	1	1	1	1	1	1	1*	1*	1*	1*	1*	1*	1*	1*
p. transversus	0	1	1	1	1	1	1	1	1	1	1	1	1	1	1	1	2	3	3
costa																			
vertebralis	0	1	1	1	1	1	1	1	1	1	2	2	3	3	3	3	3	3	3
proc. uncinatus	0	0	0	0	0	0	0	1	1	1	1	1	1	1	1	1	1	1	3

Thoracic 6

corpus																			
vertebrae	0	1	1	1	1	1	1	1	1	1	1	1	2	3	3	3	3	3	3
p. spinosus	0	1	1	1	1	1	1	1	1	1	1	1	1	1	1	1	1	1	1
p. transversus	0	1	1	1	1	1	1	1	1	1	1	1	1	1	1	1	2	3	3
costa																			
vertebralis	0	1	1	1	1	1	1	1	1	1	2	2	3	3	3	3	3	3	3

proc. uncinatus	0	0	0	0	0	0	0	0	0	0	0	0	0	0	0	0	0	0	0
Thoracic 7																			
corpus vertebrae	0	1	1	1	1	1	1	1	1	1	1	1	2	3	3	3	3	3	3
p. spinosus	0	1	1	1	1	1	1	1	1	1	1	1*	1*	1*	1*	1*	1*	1*	1*
p. transversus	0	1	1	1	1	1	1	1	1	1	1	1	1	1	1	1	2	3	3
costa vertebralis	0	1	1	1	1	1	1	1	1	1	2	2	3	3	3	3	3	3	3
proc. uncinatus	0	0	0	0	0	0	0	0	0	0	0	0	0	0	0	0	0	0	0
Lumbosacral 1																			
corpus vertebrae	0	1	1	1	1	1	1	1	1	1	1	1	1	3	3	3	3	3	3
p. spinosus	0	1	1	1	1	1	1*	1*	1*	1*	1*	1*	1*	1*	1*	1*	1*	2*	2*
p. transversus	0	1	1	1	1	1	1	1	1	1	1	1	1	1	1	1	1	2	3
Lumbosacral 2																			
corpus vertebrae	0	1	1	1	1	1	1	1	1	1	1	1	1	3	3	3	3	3	3
p. spinosus	0	1	1	1	1	1	1*	1*	1*	1*	1*	1*	1*	1*	1*	1*	1*	1*	2*
p. transversus	0	1	1	1	1	1	1	1	1	1	1	1	1	1	1	1	1	2	3
Lumbosacral 3																			
corpus vertebrae	0	1	1	1	1	1	1	1	1	1	1	1	1	3	3	3	3	3	3
p. spinosus	0	1	1	1	1	1	1*	1*	1*	1*	1*	1*	1*	1*	1*	1*	1*	1*	2*
p. transversus	0	1	1	1	1	1	1	1	1	1	1	1	1	1	1	1	1	2	3
Lumbosacral 4																			

corpus vertebrae	0	1	1	1	1	1	1	1	1	1	1	1	1	3	3	3	3	3	3
p. spinosus	0	1	1	1	1	1	1*	1*	1*	1*	1*	1*	1*	1*	1*	1*	1*	1*	2*
p. transversus	0	1	1	1	1	1	1	1	1	1	1	1	1	1	1	1	1	2	3

Lumbosacral 5

corpus vertebrae	0	1	1	1	1	1	1	1	1	1	1	1	1	2	2	2	3	3	3
p. spinosus	0	0	0	0	0	0	1*	1*	1*	1*	1*	1*	1*	1*	1*	1*	1*	1*	2*
p. transversus	0	1	1	1	1	1	1	1	1	1	1	1	1	1	1	1	1	1	2

Lumbosacral 6

corpus vertebrae	0	1	1	1	1	1	1	1	1	1	1	1	1	2	2	2	3	3	3
p. spinosus	0	1	1	1	1	1	1*	1*	1*	1*	1*	1*	1*	1*	1*	1*	1*	1*	2*
p. transversus	0	1	1	1	1	1	1	1	1	1	1	1	1	1	1	1	1	1	2

Lumbosacral 7

corpus vertebrae	0	1	1	1	1	1	1	1	1	1	1	1	1	2	2	2	3	3	3
p. spinosus	0	1	1	1	1	1	1*	1*	1*	1*	1*	1*	1*	1*	1*	1*	1*	1*	2*
p. transversus	0	1	1	1	1	1	1	1	1	1	1	1	1	1	1	1	1	1	2

Lumbosacral 8

corpus vertebrae	0	1	1	1	1	1	1	1	1	1	1	1	1	1	1	2	2	3	3
p. spinosus	0	1	1	1	1	1	1	1	1	1	1	1	1	1	1	1	1	1	3
p. transversus (diapophysis)	0	1	1	1	1	1	1	1	1	1	1*	1*	1*	1*	1*	1*	1*	1*	2*

p. transversus (parapophysis)	0	0	0	0	0	0	0	0	0	1	1	1	1	1	1	1	1	1	3*
foramen diapophysale	0	0	0	0	0	0	0	0	0	0	1	1	1	1	1	1	1	1	1

Lumbosacral 9

corpus vertebrae	0	1	1	1	1	1	1	1	1	1	1	1	1	1	1	1	2	3	3
p. spinosus	0	1	1	1	1	1	1	1	1	1	1	1	1	1	1	1	1	1	3
p. transversus (diapophysis)	0	0	0	1	1	1	1	1*	1*	1*	1*	1*	1*	1*	1*	1*	1*	1*	2*
p. transversus (parapophysis)	0	0	0	0	0	0	0	0	0	1	1	1	1	1	1	1	1	1	3*
foramen diapophysale	0	0	0	0	0	0	0	1	1	1	1	1	1	1	1	1	1	1	1

Lumbosacral 10

corpus vertebrae	0	1	1	1	1	1	1	1	1	1	1	1	1	1	1	1	2	2	3
p. spinosus	0	1	1	1	1	1	1	1	1	1	1	1	1	1	1	1	1	1	3
p. transversus (diapophysis)	0	1	1	1	1	1	1	1*	1*	1*	1*	1*	1*	1*	1*	1*	1*	1*	2*
p. transversus (parapophysis)	0	0	0	0	0	0	0	0	0	1	1	1	1	1	1	1	1	1	2*
foramen diapophysale	0	0	0	0	0	0	0	1	1	1	1	1	1	1	1	1	1	1	1

Lumbosacral 11

corpus vertebrae	0	1	1	1	1	1	1	1	1	1	1	1	1	1	1	1	2	3	
p. spinosus	0	0	0	0	0	0	1	1	1	1	1	1	1	1	1	1	1	3	
p. transversus (diapophysis)	0	1	1	1	1	1	1	1	1	1	1*	1*	1*	1*	1*	1*	1*	1*	
p. transversus (parapophysis)	0	0	0	0	0	0	0	0	0	1	1	1	1	1	1	1	1	1*	
foramen diapophysale	0	0	0	0	0	0	0	0	0	0	1	1	1	1	1	1	1	1	

Lumbosacral 12

corpus vertebrae	0	1	1	1	1	1	1	1	1	1	1	1	1	1	1	1	2	3	
p. spinosus	0	1	1	1	1	1	1	1	1	1	1	1	1	1	1	1	1	3	
p. transversus (diapophysis)	0	1	1	1	1	1	1	1	1	1	1	1*	1*	1*	1*	1*	1*	1*	
p. transversus (parapophysis)	0	0	0	0	0	0	0	0	0	1	1	1	1	1	1	1	1	1*	
foramen diapophysale	0	0	0	0	0	0	0	0	0	0	0	1	1	1	1	1	1	1	

Lumbosacral 13

corpus vertebrae	0	1	1	1	1	1	1	1	1	1	1	1	1	1	1	1	1	3	
p. spinosus	0	1	1	1	1	1	1	1	1	1	1	1	1	1	1	1	1	3	
p. transversus (diapophysis)	0	1	1	1	1	1	1	1	1	1	1	1	1	1	1	1	1	1	

p. transversus (parapophysis)	0	0	0	0	0	0	0	0	0	1	1	1	1	1	1	1	1	1	1
foramen diapophysale	0	0	0	0	0	0	0	0	0	0	0	0	0	0	0	0	0	0	0

Lumbosacral 14

corpus vertebrae	0	1	1	1	1	1	1	1	1	1	1	1	1	1	1	1	1	1	3
p. spinosus	0	1	1	1	1	1	1	1	1	1	1	1	1	1	1	1	1	1	3
p. transversus (diapophysis)	0	1	1	1	1	1	1	1	1	1	1	1	1	1	1	1	1	1	1
p. transversus (parapophysis)	0	0	0	0	0	0	0	0	0	1	1	1	1	1	1	1	1	1	1
foramen diapophysale	0	0	0	0	0	0	0	0	0	0	0	0	0	0	0	0	0	0	0

Caudal 1

corpus vertebrae	0	1	1	1	1	1	1	1	1	1	1	1	1	1	1	1	1	1	1
p. spinosus	0	1	1	1	1	1	1	1	1	1	1	1	1	1	1	1	1	1	1
p. transversus	0	0	0	0	0	1	1	1	1	1	1	1	1	1	1	1	1	1	1

Caudal 2

corpus vertebrae	0	1	1	1	1	1	1	1	1	1	1	1	1	1	1	1	1	1	1
p. spinosus	0	1	1	1	1	1	1	1	1	1	1	1	1	1	1	1	1	1	1
p. transversus	0	0	0	0	0	1	1	1	1	1	1	1	1	1	1	1	1	1	1

Caudal 3

corpus vertebrae	0	1	1	1	1	1	1	1	1	1	1	1	1	1	1	1	1	1	1
p. spinosus	0	1	1	1	1	1	1	1	1	1	1	1	1	1	1	1	1	1	1
p. transversus	0	0	0	0	0	1	1	1	1	1	1	1	1	1	1	1	1	1	1

Caudal 4

corpus vertebrae	0	1	1	1	1	1	1	1	1	1	1	1	1	1	1	1	1	1	1
p. spinosus	0	1	1	1	1	1	1	1	1	1	1	1	1	1	1	1	1	1	1
p. transversus	0	0	0	0	0	1	1	1	1	1	1	1	1	1	1	1	1	1	1

Caudal 5

corpus vertebrae	0	1	1	1	1	1	1	1	1	1	1	1	1	1	1	1	1	1	1
p. spinosus	0	1	1	1	1	1	1	1	1	1	1	1	1	1	1	1	1	1	1
p. transversus	0	0	0	0	0	1	1	1	1	1	1	1	1	1	1	1	1	1	1

Caudal 6

corpus vertebrae	0	1	1	1	1	1	1	1	1	1	1	1	1	1	1	1	1	1	1
p. spinosus	0	1	1	1	1	1	1	1	1	1	1	1	1	1	1	1	1	1	1*
p. transversus	0	0	0	0	0	1	1	1	1	1	1	1	1	1	1	1	1	1	1

Caudal 7

corpus vertebrae	0	1	1	1	1	1	1	1	1	1	1	1	1	1	1	1	1	1	1
p. spinosus	0	1	1	1	1	1	1	1	1	1	1	1	1	1	1	1*	1*	1*	1*
p. transversus	0	0	0	0	0	1	1	1	1	1	1	1	1	1	1	1	1	1	1

Caudal 8

corpus vertebrae	0	1	1	1	1	1	1	1	1	1	1	1*	1*	1*	1*	1*	1*	1*	1*
p. spinosus	0	1	1	1	1	1	1	1	1	1	1	1*	1*	1*	1*	1*	1*	1*	1*
p. transversus	0	0	0	0	0	1	1	1	1	1	1	1	1	1	1	1	1	1	1

Caudal 9

corpus vertebrae	0	1	1	1	1	1	1	1	1*	1*	1*	1*	1*	1*	1*	1*	1*	1*	1*
p. spinosus	0	1	1	1	1	1	1	1	1*	1*	1*	1*	1*	1*	1*	1*	1*	1*	1*
p. transversus	0	0	0	0	0	1	1	1	1	1	1	1	1	1	1	1	1	1	1

Caudal 10

corpus vertebrae	0	1	1	1	1	1	1	1	1*	1*	1*	1*	1*	1*	1*	1*	1*	1*	1*
p. spinosus	0	1	1	1	1	1	1	1	1*	1*	1*	1*	1*	1*	1*	1*	1*	1*	1*
p. transversus	0	0	0	0	0	1	1	1	1	1	1	1	1	1	1	1	1	1	1

Appendix A2. Copyright Acknowledgement.

The original article that forms this chapter was published in the *Zoological Journal of the Linnean Society.* Oxford University Press grants permission for this work to be reproduced in full text in this dissertation.

Bridging Text

In Chapter 2, I provide a detailed analysis of the morphological development of the axial column in *Gallus gallus.* We find that delays in ossification coincide with the formation of fusions, hinting at the presence of developmental modules independent of initial *Hox* expression patterns. This study provides greater depth to understanding axial regionalization within the context of the dinosaur-to-bird transition, while also highlighting discrepancies between molecular expression patterns, ossification sequences, and general regionalization.

Where Chapter 2 describes morphological character development and the relationship between *Hox* expression and regionalization, Chapter 3 investigates the quantification of axial column variation. This chapter represents a transition from qualitative characters to the quantification of variation, providing a direct comparison between discrete characters and surface variation within the axial column. Through the utilization of 3D modeling and spherical harmonics, I am able to create an objective and comprehensive analysis of surface morphology across an entire axial column. Chapter 3 is a novel approach to quantifying variation within the axial column, utilizing whole surface morphology. As Chapter 2 reveals the intricacies of ossification and fusion in a highly specialized avian axial column, Chapter 3 introduces an innovative technique for quantifying morphological variation and modularity in a reptilian model.

Chapter 3
Axial variation in *Caiman crocodilus*

Abstract

Understanding morphological variation and its evolutionary implications has long been a cornerstone of evolutionary biology. Traditional methods, such as discrete anatomical characters (DACs) and landmark-based geometric morphometrics (GMM), have provided valuable insights but may not capture the full extent of morphological variation. Here, we introduce a novel approach using spherical harmonics analysis (SPHARM) to quantify shape variation and regionalization in the axial column of *Caiman crocodilus*. Our method utilizes high-resolution nano-CT scans and spherical harmonics to create point distribution models, allowing for an objective analysis of whole surface morphology. We find significant serial variation concentrated near the cervical to dorsal transition, as well as the sacral complex, with Principal Component and Linear Discriminant Analyses revealing distinct regional groupings. Segmented regression models identify additional morphological subregions. Modularity analysis highlights greater integration within dorsal modules compared to other regions. Our study represents a complete surface approach to studying axial column morphology, providing insights into regionalization, integration, and developmental patterning in *Caiman crocodilus*. This methodology offers a promising avenue for exploring morphological variation in other vertebrate structures and across evolutionary scales.

Introduction

Discrete anatomical characters (DACs) have long been utilized in taxonomic, phylogenetic, developmental, and macroevolutionary contexts. Changes in the presence of

characters has provided the framework for the study of morphological variation as well as the origin of novel structures (de Beer, 1954). Understanding the drivers behind phenotypic variation is pivotal to addressing how phenotypes evolve over macroevolutionary scales. However, the question we pose is: are these characters capturing the entirety of anatomical variation and change?

Scoring discrete characters consists of determining the presence or absence of character states in distinct regions of the skeleton. Phylogenetic reconstruction of the evolution of those states may be used to account for the evolution of novelties and inferring modes of evolution (de Beer, 1954). Character coding consists of 1) discretizing the trait, 2) assessing primary homology 3) encoding the trait into a character string or vector (Wiens, 2001). Discrete character schemes allow for an accommodation of a broad range of morphologies within a single analysis, the inclusion of features that are present in a limited subset of specimens, and coding allowing for descriptors for multiple character states (Gerber, 2019). These characters provide a measure for morphological variation within and between taxa, allowing for insight into macroevolutionary processes in both paleontological and developmental contexts (Jones et al., 2018; Head & Polly, 2015; Neige, 2003; Ricklefs, 2004**)**. Understanding the processes behind character evolution is crucial for explaining evolutionary radiations (Price et al. 2010; Tobias et al. 2014; Van Bocxlaer et al. 2010), the origin of complexity and novelty (Moczek 2008; Ramirez & Michalik, 2014), and inferring phylogenies (Tarasov, 2019). However, one major drawback is there is a lack of repeatable agreed upon approaches for character coding, resulting in ambiguity and subjectivity (Tarasov, 2019).

In morphometric studies, landmarks are often used to represent specific characters but the subjectivity of landmark choice may lead to a loss of information. Geometric morphometrics

(GMM), a widely adopted approach, has provided meaningful methods for identifying and quantifying variations in shape (Bardua et al. 2019; Mitteroecker & Gunz, 2009)**.** This is typically done using landmarks, points chosen on specific structures that are homologous and recognizable across a sample group (Bookstein, 1997), semi-landmarks, and sliding semi-landmark approaches. Many landmark-based GMM studies can be found on skull variation to explore sexual dimorphism, behavior, modularity and integration, phylogenetic analyses, ecology, and evolution (e.g. Bardua et al., 2019; Drake & Klingenberg, 2010; Fabre et al., 2014; Felice et al., 2021; Foth et al., 2012**;** Godoy, 2020; Goswami, 2006; Morris et al., 2019; Openshaw et al., 2017; Palci et al., 2020; Pierce et al., 2008; Piras et al., 2014; Stayton, 2005; Tokita et al., 2016). Studies in limb shape and vertebral variation have shed light on macroevolutionary trajectories, relationship between locomotion, behavior, and ecology, as well as development (Alvarez et al. 2013; Adams & Nistri, 2010; Berio et al., 2021; Bohmer et al., 2015; Carro et al., 2018; Chamero et al., 2014; Fabre et al., 2013; Head & Polly, 2015; Lowie et al., 2022; Martin-Serra et al., 2014; Pintore et al., 2021; Randau, 2017; Scholtes et al., 2022; Stein et al., 2020; Werneberg et al., 2015). Other GMM methods quantifying variations in shape utilize linear or cross sectional measurements (Bell et al., 2011; Meachen-Samuels & Van Valkenburgh, 2009; Molnar & Watanabe, 2023; Pierce et al., 2011; Randau et al., 2016) which can potentially overlook significant biological signals, such as those linked to ecology that linear morphometric techniques were simply not powerful enough to discriminate more subtle variation in form (Randau et al., 2016). Select studies have also looked at direct comparisons of discrete characters and continuous character analyses, i.e. both linear and landmark-based geometric morphometrics to find similar results (Hetherington et al., 2015; Schaeffer et al., 2020; Villier & Eble, 2004). Despite the prevalence of landmark-based approaches, their utility is often

constrained by the requirement for replicable points in all invested structures (Ege et al., 2020). This becomes an issue for structures with spherical or rounded aspects, highly irregular shapes, or surfaces with extreme topographies (Ege et al., 2020). Including the whole surface variation may solve many of these shortfalls of landmark-based morphometrics. Utilizing whole surfaces over landmark based methods include advantages of not requiring homologous landmarks to be selected a priori, and an ability to accommodate loss or gain of 'novel' structures (Polly & MacLeod, 2008). This can be done one of three ways: semi-landmarks extending onto surfaces (Mitteröcker et al., 2004), an eigensurface analysis (Polly & MacLeod, 2008), or through spherical Fourier harmonic descriptors (SPHARM) (Shen et al., 2009) of 3D scan data. These approaches create landmarks typically in grids across the form in question, the differences solely being the methods in which the landmarks are acquired.

Here, we use spherical harmonics analysis using point distribution models (SPHARM) (Shen et al., 2009) to quantify shape variation, regionalization, and modularity of the entire vertebral surfaces in the axial column of a *Caiman crocodilu*s. I chose this approach due to the ease of using a pre-established program, and the limited coding necessary to extend the approach to the analysis of the samples in question. The pipeline from 3D scan data to point distribution model is effective for capturing surface morphology and subsequent analyses are similar to other approaches. SPHARM is the three dimensional extension of an elliptical Fourier analysis, describing the outline of a closed surface as a function that maps the distance from an origin to a point along the surface of an object (Rohlf & Archie, 1984). The function contains Fourier coefficients (Shen et al., 2009) and is expressed in terms of sine and cosine (harmonic) functions. These coefficients are determined through least squares estimation, and subsequently used to represent and reconstruct the object's original surface (Shen et al., 2009). Consequently, these

shape descriptors provide an effective base for comparing differences in shape (Macleod, 1999; Polly, 2008), or for reconstructing the evolution of shape change (McPeek et al. 2008, 2009).

Our case study focuses on the axial column as it is a relatively under-studied structure within Archosauria. Most work on the axial column has focused on functional morphology and biomechanics within Crocodylia or separate analysis of specific regions and regional transitions instead of the entire column (Chamero et al., 2014; Molnar et al., 2015; Salisbury & Frey, 2001). The vertebral column is one of the main vertebrate evolutionary novelties, conserved over the past 400 million years (Janvier, 1996). Studying the variation in axial column morphology provides a way to investigate the influence of size, locomotion, prey-size specialization, and regionalization on form-function relationships, behavior, and ecology (Buchholtz, 1998; Jones et al., 2020; Marchesi et al., 2021; Randau et al., 2016). Composed of serially homologous units with shape differentiation related to regionalization and gene expression, the axial column is often utilized to study integration and modularity (Buccholtz, 2007; Polly et al., 2001; Randau & Goswami, 2017). Through the exploration of morphological variation, regionalisation and modularity, we can gain a greater understanding of vertebrate history and evolution (Arratia et al., 2001; Berio, 2022; Buccholtz, 2007; Jones et al., 2018; Martin Serra et al., 2021; Sallan, 2012).

I chose the *Caiman* due to its relatively small size, ease in acquiring 3D morphometric data, and as an Archosaur with an axial column that is generally understood as low in complexity. Today, Archosauria is represented by more than 10,000 species of birds and 30 species of crocodylians (Scheyer et al., 2019). Crocodylians are commonly described as ‘living fossils’ due to their relatively conservative body plan (Langston et al., 1973; Meyer, 1984), conserved precaudal vertebral numbers (Mansfield & Abzhanov, 2010; Müller et al., 2010), low

genome-wide evolutionary rates, and relatively low morphofunctional disparity (Brusatte et al., 2010). Caimans are within the clade Caimaninae– a clade nested in alligatoroids, a stem-based clade defined as including *Caiman crocodilus* and all crocodylians closer to it than *Alligator mississipiensis* (Brochu, 1999). While there are several comprehensive datasets for crocodylian discrete anatomical characters (e.g. Rio & Mannion, 2021), there are no high resolution studies of extant crocodylian axial column morphological variation nor studies done to explore axial regionalization and integration.

Methods

Data Collection

Nano-CT scans using a Zeiss Xradia 520 Versa were performed on each available individual vertebra of an adult *Caiman crocodilus* (n=51). This was a single specimen of *Caiman* accessioned in the Redpath Museum under lot number RM 5242. Scans were acquired between 0.04-0.1 *um* resolution with .4x objective lens with 2x2 camera binning over a 360 degree rotation. A total of 1400 projections were taken at 80 kV and 7 W. Most scans were taken with the LE1 filter and 1 second exposure time. Each vertebra was reconstructed with Dragonfly image analysis software, Version 2022.2 for Windows. 3D meshes were cleaned up using Blender and Meshlab to remove holes, conduct isotropic resampling and smoothing, and decimate each mesh to 10,000 faces.

3D Surface generation

Spherical harmonics analyses (SPHARM) were performed using the freely available software packages Slicer (Kikinis et al., 2013) and SlicerSalt (Vicory et al., 2018). Binary segmentations were acquired in Slicer and imported into SlicerSalt to generate point distribution

models (PDMs). Bijective mapping of the surface points onto a unit sphere generated a spherical parameterization that was then expanded as a Fourier series. Spherical parameterization minimizes angular distortions while creating a continuous and uniform mapping of the surface to the surface of the unit sphere. The resultant Fourier functions were then used to compute SPHARM coefficients up to 15 degrees. PDMs with homogeneous sampling of the object surfaces were then generated from the coefficients by uniform sampling of the spherical parameterization with an icosahedron subdivision of factor 10. Alignment was performed using rigid Procrustes Alignment. This registration algorithm implicitly establishes homology between surfaces by optimally aligning their underlying parameterizations, similar to assigning landmarks to surfaces. Homology was established through directionality– anterior, posterior, left lateral, and right lateral– of each vertebra, creating a framework for each vertebra to lie within and establish surface homology for the rest of the individual vertebra. A SPHARM description was then computed from the mesh and its spherical parameterization to create a PDM totalling 1002 corresponding surface points. These surface points correspond to spatial locations of vertices across specimens to be used as surface landmarks for further analysis.

Discrete characters were compiled using Rio & Mannion's morphological dataset (Rio & Mannion, 2021) which is a comprehensive assembly of the past several decades of Crocodylomorpha phylogenetic matrices. Axial characters were mapped onto the reconstructed SPHARM models of each region's mean (Figure 3.1). Surface variation was mapped on 1000 surface landmarks generated by the SPHARM-PDMs. Average landmark coordinates were determined and plotted for each landmark and corresponding vertebra. Variation was visualized by calculating the centroid size for each landmark and assigning a color value to represent high and low centroid size (Figure 3.2).

Statistical analysis

Analyses based on PDMs were conducted in R version 2023.09.1 using the *geomorph* package (Adams et al., 2019). Preliminary analysis to visualize vertebral morphospace occupation was performed in a Principal Component Analyses (PCA; *gmprcomp*). The relationship between shape, vertebral region, and position along the axial column were evaluated using Procrustes ANCOVA using the 'procD.lm' function in geomorph (Adams et al., 2019) for R. These tests were run with a residual randomization permutation method (RRPP) (Collyer et al., 2015) with 10000 iterations to evaluate significance.

To assess SPHARM results and the successful capturing of morphological variation in the axial column, I tested for accurate regionalization and correct grouping within developmental modules and the whole vertebral body. I ran a Linear Discriminant analysis (LDA) using the *MASS* package (Ripley et al., 2013). Vertebrae were identified a priori as cervical, dorsal, sacral, or caudal, and the distinctiveness of each assigned group was quantified. LDA maximizes the separation between groups based on predictors, and in our case- the specific regions each vertebra belongs to. I also followed Jones et al.'s (2020) method of evaluating regionalization using segmented regression models based on principal components analysis. I allowed up to 7 regions, with 5 being the maximum number reported for tetrapods (Head and Polly, 2015; Jones et al., 2018; Molnar & Watanabe, 2023; Randau & Goswami, 2018). This approach takes into account vertebral integration, treating the vertebral column as a series of morphological gradients and regions based on changes in slope (Jones et al., 2020). Regionalization hypotheses were compared with an Akaike Information Criterion (AIC) value and converted to a continuous regionalization score by calculating Aikake weights from the likelihood of each hypothesis.

Integration was explored using integration.test (geomorph) and pairwise comparisons of the means across all vertebrae using the RRPP function. Size in vertebral shape was not corrected prior to the analyses of intervertebral integration as allometric effects have been suggested to be a strong contributor to integration (Randau et al., 2017). Fitted values over all permutations, least squares means, and pairwise statistics were found. Distance between vectors for LS means, or the difference in location between estimated shape change between vertebrae, was quantified and used as a proxy for exploring morphological disparity. Mean Procrustes distances between each individual vertebra and mean shape of the data was calculated. Heatmap comparisons were plotted to explore modularity by mapping pairwise comparisons across the axial column and highlighting the lowest fifth, tenth, 15th, and 25th percentiles of all the data. I removed the effects of size in order to solely explore shape variation along the axial column. A principal component analysis was run using the residuals of an allometry-free model and variation was visualized using the weighted sum of each component and respective eigenvalue. I used the first 16 principal components, capturing 95% of the variation seen across the vertebrae, multiplied by their respective eigenvalue and summed to represent each PC component.

Results

Sequential shape variation represented by SPHARM-PDM model-to-model distances reveals high variation concentrated mainly near the cervical to dorsal transition and sacral complex (Figure 3.). PCs 1 through 5 represent 87% of total variation across the whole vertebra (Figure 3.4). PC1 represented 53.7% and PC2 represented 13.9% of variation, with PC1 mostly describing size. The caudal vertebrae plot across the greatest PC1 range, with the cervicals and dorsals grouping together accordingly. The cervical grouping aligns closely with the proximal

caudals. 51% of between class variance in the whole vertebral analysis can be explained by the first linear discriminant function and 29% by the second.

The results from the pairwise comparisons between regions reveal all are significant ($p<.05$) for all groups except between dorsals and sacrals. 2B-PLS tests indicated statistically significant estimates of integration with varying strengths across the column. rPLS correlation values ranged from .89 to .99 with associated Z-scores of 10.9 and 17.6 and p values of less than .001. All Z-score values were quite high, implying the degree of integration between vertebrae was higher than that expected by chance. Pairwise distances calculated from least squares means were found with a minimum distance of .07 and a maximum distance of 0.49. The average distance is .20, with most vertebrae plotting between 1.5 and 2.5 (Figure 3.5a).

Segmented regression fitting revealed the greatest support for 7 distinct morphological subregions in the *Caiman* axial column. The first region consisted of most of the cervical vertebrae from the axis to cervical 8. The dorsal vertebrae were subdivided into an anterior and posterior region, the anterior dorsal region composed of cervical 9 to dorsal 5, and the posterior dorsal region containing dorsals 6 to 15. The sacrals plot distinctly from the rest of the population, creating an expected sacral region. I find three caudal subregions in the best fit hypothesis, the first consisting of caudals 1 to 12, then caudals 13 to 21, and finally 22 to 27 (Figure 3.5c & d). More distal caudals were not included in the analysis.

Objective modules are highlighted in the heatmaps by highlighting the lowest percentiles of the distance data (Figure 3.6). In the lowest 5th percentile, the lowest variation is seen between cervical vertebrae 6 to 8, all the dorsal vertebrae, caudal vertebrae 1 to 3, caudal vertebrae 8 to 14, caudal vertebrae 18 to 20, and caudal vertebrae 23 to 27. Highlighting the 10th percentile revealed groupings between cervical vertebra 3 to dorsal vertebra 15, caudal vertebrae

1 to 16, caudal vertebrae 18 to 20, and caudal vertebrae 23 to 27. Mapping the 15th and 25th percentiles mirror where variation is the greatest between all vertebrae, the sacral vertebrae and first caudal vertebra, as well as caudal vertebrae 20 to 23. The map of sequential axial variation shows high variation between the axis and cervical vertebrae, and a step-wise pattern of decreasing variation until cervical vertebrae 6 and 7. Variation peaks again at cervical vertebra 8 and 9, to decrease again through the mid-dorsal vertebrae. Sequential variation remains quite low amongst the dorsals, but with slightly more variation in the more posterior dorsals. Sequential variation among the sacral vertebrae, first caudal vertebra, and caudal vertebra 22 plot significantly above the fifth percentile limit, but there is also significant variation amongst the caudals with higher levels of variation around caudal vertebrae 6 through 8, and caudal vertebrae 14 to 18.

Our identification of morphological modules was based on the lowest pairwise distances between models, revealing high covariation and integration. High covariation is noted from cervical vertebrae 6 to 8, corresponding to the last three cervical vertebrae in the first region. This is noted morphologically with the most distinct anteriorly angled hypapophyses within the cervical region, along with transverse processes that have not shifted upwards towards the base of the neural arch. Dorsal 1 to 14 groups together as a module, encompassing the two dorsal regions with the exception of the anteriormost and posteriormost vertebrae. This region is morphologically grouped together by relatively long transverse processes, the lack of a hypapophysis, and parapophyses moving to the anterior edge of the transverse process. I also note high covariation between caudal vertebrae 1 and 2 that is not reflected in our regionalization analysis, but morphologically maintain strong similarities. Caudal vertebra 1 maintains two convex articular faces, while caudal vertebra 2 is procoelous. But the neural spine width and

height, as well as transverse process angle and length are relatively similar. High covariation is also seen between caudal vertebrae 8 and 14, composed of the posterior vertebrae from the first caudal region and the first couple of vertebrae from the second. This region is morphologically distinct as it encompasses the transition from a wider neural spine to a thinner more rod or needle-like neural spine shape. I note a transition from posteriorly directed transverse processes, to shorter and directed perpendicularly to the centra. From caudal vertebrae 18 to 20, I note a transition seen in the SPHARM model variation but not in the regionalization analysis. Axial variation with the neural spine shows a distinct change from the vertebra prior through a slight shift in angle posteriorly. This module is found within the posterior part of the second caudal region. Caudal vertebrae 23 through 27 can be described by a distinct decrease in neural spine presence, and is also seen in the regionalization analysis corresponding to the last caudal region.

The discrete characters utilized for phylogenetic analyses by Rio and Mannion (2021) consisted of angles and relative lengths of the neural spine, post-zygapophyses, and hypapophyses, as well as the nature of the articular facets of the cervical vertebrae. For the dorsal vertebrae, the articular faces and relative lengths of transverse processes and widths across prezygapophyses are noted. Within the sacral vertebrae, the anterior and posterior rib relations are described, and caudal vertebrae are distinguished by articular surface state, the presence of transverse processes, and chevron fusion states. Surface variation across all vertebrae reveals highest variation around the neural spine, transverse processes, the posterior articular surface, and the ventral area of the anterior articular surface. These are the areas of high variation in the region means as well, with high variation along the post-zygapophyses in dorsal and caudal vertebrae. The neural spine varies a lot in height and width, as well as in angle posteriorly. There is higher variation in the articular faces for the caudal vertebrae, and the least in sacral vertebrae

and dorsal vertebrae. There is a consistent zone of little to no variation at the base of the neural arch, where the transverse processes extend from the centra.

Upon the removal of size in shape variation, PC1 represents 29.5% of variation whilst PC2 represents 19% of variation. The weighted allometry-free PC variation is plotted in (Figure 3.5c), the absolute values of the differences between vertebrae were calculated with the lowest score difference being between caudal vertebrae 14 and 15 (.0007) and caudal vertebrae 26 and 27 (.0005). Similar to the previous analyses, we see high variation amongst the cervical vertebrae and low between the dorsals. I see the greatest differences from dorsal vertebra 13 to caudal vertebra 5 ranging from .006 to .048. The caudal vertebrae have the highest variation for PC variance, ranging from .03 to .0005.

Discussion

The results presented here are from a novel 'objective' method in the quantification of nearly all shape variation within an axial column without being limited by the selection of a limited set of homologous landmarks. Current methods have used a limited number of landmarks and characters associated with the axial column. Our motivation was to test if the entire surface variations throughout the axial column can be used to infer traditional axial modules, discover new ones, and if the variation corresponds to the discrete anatomical characters (DAC) used in phylogenetic analyses.

Concerning the latter, a few studies have compiled a comprehensive list of crocodilian characters. These include Narváez et al. (2015), based on Brochu and Storrs (2012), compiling 103 taxa, 16 extant species, and totalling to 189 characters. Of these characters, only 23 are associated with the axial column and of those 23, 17 describe the atlas and axis. The more

current comprehensive dataset was published by Rio and Mannion (2021), consisting of 330 characters. 263 characters are attributed to the skull, 30 characters to the axial column, and 14 of the 30 related solely to the atlas and axis. Although the skull is generally featured in phylogenetic character lists, the vertebral column remains an understudied structure, as the analysis of shape within a structure composed of multiple articulating discrete units poses a unique challenge (Randau et al., 2016). These datasets reflect a disparity between cranial and vertebral characters, as well as a bias towards characters solely focusing on the first two vertebrae out of the entire column. Narváez et al.'s character list does not include characters past the cervical vertebrae, whereas Rio and Mannion's does, however they are limited to 2 to 4 characters per axial region.

The utilization of the entire vertebral surface allowed us to capture greater detail of variation outside of the character states listed, as well as highlight more subtle changes throughout the axial column. There is high variation in presence, length and shape of transverse processes across the column, and yet they are only briefly noted in Rio and Mannion's dataset. Character 286 notes the width of the transverse processes within the dorsals, and Character 293 refers to their presence/absence in the caudals. Neural spine length and shape varies significantly across the column, and is thoroughly described in the axis through Characters 273-275. Neural spine extension is noted in the cervicals in Character 280, but no neural spine characters are described for the dorsal, sacral, or caudal regions. The states of the articular surfaces are a character for each vertebral region. Our analysis matches up with the character datasets through highlighted surface variation relating to the state of the articulating faces of the centra as well as absence or presence of a hypapophysis. However, only a select few areas of high variation align with these DACs. The majority of variation is not coded in currently used DACs and may offer

better insight into anatomical evolution. Notably, the intervertebral articular surfaces (centrum and zygapophyses) and rib articulations (transverse processes), and muscular attachments (neural spine, hypopophyses) present highly variable surfaces in specific regions of the axial column. The surface data presented here offers a template to begin coding novel vertebral characters for at least Crocodylia. For example, the inclusion of the changes in the neural spine and transverse processes along the axial column may be added as characters, as well as the transition of the location of the diapophysis and parapophysis. While these transitions are often noted in anatomical descriptions, their inclusion in character analyses may be beneficial to character studies on morphological variation and evolution.

Generally high levels of integration were recovered across the entire column, despite marked regionalization identified through the regionalization analysis. This however could also be a result of the sheer number of landmarks acquired from the point distribution models. Most of the thousand landmarks varied little between vertebrae and would have acted to reduce differentiation throughout the column. However, whole surface variation was able to infer regionalization within the column using several methods. Traditional vertebral modules plotted together in PC space according to region: cervical, dorsal, sacral, and caudal. Linear discriminant analyses corroborated expected general regionalization within the axial column with correct classifications for all vertebrae. Through the segmented regression model analysis however, there are distinct morphological subregions within the traditional vertebral modules. I note an anterior and posterior dorsal module, as well as an anterior, middle, and posterior caudal module. The posteriormost cervical acts as a transitional vertebra from the cervicals to dorsals, likely a reflection of a less distinct *Hox* delineation as seen in the model chicken.

Morphological changes observed at each regional boundary established through our segmented regression analysis can be seen in Figure 3.7. The transition from the posterior cervicals to anterior dorsals is reflected through a widening of the neural spine as well as an angular shift from a posterior inflection to angle more anterodorsally. There is also a dorsal shift of the placement of the transverse processes, as well as posteroventral angling of the hypapophyses. This transition marks the beginning of the anterior dorsal region, marked by sequentially increasing transverse process length and dorsoventral width. This region ends upon the transition from increasing length of transverse processes to decreasing length and increasing angle anteriorly around dorsal 6. The second dorsal regions maintains very little variation across it, with a lack of hypapophyses and a consistent length and width across the neural spines. These regions generally reveal higher variation along the cervical regions, a transitional dorsal region, to a consistent, low variation dorsal region. Interestingly, in the caudal vertebrae there are specific regions broken into anterior, middle, and posterior. These region boundaries appear to be driven mostly by neural spine shape and angle. The first caudal region contains the neural spines that are anteroposteriorly wide and dorsally angled, the second is marked by dorsally directed spines and a thinner more needle-like shape, whilst the last caudal regions is marked by a posteriorly angled neural spine that also decreases in sequential length.

Through the modularity exploration, I notice a formation of greater integration within the dorsal module in the pairwise heatmap, seen in the red ‘triangles’ as a visual representation. As one moves from the lowest 5th percentile to the lowest 20th percentile of distance data, the triangles become larger in the cervical and dorsal groupings compared to the caudals. This implies greater integration amongst the dorsals, as there is a greater similarity between dorsal 3 and dorsal 14 as compared to caudal 2 and 21. Our regionalization analysis conflicts with these

findings describing two distinct dorsal subregions, with the first five dorsals mapping into their own distinct region. This is marked by a trend of increasing transverse process length, plateauing and decreasing again after dorsal 5. I also note shape change within our principal component exploration, with the first five dorsals plotting at greater PC1 and PC2 values, then turning towards smaller values at this transition. The high integration most likely reflects the vertebral shape as a whole, with consistent centrum and neural spine shapes, as well as the dissipation of the hypapophysis.

Modularity has not been extensively studied in Crocodylia. Comparisons between regionalization and modularity patterns in other vertebrates reveal similar anterior dorsal and posterior dorsal regions to some reptiles, with one species of chameleon displaying a three-vertebra ‘cervical-dorsal’ transition region (Molnar & Watanabe, 2023) as well as a distinct module in the cervico-thoracic boundary in felids (Randau & Goswami, 2017). Our results indicate a high degree of integration around the cervico-thoracic boundary, specifically from cervical 7 to 9. In felids, this module is expanded from cervical 6 to thoracic 2. These modules were suggested to be related to the migration of cells from somites bound to the forelimbs. Jones et al. (2018) hypothesized three presacral regions to the ancestral amniote condition, with the addition of a pectoral module involving the reorganization of the pectoral girdle and the forelimb. This reorganization is also possibly linked to the evolution of the muscularisation of the diaphragm (Buchholtz et al., 2012). Comparing the regionalization and modularity analyses, there is high integration among the dorsal vertebrae with no distinct modules found within the dorsals. However, in the regionalization analysis, an anterodorsal and posterodorsal region separation is found. These findings are reminiscent of Esteban et al. 's work on covariation among the presacrals in pinnipeds. Comparing the modularity exhibited by fissipeds

(Martin-Serra et al., 2021), they find the functional modules existing in fissipeds no longer present in pinnipeds. In regards to the anterodorsal and posterodorsal modules, the separation is more blurred in pinnipeds most likely due to the functional demands of locomoting on land versus water, as sagittal locomotion is not as important in pinnepeds as in fissipeds. It is possible that there is slight regionalization and a lack of modularity due to locomotory constraints and the lack of necessity for highly mobile posterior thoracic vertebrae correlating to sagittal bending in the asymmetrical mammalian gait.

Upon removing size from the analysis, there is a greater overlap in shape amongst the dorsals, sacrals, and caudals. The cervicals and first dorsal plot closest to each other, leading us to believe that the first dorsal plays a more transitional role in axial column variation. This is also seen in Figure 3.5a and 3.5b, with an almost step-wise transition from the posterior caudals to the anterior dorsals. A similar pattern is seen in the transition from the posterior dorsals to sacrals, but with a greater difference in step size. A steeper transition occurs between the posterior caudals starting at the 7th cervical to the first dorsal. These plots also still notice a shift around dorsal 11 and after caudal 2.

These variation patterns are compared to developmental patterning in *Alligator* (Bohmer et al., 2015; Mansfield & Abzhanov, 2010). Most notably, the anterior boundary of *Hoxa5* at cervical 9 can be seen in the axial variation plots as well as the region boundaries. *Hoxc6* is expressed at the cervical-thoracic transition, but there is no clear delineation within our data to mirror its expression. This may be due to the lack of a clear expression boundary between cervical 9 and dorsal 1, as well as reflective of the cervical-dorsal morphological module. A clear boundary is present in both molecular and morphological datasets in the chicken, whereas the alligator gene expression is less clear. *Hoxa7* expressed between dorsals 2 to 8 correlates with the

second axial region of cervical vertebra 9 to dorsal vertebra 5 as well as the dorsal module identified in the 5th percentile heatmap, however it's boundaries do not correspond to specific module or region boundary identified in this analysis. This may be a reflection of expression domain changes in rib morphology and placement rather than the whole vertebral shape change as a whole.

Our patterns of regionalization and modularity can be connected to functional adaptations displayed in the behaviors of *Caiman crocodilus.* All extant crocodilians have been observed to perform a behavior known as the "death roll," in which the structure of the anterior portion of the extant crocodilian vertebral column plays a key function (Preuschoft & Klein, 2013). This is related to the presence of cervical ribs, allowing the neck to withstand torsional stresses imposed on it during death rolls. The morphology of these cervical ribs are quite unique, with short and thick proximal extensions and a dorsoventrally restricted distal portion creating an overlap between each rib to the subsequent rib. This corresponds to the first region and the second that is seen in the analysis. According to Romer (1956), the cervical-dorsal transition is also traditionally recognized by the connection between vertebrae bearing dorsal ribs and those bearing the sternal skeleton. This analysis instead reveals a modular cervico-dorsal transitional region, with regional boundaries met by a dorsal shift and enlargement of the transverse processes. In regards to the anterior and posterior dorsal regions, the shift of the parapophyses upwards to the transverse process most likely relates to a shift in rib articulation and lung expansion. Crocodylia display a unique respiratory system combining costal ventilation with a hepatic pump mechanism. The change in angle between the parapophysis and diapophysis has been found to influence the motion of ribs during breathing, with the ribless lumbar region

creating space for the diaphragm and increase space in the body cavity to ventilate the lungs (Brocklehurst et al., 2017).

This study takes into account the entire vertebra, using the entire surface rather than selected landmarks or features for pairwise comparisons along the column. This approach allowed us to conduct shape comparisons across entire surfaces rather than being limited in choosing specific landmarks, specific vertebrae, specific regions. I was able to utilize the entire axial column, finding variation within a single individual, capturing regionalization and integration in a relatively streamlined and uniform manner. To my knowledge, previous studies focusing on quantitatively identifying axial anatomical regionalization have utilized a limited number of morphometric measurements on specific regions of the axial column (Molnar & Watanabe, 2023), linear, angular and landmark approaches for 'functionally relevant' characters to homologize features along the axial column (Jones et al., 2018), homologous landmark approaches in presacral (Randau et al., 2016) and pre-cloacal (Head & Polly, 2015) axial columns. Variations of the entire vertebral surfaces reveal more anatomical modularity throughout the axial column than previously documented.

Conclusion

This study is the first attempt at complete, objective, surface variation within an entire single axial column. My focus on a single axial column demonstrates the maximal range of variation in one individual's axial column, thus forming a basis for considering evolutionarily relevant anatomical variation. My approach using spherical harmonics was not to act as a substitute for traditional discrete characters, but rather as a complementary and additive element

to studying shape variation in complex structures. Within the *Caiman* axial column, I am able to highlight regions of high anatomical variation throughout the entire, yet complex, series. Drawbacks to the utilization of spherical harmonics is the learning curve towards the utilization of Slicer and SlicerSalt with limited documentation. The acquisition of high resolution data can also become quite costly and relatively time intensive. The process however, once streamlined, generally becomes more efficient and less time intensive than the direct scoring of characters or determination and selection of individual landmarks or creating meshes for sliding surface landmarks.

This study potentially opens up a wealth of novel character sources across the axial column, as regions of high variation were identified within a single individual and raises questions regarding morphological variation within and across taxa. The expansion of vertebral variation within Crocodylia may contribute to our understanding of crocodilian locomotion, posture, ecological niche occupation– challenging the historical generalization of crocodilian axial columns with low variation and a relatively simple axial column as a whole. This work can extend towards an evolutionary or developmental perspective, incorporating more taxa or embryological data in order to explore ontogenetic or evolutionary transitions. With advancements in imaging and technology corresponding with the accessibility and ease of acquiring 3D data, these types of analyses can be further utilized in enhancing our understanding of vertebrate skeletal morphology.

Figures

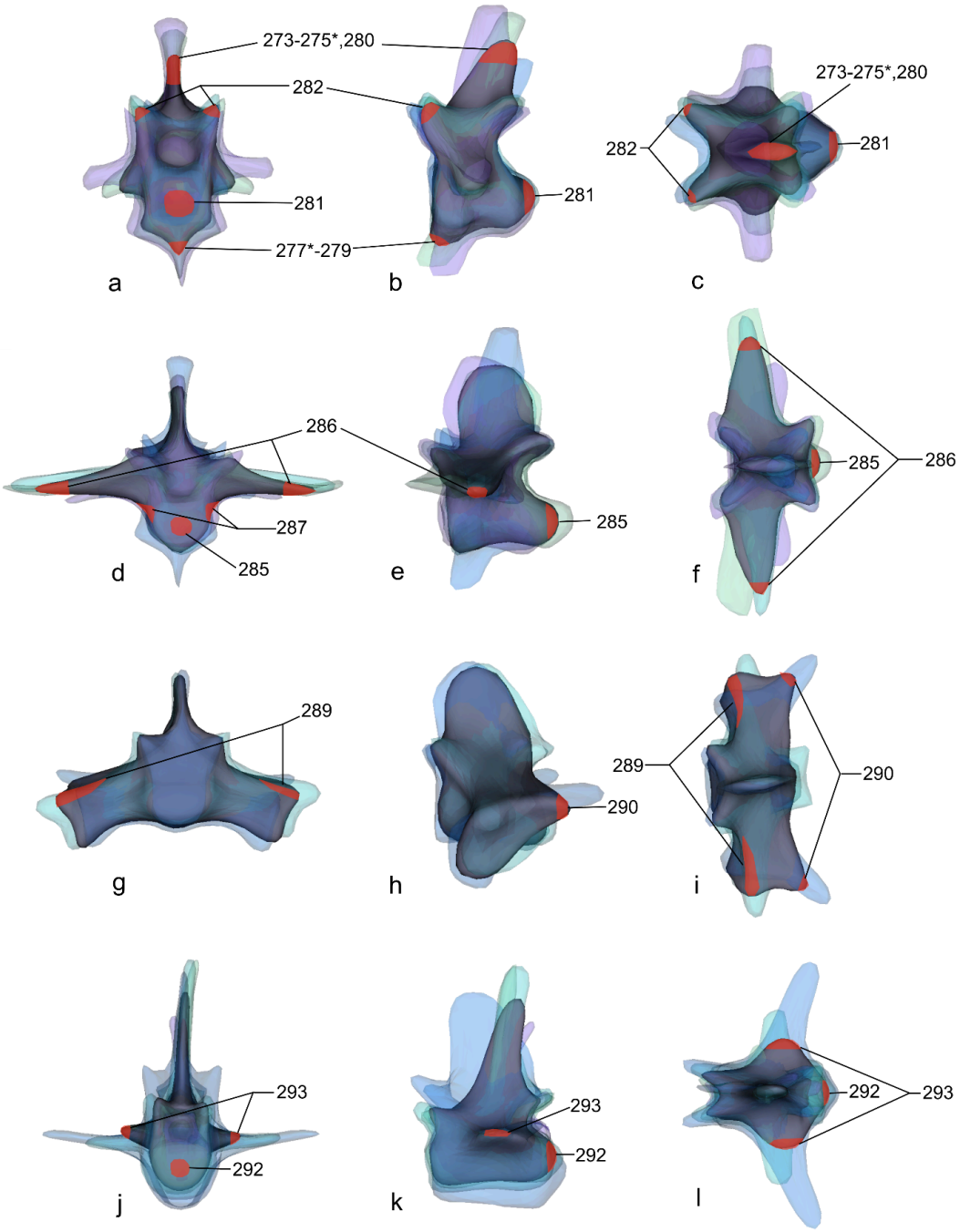

Figure 3.1. Regional variation amongst the cervicals (a-c), dorsals (d-f), sacrals (g-i), and caudals (j-l) in anterior, left lateral, and dorsal views. Discrete characters are mapped in red and labeled according to Rio and Mannion's (2021) morphological character list. The darkest vertebrae

represents the ‘mean’ shape of each region. Character numbers with an asterisk (*) apply solely to the axis.

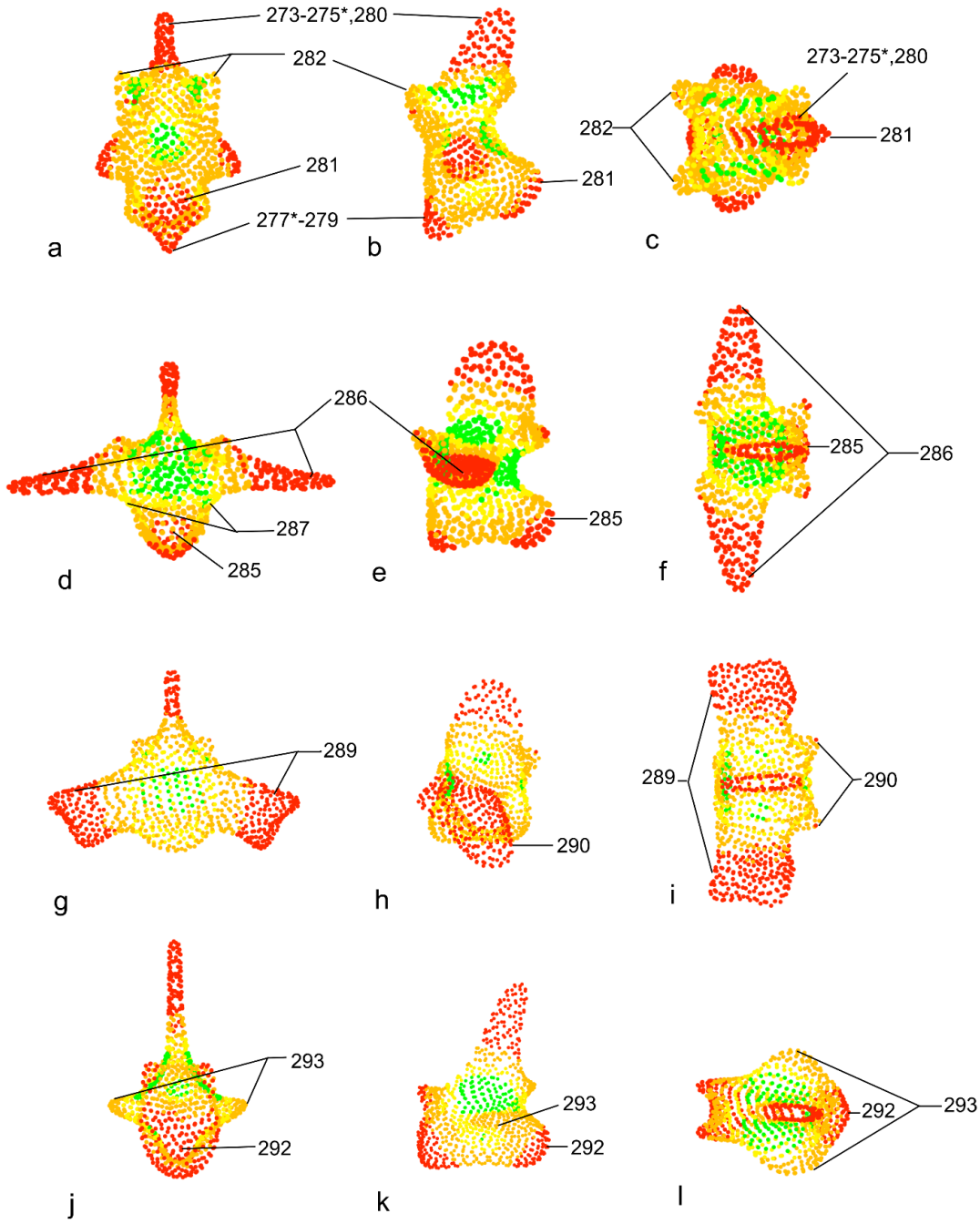

Figure 3.2. Average landmark surface variation calculated for each region using SPHARM-PDM landmarks. Individual landmark variation was calculated using the centroid size for each

landmark and assigning a color value to represent highest centroid size in red and lowest centroid size in green. Discrete characters are labeled according to Rio and Mannion's (2021) morphological character list. Character numbers with an asterisk (*) apply solely to the axis.

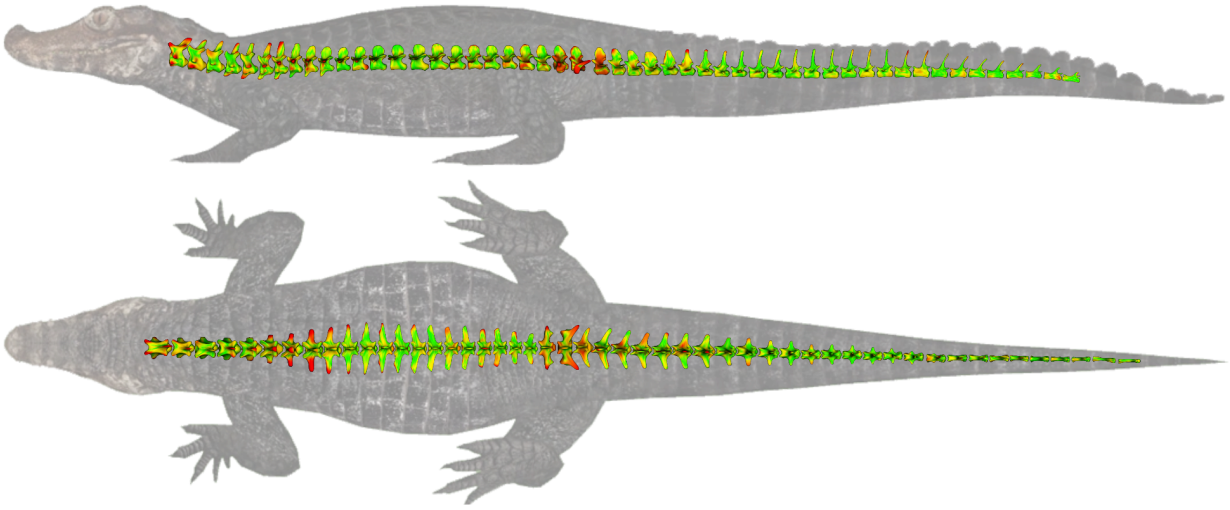

Figure 3.3. Dorsal and lateral sequential variation within the *Caiman* axial column. Regions of high variation are colored in red, and the lowest variation in green. Differences are mapped based on the vertebrae anterior to the vertebrae in question.

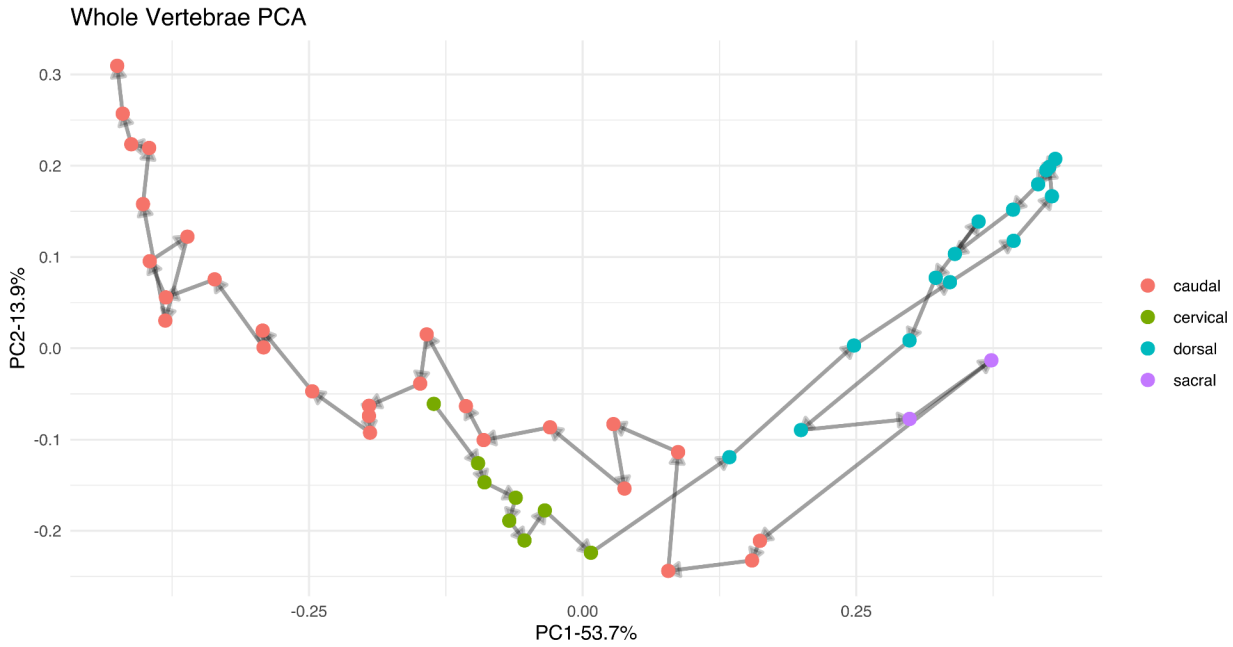

Figure 3.4. Morphospace occupation was visualized by mapping PC1 vs PC2. Regions are marked by color and anterior to posterior direction is visualized by light gray arrows.

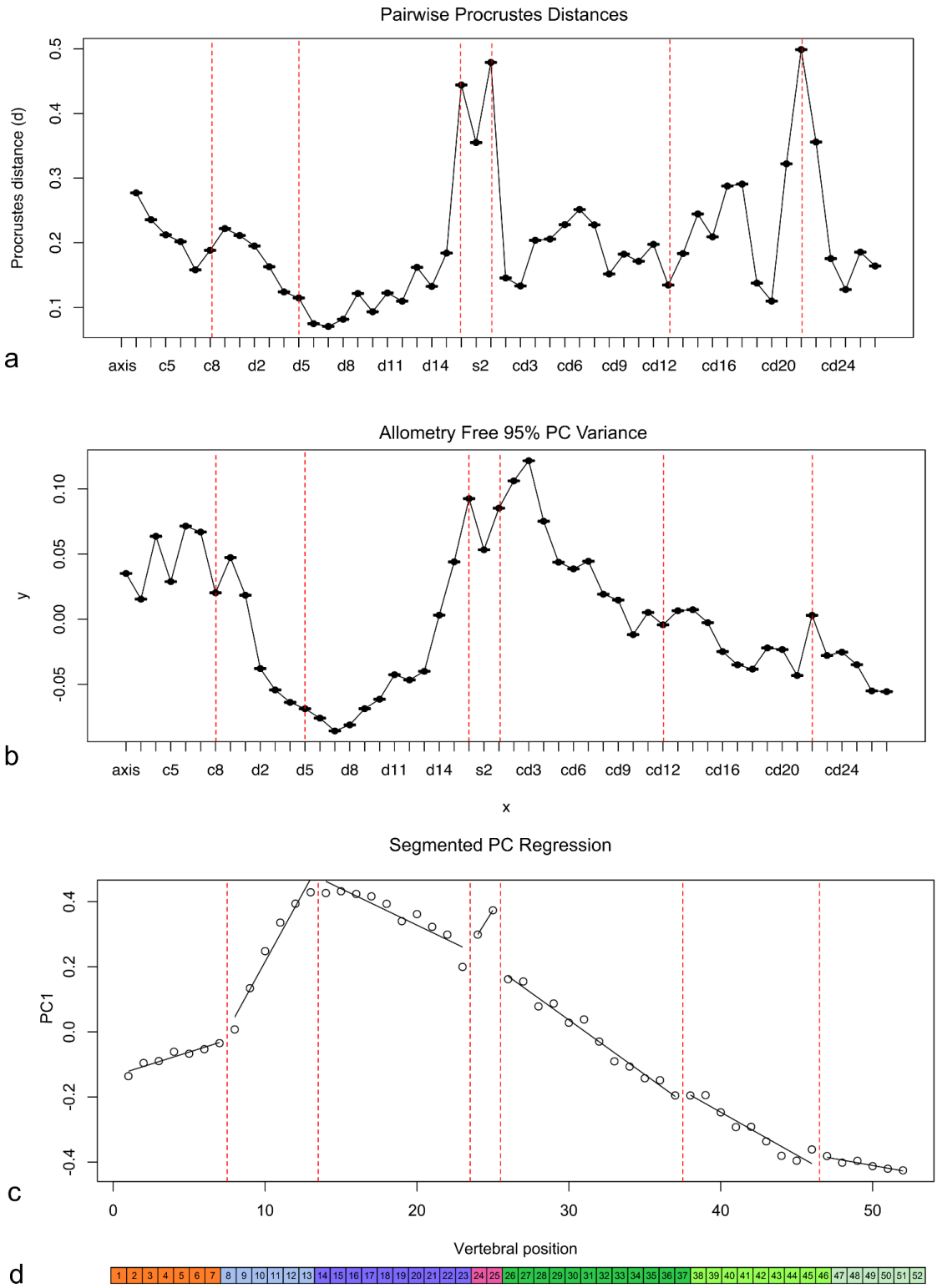

Figure 3.5. Sequential variation exploration using Procrustes distances (a), allometry-free PC variance (b), and segmented regressions to visualize regionalization using methodology provided by Jones et al. (2018) (c & d).

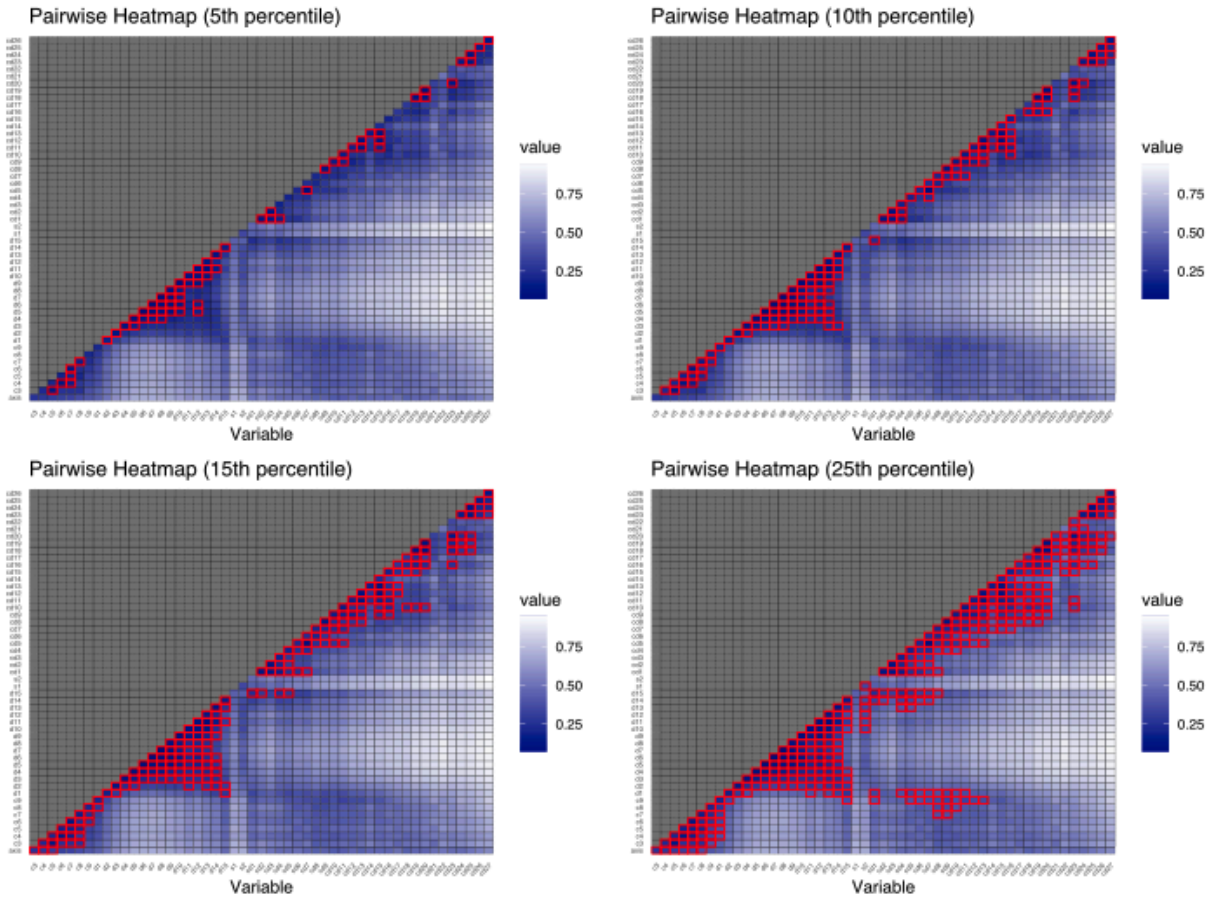

Figure 3.6. Exploring integration and modularity utilizing pairwise procrustes distances. The lowest percentile (5th, 10th, 15th, and 25th) of the data are mapped and outlined in red, with dark blue representing the lowest distances and white representing the highest.

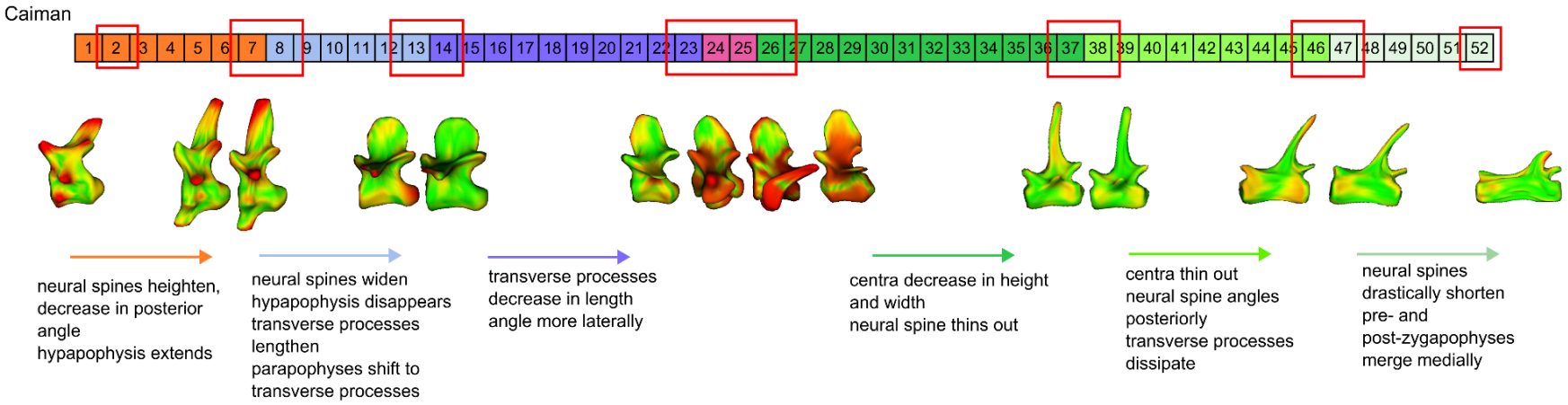

Figure 3.7. Transitional vertebra along the *Caiman crocodilus* vertebral column using SPHARM derived models. Variation is reflected by low variation in green and high variation in red. Variation is based on a Model-to-model absolute distance between preceding vertebrae. Rows of boxes represent our regionalization model, with groups of vertebrae represented by the outlined boxes,specifically those in transitional roles.

References

Adams, D. C., & Nistri, A. (2010). Ontogenetic convergence and evolution of foot morphology in European cave salamanders (Family: Plethodontidae). *BMC Evolutionary Biology, 10*, 1-10.

Adams, D. C., & Otárola‐Castillo, E. (2013). geomorph: an R package for the collection and analysis of geometric morphometric shape data. *Methods in ecology and evolution, 4*(4), 393-399.

Alvarez, A., Ercoli, M. D., & Prevosti, F. J. (2013). Locomotion in some small to medium-sized mammals: a geometric morphometric analysis of the penultimate lumbar vertebra, pelvis and hindlimbs. *Zoology, 116*(6), 356-371.

Arratia, G., Schultze, H. P., & Casciotta, J. (2001). Vertebral column and associated elements in dipnoans and comparison with other fishes: development and homology. *Journal of morphology, 250*(2), 101-172.

Bardua, C., Felice, R. N., Watanabe, A., Fabre, A.-C., & Goswami, A. (2019). A practical guide to sliding and surface semilandmarks in morphometric analyses. *Integrative Organismal Biology, 1*(1), obz016.

Bell, A., Marugán-Lobón, J., Navalón, G., Nebreda, S. M., DiGuildo, J., & Chiappe, L. M. (2021). Quantitative analysis of morphometric data of pre-modern birds: phylogenetic versus ecological signal. *Frontiers in Earth Science, 9*, 663342.

Berio, F., Bayle, Y., Riley, C., Larouche, O., & Cloutier, R. (2022). Phenotypic regionalization of the vertebral column in the thorny skate Amblyraja radiata: Stability and variation. *Journal of Anatomy, 240*(2), 253-267.

Böhmer, C., Rauhut, O. W., & Wörheide, G. (2015). Correlation between Hox code and vertebral morphology in archosaurs. *Proceedings of the Royal Society B: Biological Sciences, 282*(1810), 20150077.

Bookstein, F. L. (1997). *Morphometric tools for landmark data*.

Brochu, C. A. (1999). Phylogenetics, taxonomy, and historical biogeography of Alligatoroidea. *Journal of Vertebrate Paleontology, 19*(S2), 9-100.

Brocklehurst, R. J., Moritz, S., Codd, J., Sellers, W. I., & Brainerd, E. L. (2017). Rib kinematics during lung ventilation in the American alligator (Alligator mississippiensis): an XROMM analysis. *Journal of Experimental Biology, 220*(17), 3181-3190.

Brusatte, S. L., Benton, M. J., Lloyd, G. T., Ruta, M., & Wang, S. C. (2010). Macroevolutionary patterns in the evolutionary radiation of archosaurs (Tetrapoda: Diapsida). *Earth and Environmental Science Transactions of the Royal Society of Edinburgh, 101*(3-4), 367-382.

Buchholtz, E. A. (1998). Implications of vertebral morphology for locomotor evolution in early Cetacea. In *The emergence of whales: evolutionary patterns in the origin of Cetacea* (pp. 325-351): Springer.

Buchholtz, E. A. (2007). Modular evolution of the cetacean vertebral column. *Evolution & development, 9*(3), 278-289.

Carro, S. C. S., Louys, J., & O'Connor, S. (2018). Shape does matter: A geometric morphometric approach to shape variation in Indo-Pacific fish vertebrae for habitat identification. *Journal of Archaeological Science, 99*, 124-134.

Chamero, B., Buscalioni, Á. D., Marugán‐Lobón, J., & Sarris, I. (2014). 3D geometry and quantitative variation of the cervico‐thoracic region in Crocodylia. *The Anatomical Record, 297*(7), 1278-1291.

Cooke, S. B., & Terhune, C. E. (2015). Form, function, and geometric morphometrics. *The Anatomical Record, 298*(1), 5-28.

Collyer, M. L., & Adams, D. C. (2018). RRPP: An r package for fitting linear models to high‐dimensional data using residual randomization. Methods in ecology and evolution, 9(7), 1772-1779.

De Beer, G. (1954). Archaeopteryx lithographica: A study based upon the British Museum specimen. (No Title).

Dragonfly 2022.2 [Computer software]. Comet Technologies Canada Inc., Montreal, Canada; software available at https://www.theobjects.com/dragonfly.

Drake, A. G., & Klingenberg, C. P. (2010). Large-scale diversification of skull shape in domestic dogs: disparity and modularity. *The american naturalist, 175*(3), 289-301.

Ege, Y. C., Foth, C., Baum, D., Wirkner, C. S., & Richter, S. (2020). Adapting spherical-harmonics-based geometric morphometrics (SPHARM) for 3D images containing large cavity openings using ambient occlusion: a study with hermit crab claw shape variability. *Zoomorphology, 139*, 421-432.

Fabre, A.-C., Cornette, R., Peigné, S., & Goswami, A. (2013). Influence of body mass on the

shape of forelimb in musteloid carnivorans. *Biological Journal of the Linnean Society, 110*(1), 91-103.

Fabre, A. C., Cornette, R., Huyghe, K., Andrade, D. V., & Herrel, A. (2014). Linear versus geometric morphometric approaches for the analysis of head shape dimorphism in lizards. *Journal of morphology, 275*(9), 1016-1026.

Felice, R. N., Pol, D., & Goswami, A. (2021). Complex macroevolutionary dynamics underly the evolution of the crocodyliform skull. *Proceedings of the Royal Society B, 288*(1954), 20210919.

Foth, C., & Rauhut, O. W. (2013). Macroevolutionary and morphofunctional patterns in theropod skulls: a morphometric approach. *Acta Palaeontologica Polonica, 58*(1), 1-16.

Gerber, S. (2019). Use and misuse of discrete character data for morphospace and disparity analyses. *Palaeontology, 62*(2), 305-319.

Godoy, P. L. (2020). Crocodylomorph cranial shape evolution and its relationship with body size and ecology. *Journal of Evolutionary Biology, 33*(1), 4-21.

Goswami, A. (2006). Morphological integration in the carnivoran skull. *Evolution, 60*(1), 169-183.

Head, J. J., & Polly, P. D. (2015). Evolution of the snake body form reveals homoplasy in amniote Hox gene function. *Nature, 520*(7545), 86-89.

Hetherington, A. J., Sherratt, E., Ruta, M., Wilkinson, M., Deline, B., & Donoghue, P. C. (2015). Do cladistic and morphometric data capture common patterns of morphological disparity? *Palaeontology, 58*(3), 393-399.

Janvier, P. (1996). *Early vertebrates*: Oxford University Press.

Jones, K. E., Angielczyk, K. D., Polly, P. D., Head, J. J., Fernandez, V., Lungmus, J. K., . . . Pierce, S. E. (2018). Fossils reveal the complex evolutionary history of the mammalian regionalized spine. *Science, 361*(6408), 1249-1252.

Jones, K. E., Gonzalez, S., Angielczyk, K. D., & Pierce, S. E. (2020). Regionalization of the axial skeleton predates functional adaptation in the forerunners of mammals. *Nature ecology & evolution, 4*(3), 470-478.

Kikinis, R., Pieper, S. D., & Vosburgh, K. G. (2013). 3D Slicer: a platform for subject-specific image analysis, visualization, and clinical support. In *Intraoperative imaging and image-guided therapy* (pp. 277-289): Springer.

Langston, W., Gans, C., & Parsons, T. (1973). The crocodilian skull in historical perspective. *Biology of the Reptilia, 4*, 263-284.

Lowie, A., De Kegel, B., Wilkinson, M., Measey, J., O'Reilly, J. C., Kley, N. J., . . . Herrel, A. (2022). Regional differences in vertebral shape along the axial skeleton in caecilians (Amphibia: Gymnophiona). *Journal of Anatomy, 241*(3), 716-728.

MacLeod, N. (1999). Generalizing and extending the eigenshape method of shape space visualization and analysis. *Paleobiology, 25*(1), 107-138.

Mansfield, J. H., & Abzhanov, A. (2010). Hox expression in the American alligator and evolution of archosaurian axial patterning. *Journal of Experimental Zoology Part B: Molecular and Developmental Evolution, 314*(8), 629-644.

Marchesi, M. C., Mora, M. S., Dans, S. L., & González-José, R. (2021). Allometry and ontogeny in the vertebral column of southern hemisphere dolphins: a 3D morphofunctional approach. *Journal of Mammalian Evolution, 28*(1), 125-134.

Martín-Serra, A., Figueirido, B., & Palmqvist, P. (2014). A three-dimensional analysis of morphological evolution and locomotor performance of the carnivoran forelimb. *PLoS One, 9*(1), e85574.

Martín-Serra, A., Pérez-Ramos, A., Pastor, F. J., Velasco, D., & Figueirido, B. (2021). Phenotypic integration in the carnivoran backbone and the evolution of functional differentiation in metameric structures. *Evolution Letters, 5*(3), 251-264.

McPeek, M. A., Shen, L., & Farid, H. (2009). The correlated evolution of three-dimensional reproductive structures between male and female damselflies. *Evolution, 63*(1), 73-83.

McPeek, M. A., Shen, L., Torrey, J. Z., & Farid, H. (2008). The tempo and mode of three-dimensional morphological evolution in male reproductive structures. *The american naturalist, 171*(5), E158-E178.

Meachen‐Samuels, J., & Van Valkenburgh, B. (2009). Forelimb indicators of prey‐size preference in the Felidae. *Journal of morphology, 270*(6), 729-744.

Meyer, E. R. (1984). Crocodilians as living fossils. In *Living fossils* (pp. 105-131): Springer.

Mitteroecker, P., & Gunz, P. (2009). Advances in geometric morphometrics. *Evolutionary biology, 36*, 235-247.

Mitteroecker, P., Gunz, P., Teschler-Nicola, M., & Weber, G. (2004). New morphometric methods in Paleopathology: Shape analysis of a Neolithic Hydrocephalus.

Moczek, A. P. (2008). On the origins of novelty in development and evolution. *BioEssays, 30*(5), 432-447.

Molnar, J., & Watanabe, A. (2023). Morphological and functional regionalization of trunk vertebrae as an adaptation for arboreal locomotion in chameleons. *Royal Society Open Science, 10*(3), 221509.

Molnar, J. L., Pierce, S. E., Bhullar, B.-A. S., Turner, A. H., & Hutchinson, J. R. (2015). Morphological and functional changes in the vertebral column with increasing aquatic adaptation in crocodylomorphs. *Royal Society Open Science, 2*(11), 150439.

Morris, Z. S., Vliet, K. A., Abzhanov, A., & Pierce, S. E. (2019). Heterochronic shifts and conserved embryonic shape underlie crocodylian craniofacial disparity and convergence. *Proceedings of the Royal Society B, 286*(1897), 20182389.

Müller, J., Scheyer, T. M., Head, J. J., Barrett, P. M., Werneburg, I., Ericson, P. G., . . . Sánchez-Villagra, M. R. (2010). Homeotic effects, somitogenesis and the evolution of vertebral numbers in recent and fossil amniotes. *Proceedings of the National Academy of Sciences, 107*(5), 2118-2123.

Narváez, I., Brochu, C. A., Escaso, F., Pérez-García, A., & Ortega, F. (2015). New crocodyliforms from southwestern Europe and definition of a diverse clade of European Late Cretaceous basal eusuchians. PLoS One, 10(11), e0140679.

Neige, P. (2003). Spatial patterns of disparity and diversity of the Recent cuttlefishes (Cephalopoda) across the Old World. *Journal of Biogeography, 30*(8), 1125-1137.

Openshaw, G. H., D'Amore, D. C., Vidal-García, M., & Keogh, J. S. (2017). Combining geometric morphometric analyses of multiple 2D observation views improves interpretation of evolutionary allometry and shape diversification in monitor lizard (Varanus) crania. *Biological Journal of the Linnean Society, 120*(3), 539-552.

Palci, A., Caldwell, M. W., Hutchinson, M. N., Konishi, T., & Lee, M. S. (2020). The morphological diversity of the quadrate bone in squamate reptiles as revealed by high‐resolution computed tomography and geometric morphometrics. *Journal of Anatomy, 236*(2), 210-227.

Pierce, S., Clack, J., & Hutchinson, J. (2011). Comparative axial morphology in pinnipeds and its correlation with aquatic locomotory behaviour. *Journal of Anatomy, 219*(4), 502-514.

Pierce, S. E., Angielczyk, K. D., & Rayfield, E. J. (2008). Patterns of morphospace occupation

and mechanical performance in extant crocodilian skulls: a combined geometric morphometric and finite element modeling approach. *Journal of morphology, 269*(7), 840-864.

Pintore, R., Houssaye, A., Nesbitt, S. J., & Hutchinson, J. R. (2022). Femoral specializations to locomotor habits in early archosauriforms. *Journal of Anatomy, 240*(5), 867-892.

Piras, P., Buscalioni, A. D., Teresi, L., Raia, P., Sansalone, G., Kotsakis, T., & Cubo, J. (2014). Morphological integration and functional modularity in the crocodilian skull. *Integrative zoology, 9*(4), 498-516.

Polly, P. D. (2008). Adaptive zones and the pinniped ankle: a three-dimensional quantitative analysis of carnivoran tarsal evolution. In *Mammalian evolutionary morphology: A tribute to Frederick S. Szalay* (pp. 167-196): Springer.

Polly, P. D., Head, J. J., & Cohn, M. J. (2001). Testing modularity and dissociation: the evolution of regional proportions in snakes. *Beyond heterochrony: the evolution of development*, 307-335.

Polly, P. D., & MacLeod, N. (2008). Locomotion in fossil Carnivora: an application of eigensurface analysis for morphometric comparison of 3D surfaces. *Palaeontologia Electronica, 11*(2), 10-13.

Preuschoft, H., & Klein, N. (2013). Torsion and bending in the neck and tail of sauropod dinosaurs and the function of cervical ribs: insights from functional morphology and biomechanics. *PLoS One, 8*(10), e78574.

Price, S. A., Wainwright, P. C., Bellwood, D. R., Kazancioglu, E., Collar, D. C., & Near, T. J. (2010). Functional innovations and morphological diversification in parrotfish. *Evolution, 64*(10), 3057-3068.

Ramírez, M. J., & Michalik, P. (2014). Calculating structural complexity in phylogenies using ancestral ontologies. *Cladistics, 30*(6), 635-649.

Randau, M., Cuff, A. R., Hutchinson, J. R., Pierce, S. E., & Goswami, A. (2017). Regional differentiation of felid vertebral column evolution: a study of 3D shape trajectories. *Organisms Diversity & Evolution, 17*, 305-319.

Randau, M., Goswami, A., Hutchinson, J. R., Cuff, A. R., & Pierce, S. E. (2016). Cryptic complexity in felid vertebral evolution: shape differentiation and allometry of the axial skeleton. *Zoological Journal of the Linnean Society, 178*(1), 183-202.

Ricklefs, R. E. (2004). Cladogenesis and morphological diversification in passerine birds. *Nature, 430*(6997), 338-341.

Rio, J. P., & Mannion, P. D. (2021). Phylogenetic analysis of a new morphological dataset elucidates the evolutionary history of Crocodylia and resolves the long-standing gharial problem. *PeerJ, 9*, e12094.

Ripley, B., Venables, B., Bates, D. M., Hornik, K., Gebhardt, A., Firth, D., & Ripley, M. B. (2013). Package 'mass'. Cran r, 538, 113-120.

Rohlf, F. J., & Archie, J. W. (1984). A comparison of Fourier methods for the description of wing shape in mosquitoes (Diptera: Culicidae). *Systematic Zoology, 33*(3), 302-317.

Romer, A. S. (1956). The early evolution of land vertebrates. *Proceedings of the American Philosophical Society*, 100(3), 157-167.

Salisbury, S. W., & Frey, E. (2001). A biomechanical transformation model for the evolution of semi-spheroidal articulations between adjoining vertebral bodies in crocodilians. *Crocodilian biology and evolution*, 85-134.

Sallan, L. C. (2012). Tetrapod-like axial regionalization in an early ray-finned fish. *Proceedings of the Royal Society B: Biological Sciences, 279*(1741), 3264-3271.

Schaeffer, J., Benton, M. J., Rayfield, E. J., & Stubbs, T. L. (2020). Morphological disparity in theropod jaws: comparing discrete characters and geometric morphometrics. *Palaeontology, 63*(2), 283-299.

Scheyer, T. M., Hutchinson, J. R., Strauss, O., Delfino, M., Carrillo-Briceño, J. D., Sanchez, R., & Sánchez-Villagra, M. R. (2019). Giant extinct caiman breaks constraint on the axial skeleton of extant crocodylians. *Elife, 8*, e49972.

Scholtes, S. J., Arntzen, J. W., Ajduković, M., & Ivanović, A. (2022). Variation in vertebrae shape across small‐bodied newts reveals functional and developmental constraints acting upon the trunk region. *Journal of Anatomy, 240*(4), 639-646.

Shen, L., Farid, H., & McPeek, M. A. (2009). Modeling three-dimensional morphological structures using spherical harmonics. *Evolution, 63*(4), 1003-1016.

Stayton, C. T. (2005). Morphological evolution of the lizard skull: a geometric morphometrics survey. *Journal of morphology, 263*(1), 47-59.

Stein, M. D., Hand, S. J., Archer, M., Wroe, S., & Wilson, L. A. (2020). Quantitatively assessing mekosuchine crocodile locomotion by geometric morphometric and finite element

analysis of the forelimb. *PeerJ, 8*, e9349.

Tarasov, S. (2019). Integration of anatomy ontologies and evo-devo using structured Markov models suggests a new framework for modeling discrete phenotypic traits. *Systematic biology, 68*(5), 698-716.

Tobias, J. A., Cornwallis, C. K., Derryberry, E. P., Claramunt, S., Brumfield, R. T., & Seddon, N. (2014). Species coexistence and the dynamics of phenotypic evolution in adaptive radiation. *Nature, 506*(7488), 359-363.

Tokita, M., Yano, W., James, H. F., & Abzhanov, A. (2017). Cranial shape evolution in adaptive radiations of birds: comparative morphometrics of Darwin's finches and Hawaiian honeycreepers. *Philosophical Transactions of the Royal Society B: Biological Sciences, 372*(1713), 20150481.

Van Bocxlaer, I., Loader, S. P., Roelants, K., Biju, S., Menegon, M., & Bossuyt, F. (2010). Gradual adaptation toward a range-expansion phenotype initiated the global radiation of toads. *Science, 327*(5966), 679-682.

Vicory, J., Pascal, L., Hernandez, P., Fishbaugh, J., Prieto, J., Mostapha, M., . . . Liu, Z. (2018). *Slicersalt: Shape analysis toolbox.* Paper presented at the Shape in Medical Imaging: International Workshop, ShapeMI 2018, Held in Conjunction with MICCAI 2018, Granada, Spain, September 20, 2018, Proceedings.

Villier, L., & Eble, G. J. (2004). Assessing the robustness of disparity estimates: the impact of morphometric scheme, temporal scale, and taxonomic level in spatangoid echinoids. *Paleobiology, 30*(4), 652-665.

Werneburg, I., Wilson, L. A., Parr, W. C., & Joyce, W. G. (2015). Evolution of neck vertebral shape and neck retraction at the transition to modern turtles: an integrated geometric morphometric approach. *Systematic biology, 64*(2), 187-204.

Wiens, J. J. (2001). Character analysis in morphological phylogenetics: problems and solutions. *Systematic biology, 50*(5), 689-699.

Appendix B

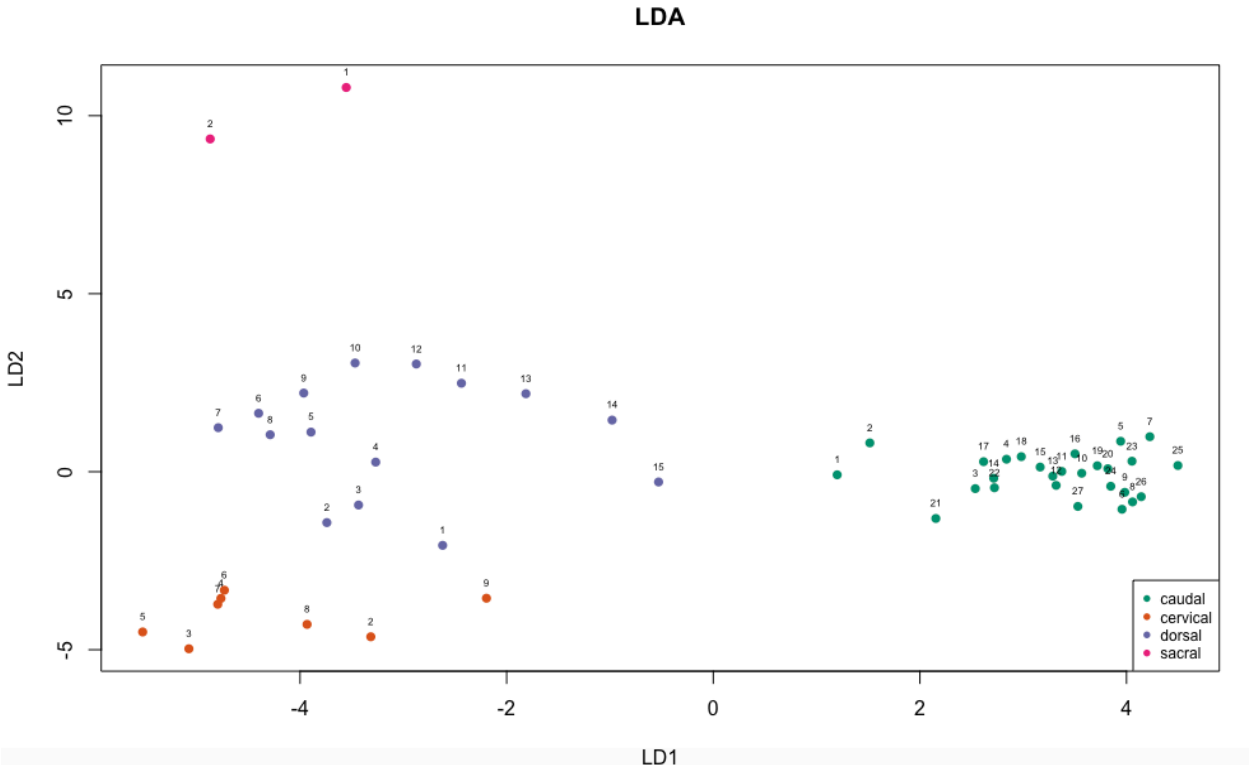

Appendix B1. Linear discriminant analysis was conducted on all vertebrae in the axial column to determine correct grouping among regions. All vertebrae were plotted and classified based on region, and cross-referenced with anatomical markers to determine grouping accuracy of the SPHARM models provided.

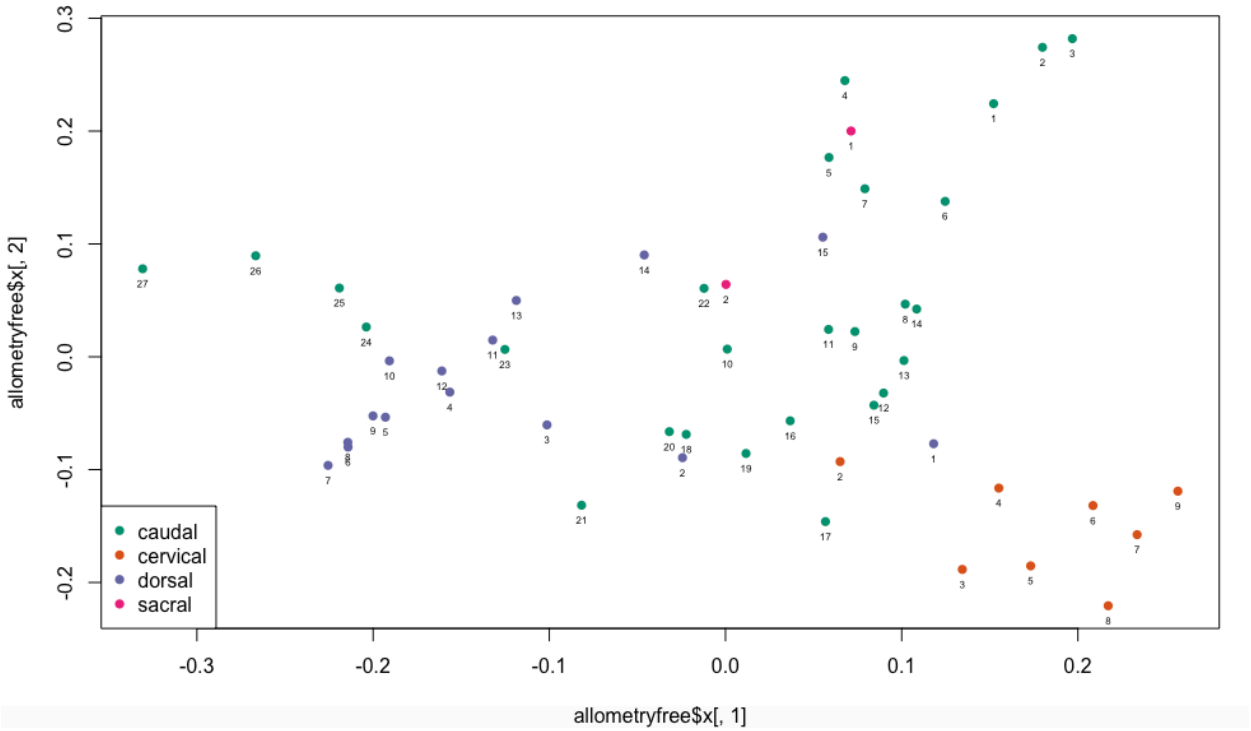

Appendix B2. PC1 and PC2 after size was removed from the analysis. We allowed size to remain in our general analyses as each vertebrae belonged to a single individual. Shape variation including size was inherent, but exploratory patterns were visualized to help assess general patterns in variation.

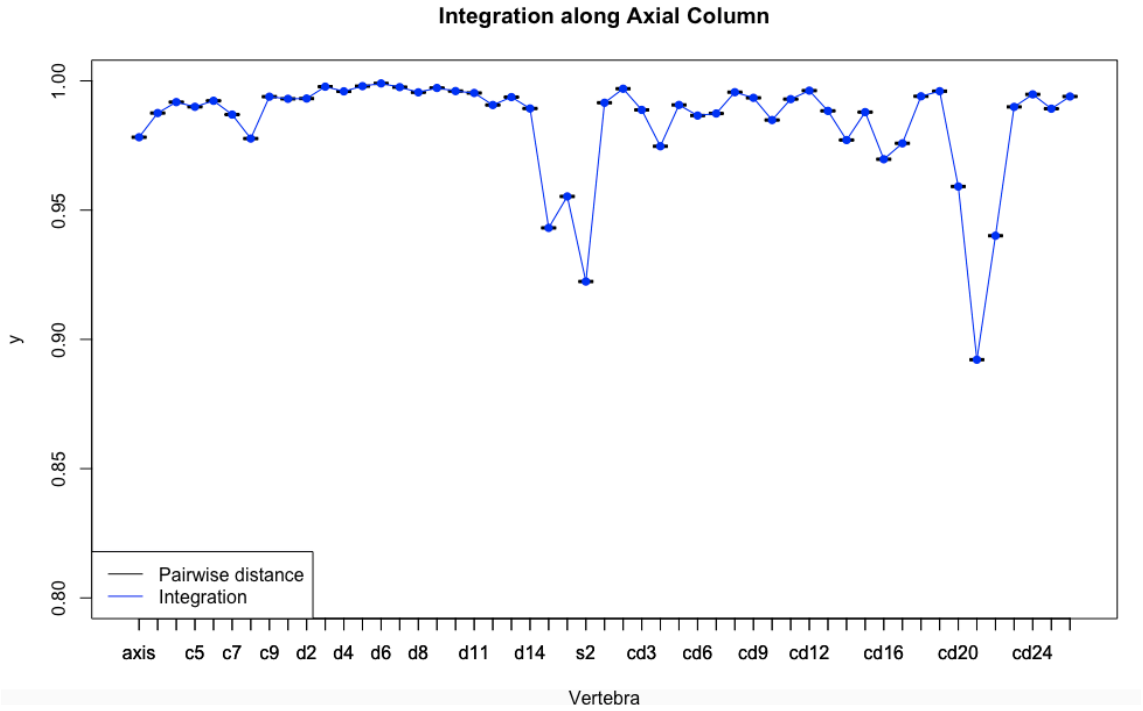

Appendix B3. Integration along the axial column was plotted revealing high integration along the axial column except for dips around the dorsal-sacral transition and a mid-caudal region. Integration was the most stable throughout the dorsals, as the cervicals and caudals see more varied covariation between vertebrae.

Appendix B4. Table of integration scores, distances, and Z-scores between pairwise vertebrae.

A	B	d	UCL	r.pls	Z	P.value
axis	c3	0.277086886423655	0.840672862235318	0.978193475101197	13.7906040705774	0.001
c3	c4	0.235643778080588	0.824428928837857	0.987552029446745	13.8111498919834	0.001
c4	c5	0.212203280721312	0.817207838345477	0.991784247887814	15.200416271175	0.001
c5	c6	0.201786171460189	0.836177123837776	0.989968295460478	14.98905650985	0.001
c6	c7	0.158133526138301	0.844640565263023	0.99229818114961	15.2022368539082	0.001
c7	c8	0.188356935834735	0.844640565263021	0.986960026533113	15.1393509680334	0.001
c8	c9	0.22190761738427	0.826489680913076	0.977690235987822	15.615822500318	0.001
c9	d1	0.211190701259717	0.837099100233434	0.99387643996168	12.9831994059366	0.001
d1	d2	0.194991119731673	0.831763594179004	0.993058303732991	14.1708368332115	0.001
d2	d3	0.162914459051355	0.846144313596295	0.99316603838834	14.6522535493459	0.001
d3	d4	0.123924841940095	0.830783585948102	0.997753758069329	16.0662424868119	0.001
d4	d5	0.1146401816785	0.841666721936595	0.995952465271005	14.3687719427894	0.001
d5	d6	0.0748721247337736	0.837390748221595	0.997954550629176	15.0103973909474	0.001
d6	d7	0.0704832350683948	0.837308706741445	0.999015104373942	15.6445811466673	0.001
d7	d8	0.0816144630806755	0.821311058746974	0.997572355558123	15.29911683881	0.001
d8	d9	0.121571437007091	0.807709017879191	0.995571948031074	15.0135805701775	0.001
d9	d10	0.0932611128219265	0.842913467416186	0.997253336288251	13.597660448065	0.001
d10	d11	0.122304918009779	0.824276314857739	0.996054930214397	13.5466460936163	0.001
d11	d12	0.109640432244313	0.840672862235322	0.995316881155705	15.7315902090982	0.001
d12	d13	0.161987894712144	0.835856125526459	0.990659748751313	14.4182007222294	0.001
d13	d14	0.132454491949708	0.828898663903187	0.993720740702533	16.7559125680641	0.001
d14	d15	0.18396482679589	0.844494030431742	0.989310741531729	16.1422762061098	0.001
d15	s1	0.444016112724495	0.846533087785697	0.943129071198197	12.6501349260858	0.001
s1	s2	0.355003282389883	0.8475240756444	0.955297101657921	16.4859738768279	0.001
s2	cd1	0.478993879852151	0.842913467416186	0.922387989867558	14.5316237845857	0.001
cd1	cd2	0.145485804021281	0.835877104786913	0.991536138256584	17.6150371172826	0.001
cd2	cd3	0.133195281641791	0.830583659600552	0.996961259188647	17.566680216326	0.001

cd3	cd4	0.203802245834592	0.828980334719028	0.988771471599946	15.4380879323189	0.001
cd4	cd5	0.205695071194148	0.850183438225044	0.974700500776533	15.1214843170659	0.001
cd5	cd6	0.22803896031338	0.837842636475882	0.990685513958057	16.6481921025717	0.001
cd6	cd7	0.251481739722384	0.834363412196389	0.986578445769708	17.1861611660598	0.001
cd7	cd8	0.227629853858795	0.837739694457486	0.987386986107066	14.6423341052126	0.001
cd8	cd9	0.151705677584235	0.852784217774352	0.995615630510676	15.0577814143061	0.001
cd9	cd10	0.182311197564892	0.837842636475884	0.993435921425289	13.6949451569748	0.001
cd10	cd11	0.171279695934122	0.829031914099602	0.984851455854365	15.187521123207	0.001
cd11	cd12	0.197478682208203	0.837712376645363	0.992939214776322	15.8521520711136	0.001
cd12	cd13	0.134505610997981	0.80770901787919	0.996218196268034	16.0035775777608	0.001
cd13	cd14	0.183348639274736	0.837346725842422	0.988392606110387	14.1946522116978	0.001
cd14	cd15	0.244507473328384	0.845683640460362	0.97711445787982	12.9008501672407	0.001
cd15	cd16	0.209119659597125	0.848237806276276	0.987914159119972	13.2789668396818	0.001
cd16	cd17	0.287720572173666	0.820607219160121	0.969686067413612	11.7904208364702	0.001
cd17	cd18	0.290705458743936	0.830532080219974	0.975844827997432	13.2282912457729	0.001
cd18	cd19	0.137492981861548	0.842913467416186	0.994037366535996	11.7872792594675	0.001
cd19	cd20	0.109735970668086	0.819603358841353	0.996001162411974	11.9265987169189	0.001
cd20	cd21	0.32212869687836	0.834362962163521	0.959136662852887	13.560297091721	0.001
cd21	cd22	0.498840788536456	0.842992251210231	0.89214598307036	10.9575452328618	0.001
cd22	cd23	0.35572795942721	0.837408195533392	0.94009944599505	10.4082158085726	0.001
cd23	cd24	0.175444340704472	0.834953241060106	0.989936874244898	11.5566688561636	0.001
cd24	cd25	0.127593252128425	0.845068842974922	0.994778424791124	11.6905164392244	0.001
cd25	cd26	0.185561260924645	0.836173888590883	0.989231174145289	12.8460867064629	0.001
cd26	cd27	0.164045718229953	0.828898663903189	0.99395753176911	11.1397327310835	0.001

Bridging Text

Chapters 2 and 3 employ different methodologies to explore the axial columns of Archosauria. Chapter 3 outlines a novel approach for quantifying axial column variation within a single species, *Caiman crocodilus*, utilizing high resolution 3D models to analyze whole surface morphology. This approach establishes a comprehensive framework for inferring modularity and integration across the entire axial column, contrasting the efficacy of discrete anatomical characters with surface models in capturing morphological variation and quantifying modularity. Chapters 2 and 3 represent a transition from qualitative characters to the quantification of variation, providing a direct comparison between discrete characters and surface variation within the axial column.

Building on these insights, Chapter 4 extends this methodology across a broader spectrum of taxa within Crocodylia. Utilizing the established approach in Chapter 3, this study aims to assess its effectiveness in quantifying axial column variation across species. Utilizing a similar framework, I quantify shape variation and determine modularity and integration within each taxa. I identify regional and modularity differences among taxa, as well as establish a statistical framework for comparisons and future studies. Our results reveal greater complexity than previously thought, with regionalization and modularity reflecting different ecological and functional roles within each taxa. This approach not only enhances our understanding of vertebral morphology and its evolutionary implications, but also emphasizes the intricate adaptations within Crocodylian axial skeletons.

Chapter 4
Axial column variation, regionalization, and modularity in Crocodylia

Abstract

Crocodylians have traditionally been viewed as having relatively typical axial columns divided into a cervical, dorsal, sacral, and caudal series. This study utilizes a novel, whole surface methodology to investigate anatomical regionalization, integration, and modularity within the axial skeletons of five species distributed among extant Crocodylia. Our analysis reveals significant regional and morphological diversity across different taxa. I employ spherical harmonic modeling to quantify shape variation, calculate Procrustes distances, and perform regression models and pairwise tests. The results demonstrate a high degree of variation, with regional boundaries varying by one or two vertebrae among taxa. Our modularity exploration identified differing degrees of modularity among taxa and up to two cervical modules, up to five dorsal modules, and up to two caudal modules among taxa. Functional considerations, including locomotion, respiration, and the 'death roll' behavior, were explored in the framework of vertebral morphology, modularity, and regional transitions. The innovative use of spherical harmonics and complete surface analysis enables a detailed, objective comparison of axial columns, highlighting the complex evolutionary history and functional adaptations in Crocodylia. Despite the challenges in processing times and troubleshooting, this methodology allows for comprehensive analyses with minimal subjectivity, offering new insights into vertebral morphology and its evolutionary implications. This work underscores the intricate and varied nature of crocodylian axial skeletons, paving the way for further research integrating more taxa, molecular data, and ontogenetic studies.

Introduction

The axial column serves as a remarkable window into the intricate tapestry of development and evolution in vertebrates. The axial column and elemental vertebrae are an evolutionary novelty of Vertebrata and have been conserved over 400 million years (Janvier, 1996). Morphological variation in the vertebral column provides insights into evolutionary trends among vertebrates specifically as it plays a fundamental role in skeletal support and locomotion, making them ecologically and functionally significant (Buccholtz, 1998; Jones et al., 2020; Marchesi et al., 2021; Randau et al 2016). Limited morphometric studies of vertebral form have demonstrated ecological specializations and developmental patterning reflected in the morphology of individual vertebrae, as well as along the entire spine (Böhmer et al. 2015; Chen et al. 2005; Head & Polly, 2015; Jones and German, 2014; Jones & Pierce 2016; Kida et al. 1999; Pierce et al., 2013; Randau et al. 2016; Shapiro, 2007; Ward & Mehta, 2014; Werneburg et al. 2015). By studying the variation in axial column morphology, we can gain insight to the influence of size, locomotion, prey-size specialization, and regionalization on form-function relationships, behavior, and ecology (Buchholtz, 1998; Jones et al., 2020; Marchesi et al., 2021; Randau et al., 2016). Composed of serially homologous units with shape differentiation and regionalization influenced by early developmental gene expression and the above functional aspects, the axial column is often utilized to study integration and modularity (Buccholtz, 2007; Polly et al., 2001; Randau & Goswami, 2017).

Vertebral morphology and regional identity can also be used as a proxy for embryological and molecular aspects of evolution. The number of vertebrae corresponds with the number of somites, added sequentially from anterior to posterior in pairs at regular intervals along the axis

(Christ et al., 2000). Region boundaries and vertebral identity are coupled with several Homeobox (Hox) gene expression boundaries (Burke et al., 1995; Richardson, 1999), with combinations of active genes patterning the anterior to posterior axis. Several Hox gene expression boundaries consistently correspond to certain regional transitions along the axial column such as *Hoxc5 and Hoxc6* in regards to the cervical-thoracic transition and *Hoxa9, Hoxb9,* and *Hoxc9*, with the thoracic-lumbar. However, there are expression boundaries that do not line up with these traditional anatomical boundaries but could be involved in other aspects such as patterning axial ossification patterns (Bui & Larsson, 2021).

Tetrapod axial columns are typically composed of four regions: cervical, dorsal, sacral, and caudal. Mammals, crocodylians, and birds have an additional lumbar region lacking ribs between the ribbed thoracic and sacral vertebrae. This regionalization is intricately linked to locomotion and ventilation, providing valuable insights into form-function relationships (Johnson & Shapiro, 1998). Morphological regionalization has been studied mostly in mammals (Burke et al., 1995; Jones et al., 2020; Mallo et al., 2010) due to their highly constrained vertebral counts but highly disparate morphologies (Jones et al., 2020). Vertebral regions have also been identified in several non-mammalian vertebrates such as the sea lamprey (Chevrinais et al., 2018), zebrafish (Morin-Kensicki et al., 2002), lungfish (Johanson et al., 2005), and the thorny skate (Berio et al., 2021). However, a comprehensive look at vertebral quantitative variation and regionalization patterns is absent.

Bolker (2000) defines modules as fundamental developmental units characterized by internal integration, hierarchical organization, specific physical locations, and the potential for developmental and evolutionary transformation. Modularity is closely tied to the concept of integration, referring to the covariation of traits within an organism due to genetic,

developmental, and functional relationships (Esteban et al., 2023). With modularity being easiest to recognize in structures with discrete homologous elements and distinct levels of organization (Buccholtz, 2007), the vertebral column acts as a proxy for modularity due to its various levels of organization. The axial column is a serially homologous structure, with individual vertebrae representing the discrete units with variation distributed throughout (Buccholtz, 2007). With the ability to measure and map out variation along the axial column, we can identify boundaries and interactions between sets of functional traits, providing insight into evolvability and adaptive evolution **(**Esteban et al., 2023).

Crocodylia, together with Aves, define the crown groups of Archosauria with a fossil record over 250 million years. Crocodylomorpha, a group that includes crocodilians and their extinct relatives, originated during the Late Triassic and radiated into a wide range of ecological specializations ranging from marine, to terrestrial, to amphibious, and even several herbivorous taxa (Erickson et al., 2012; Mannion et al., 2015). Today however, Crocodylia consists of only about two dozen species of crocodiles, alligators, caimans, and gharials. Characterized by elongated bodies, powerful jaws, armored skin, and streamlined tails, crocodilians are well-adapted for life in amphibious habitats. Studies on the axial columns within Crocodylia have mostly focused on functional morphology and biomechanics, or separate analysis of specific regions and regional transitions instead of the entire column (Chamero et al., 2014; Molnar et al., 2015; Salisbury & Frey, 2001).

Crocodylian axial columns display procoelic vertebral articulations in cervical and dorsal vertebrae allowing for enhanced angular movement that is particularly beneficial for the semi-aquatic lifestyle of crocodiles (Chamero et al. 2014; Troxell, 1925). Other work has determined crocodilian vertebral articulations to act to stabilize the spine against shear stresses,

providing a more stable articulation, particularly during terrestrial locomotion seen in extant crocodilians such as a sprawling “low-walk”, “high-walk” and gallop (Fronimos & Wilson, 2017; Salisbury & Frey, 2001). Early contributions on vertebral shape hypothesize that the acquisition of this type of articulation was a key to skeletal modification that led to the emergence of Crocodylia as a whole (Benton & Clark, 1988; Chamero et al., 2014). Crocodilians also possess a biconvex first caudal vertebrae for further stabilization of the spine (Fronimos & Wilson, 2017) or for enhanced proximal tail mobility (Troxell, 1925). The rest of the tail typically displays concavo-convex joints, transitioning to amphiplatyan articulations distally, allowing for increased flexibility moving from the sacrum to the end of the tail. Coupling of these innovations have been suggested to biomechanically constrain both the musculoskeletal and dermatoskeletal systems, which in turn restrained decisive phenotypic changes among major crocodylian clades (Cleuren & De Vree, 2000). Today, Crocodylia displays a highly conserved body plan across clades, as Crocodylide, Alligatoridae, and *Gavialis* maintain the similar musculoskeletal axial morphologies (Cleuren & De Vree 2000; Seidel, 1978; Tsuihiji 2005; 2007).

Quantitative variation throughout the rest of the axial column has been generally understudied, with only one study focusing on the cervico-thoracic transition (Chamero et al., 2014) and another examining the general regionalization of presacral vertebrae in *Alligator* in the context of mammal regionalization (Jones et al., 2020). The present study aims to examine the intraspecific and interspecific variability of axial columns in Crocodylia using geometric morphometric methods on the complete surfaces of each vertebra. Through the exploration of morphological variation, regionalisation and modularity, we can gain a greater understanding of

vertebrate history and evolution (Arratia et al., 2001; Berio et al., 2021; Buccholtz, 2007; Jones et al., 2020; Martin Serra et al., 2021; Sallan, 2012; Woltering, 2012).

Methods

Data Collection

Nano-CT scans using the Zeiss Xradia 520 Versa were performed on each available individual vertebra of an adult *Caiman crocodilus* (n=51). *Caiman* scans were acquired between 0.04-0.1 *um* resolution with .4x objective lens with 2x2 camera binning over a 360 degree rotation. A total of 1400 projections were taken at 80 kV and 7 W. Most scans were taken with the LE1 filter and 1 -3 second exposure time. CT data of *Crocodylus acutus, Alligator mississippiensis, Gavialis gangeticus, Tomistoma schlegelii,* and *Crocodilus porosus* were acquired via Morphosource (Table 4.1). Atlantal vertebrae for each specimen were excluded from the analysis due to their lack of a closed surface, and incompatibility with SPHARM software. Caudal 1 to 20 were reconstructed for each specimen. Each vertebra was reconstructed with Dragonfly image analysis software (Object Research Systems Inc.). Meshes were reconstructed separately as centrum and neural arch and then as the vertebra as a whole. 3D meshes were cleaned up using Blender and Meshlab. In Blender, non-manifold edges were identified and removed. Each model then underwent a hole removal process, followed by a three-step Laplacian Smooth including one-dimensional boundary smoothing and Cotangent weighting. Following smoothing, I simplified the mesh using Quadric based Edge Collapse, with a target number of faces at 10,000 and quality threshold of .3.

3D Surface generation

Spherical harmonics analyses (SPHARM) were performed using freely available software, Slicer (Kikinis et al., 2013) and SlicerSalt (Vicory et al., 2018). Binary segmentations were acquired in Slicer and imported into SlicerSalt to generate point distribution models (PDMs). Bijective mapping of the surface points onto a unit sphere generated a spherical parameterization that was then expanded as a Fourier series. Spherical parameterization minimizes angular distortions while creating a continuous and uniform mapping of the surface to the surface of the unit sphere. The resultant Fourier functions were then used to compute SPHARM coefficients up to 15 degrees. PDMs with homogeneous sampling of the object surfaces were then generated from the coefficients by uniform sampling of the spherical parameterization with an icosahedron subdivision of factor 10. Alignment was performed using rigid Procrustes Alignment. This registration algorithm implicitly establishes homology between surfaces by optimally aligning their underlying parameterizations, similar to assigning landmarks to surfaces.

Statistical analysis

Analyses based on PDMs were conducted in 2023.09.1 using the *geomorph* package (Adams et al., 2019). Preliminary analysis to visualize vertebral morphospace occupation was performed in multiple Principal Component Analyses (PCA; *gmprcomp*). These tests were run with a residual randomization permutation method (RRPP) (Collyer et al., 2015) with 10000 iterations to evaluate significance and variables for size were log-transformed.

I followed Jones et al.'s (2020) method of evaluating regionalization using segmented regression models based on principal components analysis. I allowed up to 7 regions, with 5 being the maximum number reported for tetrapods (Head & Polly, 2015; Jones et al., 2018; Molnar & Watanabe, 2023; Randau & Goswami, 2018). This approach takes into account vertebral

integration, treating the vertebral column as a series of morphological gradients and regions based on changes in slope (Jones et al., 2020). Regionalization hypotheses were compared with an Akaike Information Criterion (AIC) value and converted to a continuous regionalization score by calculating Aikake weights from the likelihood of each hypothesis.

Distance between vectors for LS means, or the difference in location between estimated shape change between vertebrae, was quantified and used as a proxy for exploring morphological disparity. Heatmap comparisons were plotted to explore modularity by mapping pairwise comparisons across the axial column and highlighting the lowest fifth, tenth, 15th, and 25th percentiles of all the data.

Results

Principal component analysis for all vertebrae was conducted. PC's 1 through 4 represent 77% of all variation. PC1 represents 52.4% of variation and PC2 represents 11.3% of variation with PC1 mainly describing size. I plotted each taxon within the same PC space by region. *Caiman* dorsal vertebrae plot the greatest variation along PC1 and PC2. For *Alligator mississippiensis,* compared to the cervical vertebrae and dorsal vertebrae, the caudal vertebrae have the lowest variation along PC1. The cervical vertebrae display the lowest range across PC2. Comparative PC results reveal different clustering of all of the regional vertebrae across taxa. *Caiman* cervical vertebrae cluster closer than *Alligator* and *Crocodylus* with cervical vertebrae plotting along a greater PC1 range. *Gavialis* and *Tomistoma* cervicals also plot tightly together. The dorsals in PC space see an inflection from larger to smaller PC1 values, the least drastic found in *Alligator* but still present nonetheless. *Caiman* and *Tomistoma* caudal vertebrae plot similarly with *Caiman* on a greater scale along the PC1 axis compared to *Tomistoma*, while

Crocodylus and *Alligator* caudal vertebrae plot in a more clustered-manner. Gavialis stands out with most variation being found along PC2 (Figure 4.1).

Region modeling for the five sampled taxa recovers six to seven regions, with most of the boundaries of shared regions varying by one or two vertebrae. Traditional and segmented regionalization are visualized in each taxa from Figures 4.2 to 4.6. The boundary between regions one and two typically describes the transition from cervical vertebrae to thoracic vertebrae . In *Alligator*, the cervical vertebrae recovers two regions, with a boundary between the second and third region overlapping a cervico-thoracic region for the rest of the taxa. This boundary falls between vertebrae 9 and 10, with the cervical vertebrae being split in two regions between vertebrae 6 and 7. In the other taxa, the boundary between regions one and two fall between vertebrae 8 and 9 (*Caiman*); 7 and 8 (*Crocodylus, Gavialis, Tomistoma*). The dorsal vertebrae, or vertebrae 10 to 24, are split in two regions in *Caiman*, and three regions in *Alligator, Crocodylus, Gavialis*, and *Tomistoma*. The anterior dorsal regions posterior boundaries are found between vertebrae 12 and 13 (*Alligator*), 14 and 15 (*Caiman* and *Crocodylus*), 12 and 13 (*Gavialis*), and 13 and 14 (*Tomistoma*). In the taxa displaying three dorsal regions, another boundary between vertebrae 19 and 20 or dorsal vertebrae 10 and 11 (*Alligator* and *Crocodylus*), vertebrae 18 and 19 or dorsal vertebrae 9 and 10 (*Gavialis* and *Tomistoma*) is recovered. All taxa recover a single sacral region composed of sacral vertebrae 1 and 2. Two taxa recover two caudal regions and one taxa recovers three caudal regions. This boundary is found between caudal vertebrae 7 and 8 in *Crocodylus,* caudal vertebrae 2 and 3 in *Caiman*, and 5 and 6 in *Tomistoma*.

Pairwise distances were calculated in order to explore regionalization and modularity along the axial column. I utilized the lowest percentile and the highest integration amongst

vertebrae to identify morphological modules. Modularity is visualized using heatmaps by highlighting the lowest distances in the lower 5th, 10th, 15th, and 25th percentiles. In *Alligator mississippiensis* our minimum distance calculated between vertebrae was 0.076 with our maximum being 0.73. The lower bounds of the data as lowest percentile cut-offs were 0.14, 0.18, 0.21, and 0.28 for the 5th, 10th, 15th, and 15th percentiles respectively. Sequential axial variation reveals higher differences between the posterior cervical vertebrae and anterior dorsal vertebrae, the sacral complex, and posterior caudal vertebrae. We see higher distances between caudal vertebra 9 and dorsal vertebra 1 (0.23), as well as dorsal vertebrae 1 and 2 (0.25). The largest Procrustes distances are seen from the transitions from dorsal vertebra 15, the sacral vertebrae, and the first caudal vertebra with values of 0.45 (dorsal 15 to sacral 1), 0.32 (sacral 1 to sacral 2), and 0.55 (sacral 2 to caudal 1). Another spike in pairwise distances is also seen from caudal 9 to 10 with a distance of 0.22. Using the lowest 5th percentile of Procrustes distances, I calculated 6 separate modules along the axial column. These consist of an anterior cervical module, containing cervical 3 to cervical 7. An anterior, middle, and posterior dorsal module, containing dorsals 4 to 6, 8 to 10, and 13 to 15 respectively. I also calculated two caudal modules, an anterior caudal module consisting of caudals 1 to 8, and a posterior module containing caudals 11 to 12.

For *Caiman crocodilus*, the lowest Procrustes distance between vertebrae was 0.1 and the highest distance was 0.78. For the *Caiman*, the lowest 5th percentile was represented by all values from 0 to 0.2. For the 10th percentile: 0 to 0.23, for the 15th: 0 to 0.289, and for the 25th: 0 to 0.36. Axial variation was also plotted sequentially, revealing high differences in the anterior cervical vertebrae (0.29 between axis and cervical 3), transition into the sacral vertebrae (0.45 between dorsal vertebra 15 and sacral vertebra 1, 0.38 between sacral vertebrae 1 and 2, and 0.42

from sacral vertebra 2 to caudal vertebra 1), and anterior caudal vertebrae (0.42 between caudal vertebrae 3 and 4). In the *Caiman* analysis, seven modules are identified. Two posterior cervical modules, four dorsal modules, and a posterior caudal module. The two cervical modules consist of cervicals 6 and 7, followed by 8 and 9. The dorsals are also organized into four sections, dorsals 1 and 2, 3 to 5, 6 to 11, then 12 to 14. The caudal module contains caudals 7 to 11.

Our analysis for *Crocodylus acutus* resulted in a minimum vertebral distance of 0.07 and a maximum of 0.7. The cut-offs for the lowest 5th, 10th, 15th, and 25th percentiles were calculated at 0.14, 0.19, 0.23, 0.30 respectively. The greatest distance differences are noted between cervical vertebrae 7 and 8 (0.3) and dorsal vertebra 15 to sacral vertebra 1 (0.47) and sacral vertebra 2 to caudal vertebra 1 (0.45). The rest of the vertebrae maintain differences between 0.1 and 0.2, with the upper end of distances mapping around the anterior cervicals, anterior and mid-dorsals, and posterior caudals. Using the 5th percentile of the distance data, I determined 7 separate modules across the axial column. These include a mid-cervical series, a cervical-dorsal module, three dorsal modules, and two caudal modules. The mid-cervical series consists of cervicals 5 and 6, the cervical-dorsal module contains cervicals 8 through 9 and dorsals 1 and 2. The three dorsal modules group from dorsals 4 to 8, 10 and 11, and 12 and 14. The caudal modules consisted of caudals 1 to 8 and caudals 9 and 10.

In *Gavialis gangeticus*, I found a minimum Procrustes distance of 0.08 and a maximum of 0.85. The lowest 5th percentile ranged from 0 to 0.14, the 10th percentile from 0 to 0.18, the 15th percentile from 0 to 0.22, and the 25th percentile from 0 to 0.27. Most of the data lies between 0.1 and 0.15, with high variation peaks occurring between the axis and cervical 3 at 0.24, dorsal vertebrae 3 and 4 at 0.22, dorsal vertebrae 12 and 13 at 0.21, dorsal vertebra 15 and sacral vertebra 1 at 0.46, sacral vertebra 2 to caudal vertebra 1 at 0.66. I also see smaller relative

peaks between caudal vertebrae 6 and 9 from 0.22 to 0.19. I identified 8 separate modules, with two cervical modules, four dorsal modules, and two caudal modules. The anterior cervical module contains cervical vertebrae 3 to 7, and the posterior cervical module contains cervical vertebrae 8 and 9. The dorsal modules consist of two anterior dorsal modules, with the first consisting of dorsals 1 to 3, and the second consisting of dorsal vertebrae 4 and 5. The posterior dorsal modules consist of dorsals 6 through 12, and the posteriormost dorsal module consists of dorsals 14 and 15. The caudal modules are separated from caudal vertebrae 1 to 5 and then another module of caudal vertebrae 10 and 11.

Finally, for *Tomistoma schlegelii* the minimum calculated Procrustes distance between vertebrae was found to be 0.08 and the maximum to be 0.7. The heatmap exploration included percentile cut-offs at 0.16, 0.2, 0.24, and 0.3 for the 5th, 10th, 15th, and 25th percentiles respectively. The majority of plotted distances between sequential vertebrae ranged from 0.1 and 0.2, with greater variation seen between dorsal vertebrae 2 and 3 at 0.22, dorsal vertebrae 12 and 13 at 0.23, dorsal vertebra 15 and sacral vertebra 1 at 0.47, sacral vertebra 1 and sacral vertebra 2 at 0.29, sacral vertebra 2 and caudal vertebra 1 at 0.4, and caudal vertebra 7 and vertebra 8 at 0.19. I identify 5 separate modules through our integration exploration. The first module is a cervical and anterior dorsal module, consisting of the vertebrae from cervical vertebra 3 to dorsal vertebra 1. This is followed by two dorsal modules, dorsals 5 to 9, and dorsals 14 and 15. The caudal vertebrae are also split into modules with caudal vertebrae 2 to 7 forming the first, and caudal vertebrae 8 to 12 forming the second.

Discussion

Our results show that the axial column of Crocodylia is highly regionalized with all taxa displaying more regions than the expected traditional breakdown. Moreover, regional boundaries varied between taxa but to a limited degree. The first post axial region is morphologically consistent with cervical rib attachment surfaces, as the dorsal regions seem to be divided by the orientation of the rib attachment surfaces. The transition between regions one and two in all taxa can be seen in the principal component data, typically indicated by inflections and gaps between plotted clusters. The second region is characterized by a slight increase in size in the cervicals, with an elongation of the transverse processes and hypapophyses, as well as a more drastic shift of the transverse process dorsally (from the center of the centra to the base of the neural arch). The third and fourth regions, if present in the dorsal vertebrae, generally consist of a shift in angle and size of the transverse processes and the presence and orientation of the diapophysis. All taxa exhibit a separate sacral region and caudal region, with *Crocodylus* and *Tomistoma* displaying two caudal regions and *Caiman* displaying three caudal regions (Figure 4.7).

A degree of conservatism across the cervical to dorsal regional boundary transition is present across all taxa, with the boundary varying by only one to two vertebrae. This boundary exists between cervical vertebrae 7 and 8 in *Crocodylus, Gavialis, and Tomistoma*, 8 and 9 for *Caiman,* and 9 and 10 for Alligator. In *Caiman*, the first regional transition is marked by the dorsal shift of the transverse processes without elongation. In *Tomistoma*, this transition is also marked by higher transverse process placement pre-elongation, the hypapophyses is less exaggerated and angled more ventrally compared to *Caiman.* The neural spine is also shorter, thinner, and angled more posteriorly. The transition from region 1 and 2 is also marked by a widening of the neural spine anteroposteriorly, and it being slightly shorter. While this transition is variable among the sampled taxa, it is generally encompassed by the shift in the location and

direction of the diapophysis, as it projects ventrally from the neural arch in proximal cervical vertebrae to the projecting horizontally and laterally from the transverse processes towards the dorsal vertebrae. *Caiman*, *Gavialis*, and *Crocodylus* have a more gradual transition of the diapophyseal surface moving to the base of the neural arch. In these taxa, the region boundary is placed in the middle of the transition, also accompanied by a slight anteroposterior widening and shortening of the neural arch. The boundary from regions 2 and 3 is marked by the inflection from increasing transverse process length to decreasing transverse process length for *Caiman*, *Gavialis, Tomistoma*, and *Crocodylus*. This transition is homologous to the transition between regions 3 to 4 in *Alligator*. *Alligator, Crocodylus, Gavialis* and *Tomistoma*, display three dorsal regions. The first dorsal region is homologous to the first dorsal region in *Caiman*, which incorporates the posterior cervicals and the most anterior dorsals prior to the expansion and extension of the transverse processes, as well as a loss of the hypapophyses. The second dorsal region is marked by the slight decrease in transverse process length but general uniformness to dorsal vertebrae shape overall. The third dorsal region is reflective of the transition to the lumbar, or rib-less vertebrae. *Caiman*, *Crocodylus*, and *Tomistoma* display multiple caudal regions, marked by a transition of the angle of the transverse processes from perpendicular to the centra to slightly anterior facing *Crocodylus* and *Tomistoma*. In *Caiman*, the transition is early with a small anterior region mostly driven by size and transverse process shape. These breakpoints can also be seen in the PC data.

Our modularity exploration reveals up to two cervical modules, up to five dorsal modules, and up to two modules in the tail for all taxa (Figure 4.8). Modules identified here were calculated by determining the highest covariation through pairwise tests. There remains high variation in the makeup of each module across taxa. *Alligator* and *Gavialis* display large cervical

modules, consisting of cervical vertebrae 3 to 7, with all of Tomistoma's cervicals including the first dorsal constituting one module. *Gavialis* and *Caiman* share a module of cervical vertebrae 8 and 9 together. These modules may act homologously as transitional modules between cervicals and thoracics. Within the dorsal region, the distribution of modules varies immensely across taxa. Across most taxa however, I do see a consistent mid-dorsal and posterior-dorsal module. The mid-dorsal module typically contains the thoracic vertebrae with elongated transverse processes, and a posterior boundary of the transition from thoracic to lumbar. The posterior-dorsal module typically contains the last two to three dorsals prior to the sacral vertebrae. These can be described as containing shortened and thinned anteroposterior transverse processes and a lack of rib attachment points. In *Alligator*, *Caiman*, *Tomistoma*, and *Gavialis,* the caudal modules include the anterior and posterior caudal vertebrae, with slight variations such as the exclusion of the first caudal vertebra in *Tomistoma* and the last caudal vertebra in *Gavialis*. This dual module is only seen in the regionalization data in Crocodylus.

There are varying levels of integration in the cervical vertebrae of the taxa studied, and little to no pattern to be followed across sampled cervical vertebrae. *Alligator, Gavialis*, and *Tomistoma* show the highest amount of integration amongst their cervical vertebrae, with *Tomistoma* revealing high integration between their cervical vertebrae and anterior dorsal vertebrae. The most variance among the cervical vertebrae is seen in *Caiman* and *Crocodylus*, with high integration seen solely in their posterior cervical vertebrae. In studies conducted within Aves, their closest living relatives, studies have commonly identified three cervical regions within the avian neck: a cranial, middle, and caudal region (excluding the atlas and axis) (Boas, 1929; Cobley et al., 2013; Dzemski & Christian, 2007; Zweers et al., 1987). These regions have typically been characterized by morphology and joint mobility, as the number of functional

regions has seemingly varied across species and studies (Krings et al., 2014). The avian neck is highly variable in terms of cervical count, flexibility, and its relation to ecology and behavior. Compared to Crocodylia, the evolutionary occurrence of specific modules along the avian neck most likely allowed or drove the variation of the avian neck. The lack of specific modules and integration patterns in the Crocodilian neck may be a reflection of the conserved cervical counts and behaviors shared amongst taxa.

Studies have found modules reflective of the 'cervical dorsal transition' specifically in felids and chameleons. In felids, this distinct module is composed of vertebrae from cervical vertebra 6 to thoracic vertebra 2, as developmental covariation has been suggested based on the migration of cells from somites (Randau & Goswami, 2017), as well as the potential involvement in the evolution of the muscularisation of the diaphragm (Buccholtz et al, 2012). One study focusing on chameleon regionalization found one taxa with a three vertebra 'cervical-dorsal transition' module (Molnar & Watanabe, 2023). Our results suggest a similar pattern seen in *Tomistoma* displaying a module from cervical vertebra 3 to dorsal vertebra 1, and *Crocodylus* with a module from cervical vertebra 8 to dorsal vertebra 2. Molnar and Watanabe (2023) also found a two vertebrae 'lumbar' module in chameleons, also seen in felids by Randau and Goswami (2017). This 'thoracolumbar module' is thought to facilitate or be driven by homeotic changes between thoracic and lumbar regions promoting variation without changing count (Randau & Goswami, 2017).

Expression data for *Alligator mississippiensis* (Böhmer et al. 2015; Mansfield & Abzhanov, 2010) compared with region and module boundaries across Crocodylia shows *Hoxb4* and *Hoxd4* expressed at the boundary between the atlas-axis complex and cervical 3. *Hoxa5* is strongly expressed from cervical 9 to thoracic 3, while weakly present in thoracic 4 to 7. Relative

to regions and modules calculated in this study, I note a general correspondence with one or two vertebrae varying to region two in *Tomistoma, Gavialis, Caiman*, *Crocodylus* and region three in *Alligator.* In the identified modules however, I only note in *Crocodylus* the second module, consisting of cervical vertebra 8 to dorsal vertebra 2, and modules 1 and 2 flanking the region in *Alligator* cervical vertebra 8 to dorsal vertebra 3. *Hoxc6* and *Hoxc8* express at the cervico-thoracic boundary, between cervical vertebra 9 and dorsal vertebra 1. Our data reveal in *Alligator,* for the boundary between region 2 and 3 to match said boundary. *Caiman* varies by one vertebrae, as the boundary between region 1 and 2 occurs at cervical vertebra 8, in *Crocodylus, Tomistoma,* and *Gavialis* it occurs at cervical vertebra 7. While the traditional molecular boundary is not seen within our regionalization analysis, it is noted in the boundaries between some modules specifically in *Caiman* and *Gavialis*. I also note a division in morphology between cervical vertebra 9 and dorsal vertebra 1, typically in the ribs, suggesting gene expression affects other areas of morphology separate from entire regional changes. In the lateral plate mesoderm, *Hoxc8* extends from thoracic vertebra 9. I note in *Gavialis* and *Alligator* the transition from region 3 and 4 matches this boundary, while in *Tomistoma* this transition varies by one vertebra, occurring at dorsal 10. This may relate to respiratory function and the intracolumnar change associated with rib attachments and costal ventilation. Only limited axial Hox expression patterns are known for *Alligator*. The regional variations shown here for other crocodylians may provide a guide to discovering if axial Hox expression variations match the osteological variations reported here.

Functional considerations among the compared patterns in developmental, morphological, regional, and module groupings include specific morphologies related to locomotion and respiration. Crocodylians use a wide range of terrestrial locomotor behaviors

including sprawling, high-walking, and asymmetrical gaits such as bounding and galloping otherwise seen only in mammals (Renous et al 2002). As semi-aquatic animals, they display axial swimming, characterized by swimming with adducted limbs while the trunk remains fairly straight, and thrust being produced by the undulation of the tail (Salisbury & Frey, 2001). A feeding behavior also includes the 'death roll', or rotational feeding, used to subdue and dismember large prey through spinning around the longitudinal axis of their body (Drumheller et al., 2019; Fish et al., 2007). Crocodylians also possess a unique respiratory system that combines costal ventilation with a hepatic pump mechanism (Brocklehurst et al., 2018). These behaviors and functional systems are closely tied to axial column morphology and variation as will be discussed below.

Crocodylians are capable of both lateral trunk bending and dorsoventral flexion, and changes in morphological regionalization may not reflect anatomical changes enabling dorsoventral flexion. Flexibility in the crocodylian axial column is greatly influenced by the zygapophyses, ribs, musculature, cartilaginous elements, and ligaments, and is generally independent of centrum articular face morphology (Fronimos & Wilson, 2017; Molnar et al., 2014). There is a pattern of posteriorly-decreasing lateral flexibility in the lumbar region, noted in *Alligator* (Fronimos & Wilson, 2017) which is semi-reflected in the regionalization analysis of *Alligator* conducted here. We see shorter, smaller regions along the cervical vertebrae, with a generally short anterior dorsal region moving towards two larger middle and posterior dorsal regions. Stiffness was found to be the highest at the lumbosacral joint in *C. niloticus*, suggesting a need to generate large movements about this joint for bounding and galloping to produce an appreciable degree of flexion/extension (Molnar et al., 2014). Our results reveal high amounts of

integration and modularity surrounding the lumbosacral joint and into the tail. These patterns however, cannot be identified in the other taxa.

The high integration calculated among the cervicals, as well as a distinct first region may be related to the "death roll" behavior. All extant crocodylians have been observed to perform a "death roll" behavior except for *Paleosuchus palpebrosus* (Drumheller et al., 2019; Preuschoft & Klein, 2013). Within the calculated first region, the cervicals maintain ventrally directed and short transverse processes, with the diapophysis lying below the parapophysis on the centrum. Upon the transition to region two, transverse processes lift so the diapophysis is directed ventro-laterally in line with the top of the centrum, or base of the neural arch. Among the sampled taxa, all the vertebrae within the first region also display shorter, thinner and posteriorly angled neural spines. This region contains cervicals bearing morphologically unique cervical ribs– extending from each vertebra, lying nearly parallel to the centrum, and overlapping with the cervical ribs of the subsequent vertebra. This structure resists torsional stresses imposed on the neck during death rolls (Preuschoft & Klein, 2013). This is reflected in the location of the diapophysis and parapophysis, the attachment points of the tuberculum and capitulum of each rib respectively, as the space between the attachment points allows for twisting forces to be maintained from the neck's longitudinal axis (Preuschoft & Klein, 2013).

Crocodylian respiration is also closely linked to the changes in angle between the diapophysis and parapophysis. Crocodylia displays a unique respiratory system combining costal ventilation with a hepatic pump mechanism. During costal ventilation, an intracolumnar change in angle between the parapophysis and diapophysis influences the motion of ribs during breathing (Brocklehurst et al., 2017). This transition is seen between our calculated regions two and three, in *Alligator* between three and four, and can be described as a boundary constrained

by respiratory function. Our results reveal a third dorsal region in *Alligator, Gavialis,* and *Tomistoma*, reflective of the described ribless lumbar region which creates space for the diaphragmaticus muscle. The diaphragm is connected to the liver, and moves caudally to increase space in the body cavity to assist ventilation during higher activity while also controlling buoyancy in water (Rose et al., 2021). This region corresponds to the division between the vertebrae with the last sternal rib and the vertebrae with the first shorter non-sternal rib within the dorsal region.

Interestingly, *Gavialis* have three rib-less dorsal vertebrae compared to the non-*Gavialis* species, usually four or five. This pattern is noted within the modularity calculations, but not within the regionalization models. The functional relevance is also unclear in terms of locomotion. In secondary aquatic animals (cetaceans and ichthyosaurs), it is generally known that the aquatic locomotor adaptation involves initial reduction and a subsequent increase in trunk vertebral stiffness (Buccholtz, 2001). In Crocodyliformes, aquatic Thalattosuchians show increased intervertebral range of motion compared to semi-aquatic crocodylian (*C. niloticus*) suggesting the same pattern may be applied to crocodylomorph aquatic adaptation (Molnar et al., 2015). Both the *Caiman* and *Gavialis* display high integration along their axial columns, with modules containing mostly all of their presacral vertebrae. As two taxa that are generally more aquatic than the other taxa, we can infer the more uniform presacral shapes allow for generation of constant undulatory waves and increase in efficiency of aquatic locomotion (Iijima et al., 2018).

Crocodylian tail morphology and function is tightly coupled with musculature and the mechanical properties of the dermis encasing it (Salisbury & Frey, 2000). *Tomistoma, Crocodylus,* and *Alligator* display high integration from caudals one through twelve, generally

split into two large groupings. These groups are revealed in the regionalization analysis for *Crocodylus* solely. The boundaries between the integrated modules are typically reflected by a reduction in the zygapophyses, leading to the inability to limit tail mobility and flexibility in the tail (Mallison & Schwarz, 2015). The *Caiman* and *Gavialis* have one and two modules respectively, but typically reveal less integration overall with smaller modules. *Gavialis* is unique among the extant taxa as they lack the dermal accessories along their tail, allowing for a greater capacity for lateral flexion during swimming (Salisbury & Frey, 2000). *Gavialis* tail modularity does include two small modules, but are comparatively smaller with implications for more flexibility for movement. Comparisons to muscle insertions, specifically the caudofemoralis muscle (CFL), reveal no direct correspondence to regional or module boundaries except for in the *Caiman*. The caudofemoralis muscle originates from around caudal vertebrae 3 to 15 in *Alligator* according to an early Romer (1923) description, and another study notes attachment at caudal vertebrae 4 to 11 (Wilhite, 2023). The CFL acts as the primary hind-limb retractor, as well as plays a role in lateral flexion of the tail. High integration modules and general morphological region boundaries among the tails of the extant sampled taxa may be related to other factors.

Conclusion

This study employs a novel, highly objective methodology to explore regionalization, integration, and modularity in Crocodylia, challenging the traditional view of a ‘simple’ regionalized axial column. Our findings reveal significant regionalization and heterogeneity within the axial columns of crocodylians, with notable variation between taxa. Despite this diversity, there is a degree of conservatism however with similar regional boundaries, varying often by only one or two vertebrae.

This study utilizes an objective, complete surface approach to analyzing variation, regionalization, and modularity across various axial columns. Using whole surface landmarks, we are able to determine total shape variation between vertebrae, as well as calculate Procrustes distance and quantify total difference between structures. The application of various analyses, specifically spherical harmonics, regression models, and pairwise tests, has created an opportunity to look at modularity in-depth. This 'whole surface' approach highlights several subtle axial regionalizations not identified before.

Drawbacks of the utilization of spherical harmonics are that it can be time intensive, may require a significant amount of troubleshooting, and working with different resolution scales of specimens affects the processing times of various models. However, the ability to use minimal landmarks, acquire the entirety of a surface, and compare the axial columns of multiple taxa with minimal subjectivity nor the need to identify landmarks on each vertebrae, creates the opportunities for deeper analyses with a higher number of taxa and broader ontogenetic sampling. This study underscores the complexity and diversity of vertebral morphology in Crocodylia, demonstrating that their axial regionalization is far from simple. The objective methodology applied here paves the way for future research to further explore these patterns, their functional implications, and their developmental histories in greater detail.

Tables

Table 4.1. Specimen data, CT resolution, and regionalization data

Taxa	**Specimen ID**	**Holder**	**Resolution (mm)**	**Regions**	**sumRss**	**AICc**	**delta AIC**
Caiman crocodilus	RM5242	Redpath Museum	.04-.1	7	0.145	-1862	18.21
Gavialis gangeticus	UF Herp 33421	Florida Museum of Natural History	.08741	6	0.026	-1060	9.08
Crocodylus acutus	UF Herp 20561	Florida Museum of Natural History	.97785	7	0.028	-1052	30.92
Tomistoma schlegelii	UF Herp 33422	Florida Museum of Natural History	.08676	7	0.015	-818.7	24.63
Alligator mississippiensis	UF Herp 21461	Florida Museum of Natural History	.08635	7	0.021	-778.6	39

Figures

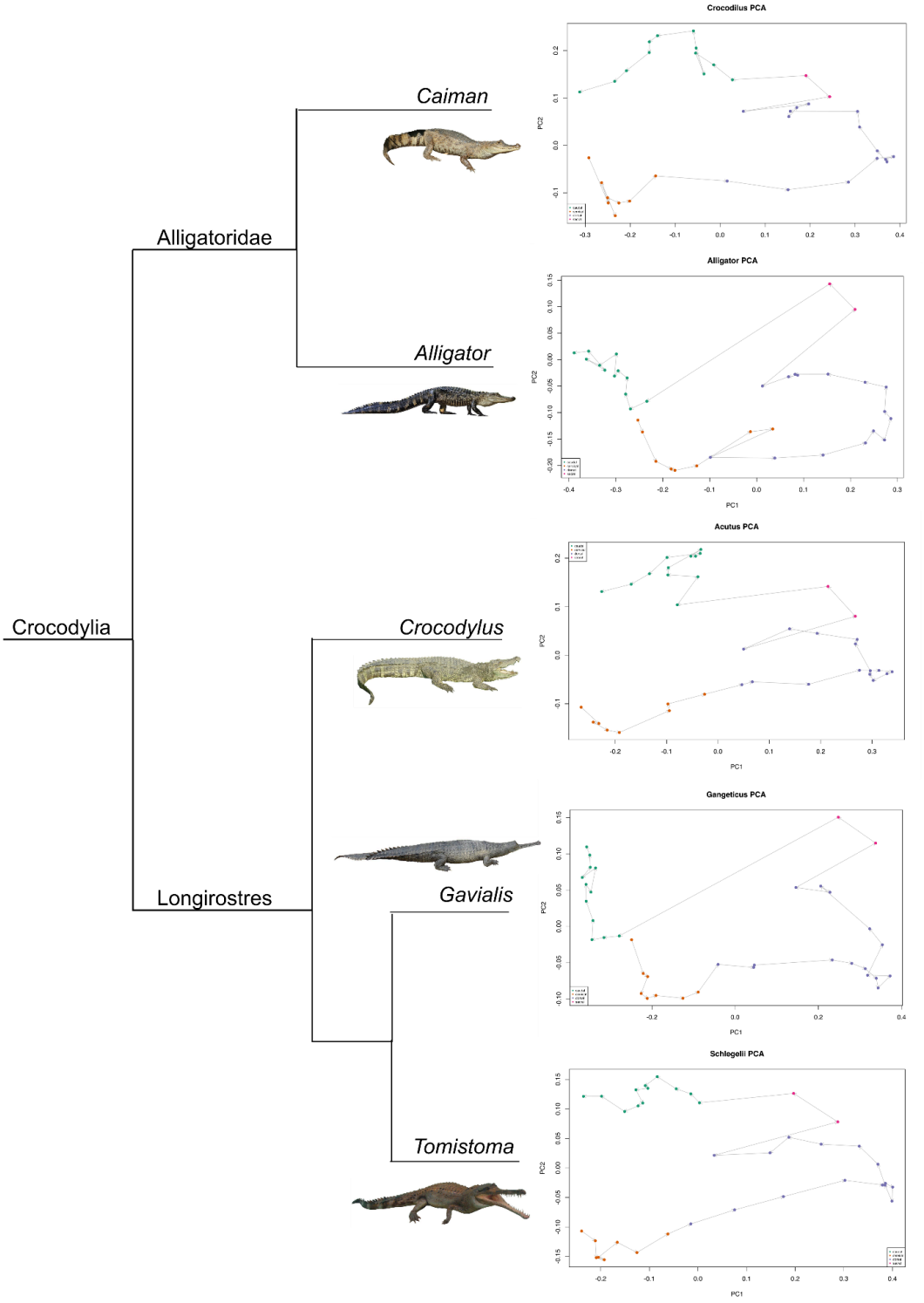

Figure 4.1. Simplified Crocodylia phylogeny displaying varying morphospace occupation of vertebrae plotting PC1 vs PC2.

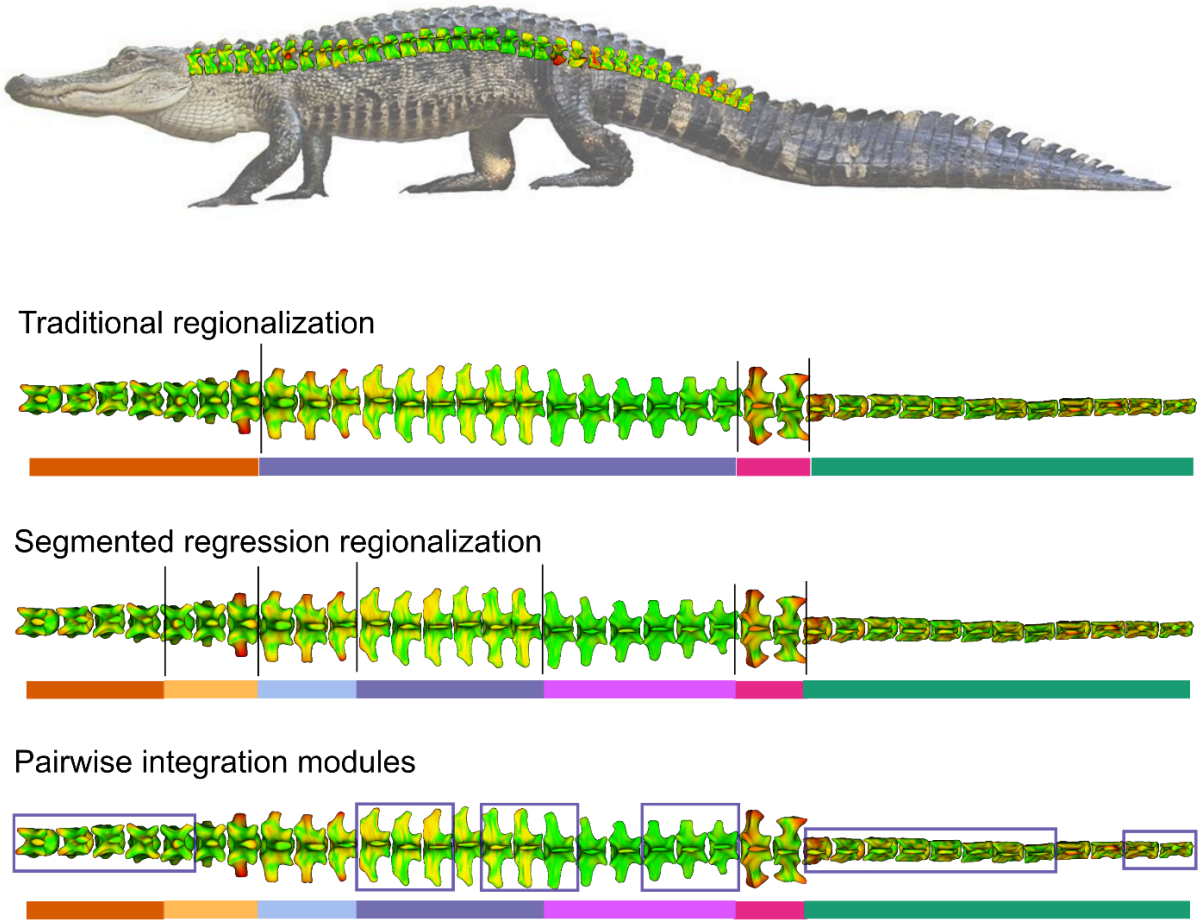

Figure 4.2. *Alligator mississippiensis* axial variation, traditional regionalization, and calculated regionalization and modularity. Each vertebrae above is a representation of the Model-to-Model distance between itself and the vertebra anterior to it. For example, the anteriormost vertebra is the shape difference between the axis and cervical 3, with the differences between the vertebrae highlighted onto cervical 3. Life reconstruction by Gareth Rasberry, used under Creative Commons Attribution-Share Alike 3.0 Unported license.

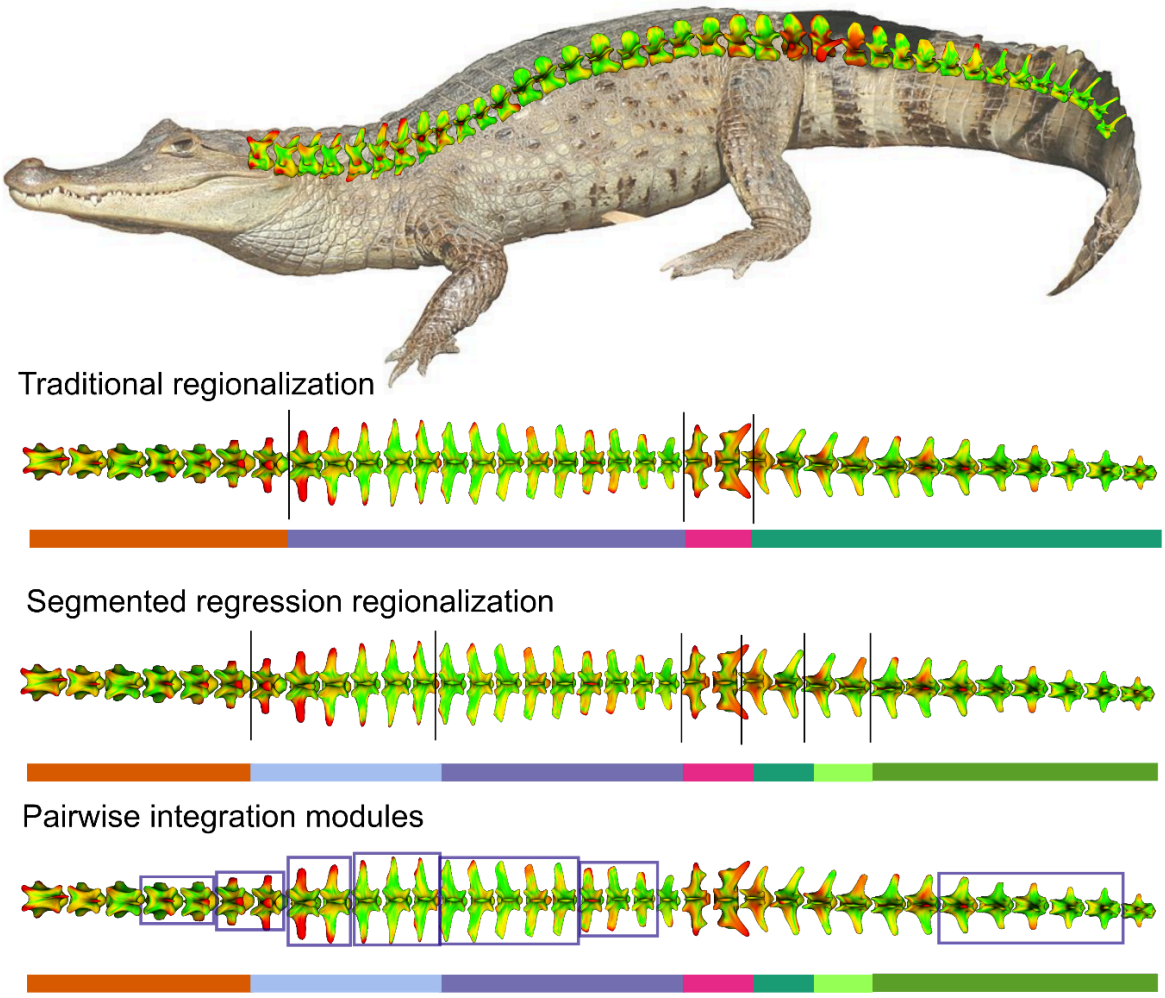

Figure 4.3. *Caiman crocodilus* axial variation, traditional regionalization, and calculated regionalization and modularity. Each vertebrae above is a representation of the Model-to-Model distance between itself and the vertebra anterior to it. For example, the anteriormost vertebra is the shape difference between the axis and cervical 3, with the differences between the vertebrae highlighted onto cervical 3. Life reconstruction by Berrucomons, used under Creative Commons Attribution-Share Alike 3.0 Unported license.

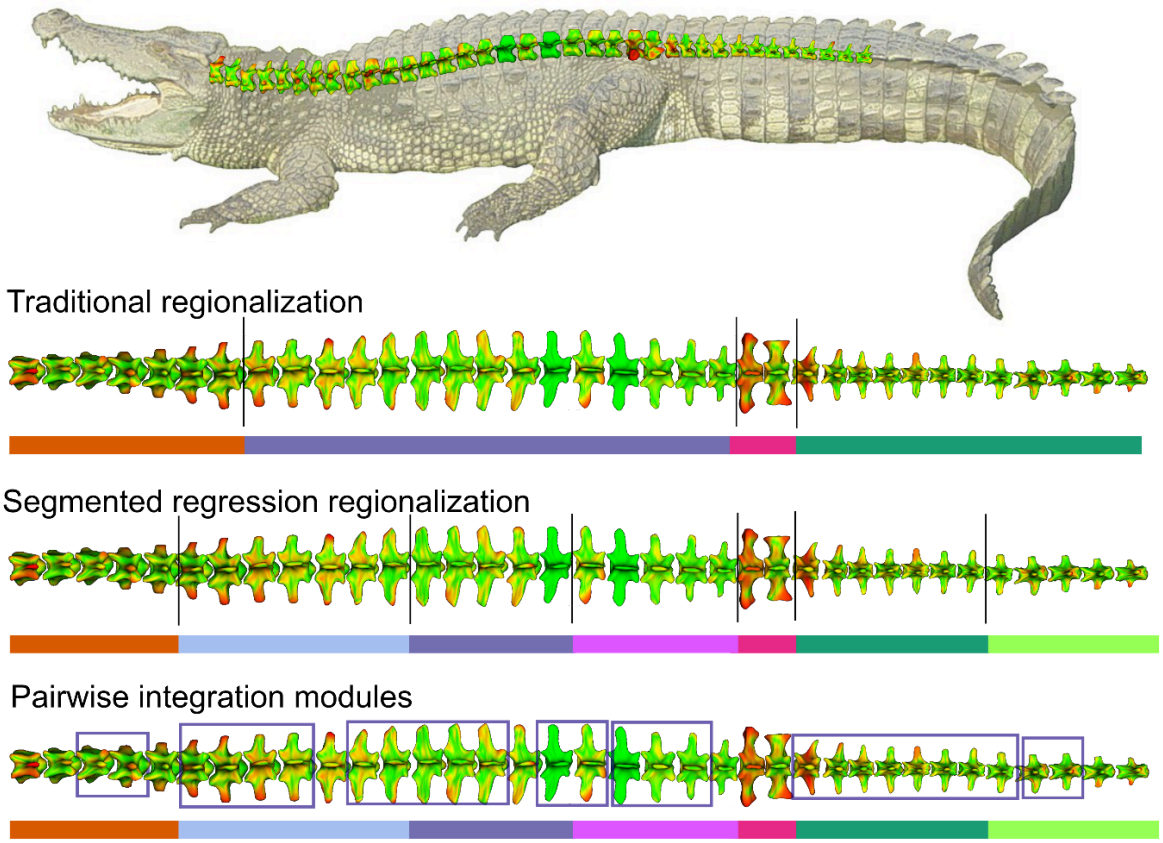

Figure 4.4. *Crocodylus acutus* axial variation, traditional regionalization, and calculated regionalization and modularity. Each vertebrae above is a representation of the Model-to-Model distance between itself and the vertebra anterior to it. For example, the anteriormost vertebra is the shape difference between the axis and cervical 3, with the differences between the vertebrae highlighted onto cervical 3. Life reconstruction by Rlevse published into the public domain.

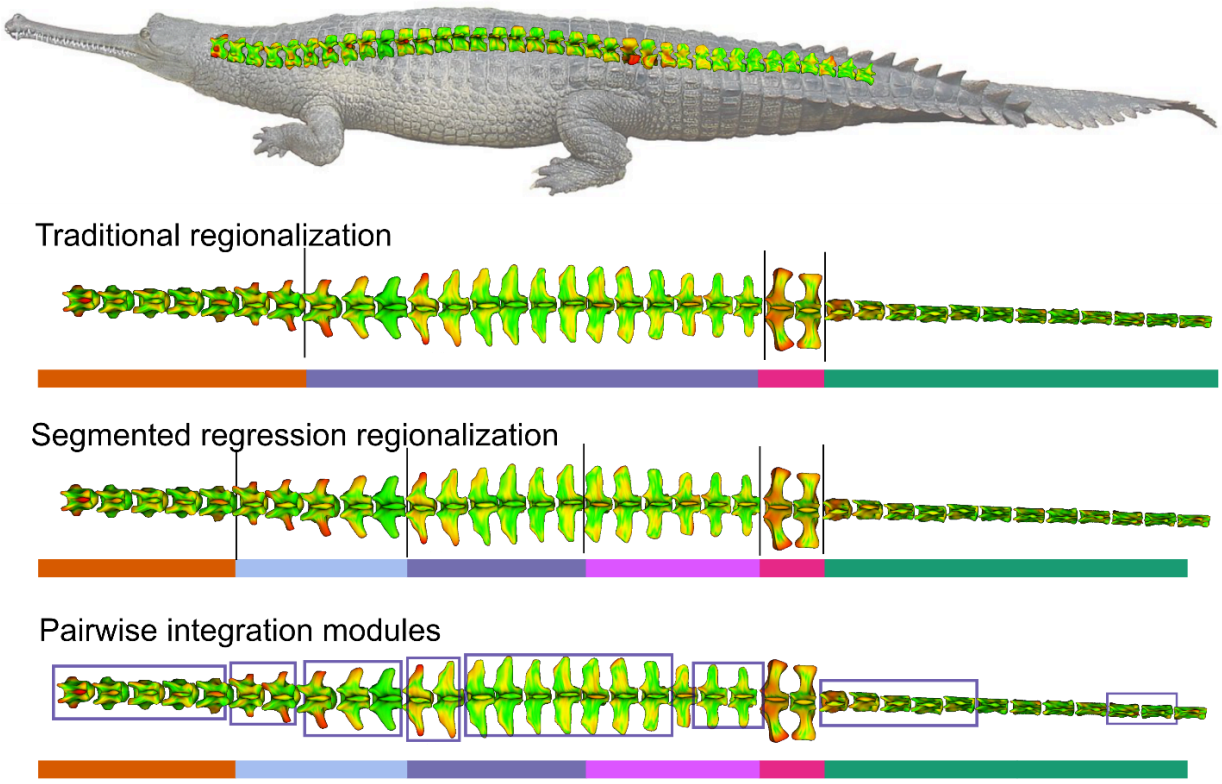

Figure 4.5. *Gavialis gangeticus* axial variation, traditional regionalization, and calculated regionalization and modularity. Each vertebrae above is a representation of the Model-to-Model distance between itself and the vertebra anterior to it. For example, the anteriormost vertebra is the shape difference between the axis and cervical 3, with the differences between the vertebrae highlighted onto cervical 3. Photo taken at San Antonio Zoo published in the public domain.

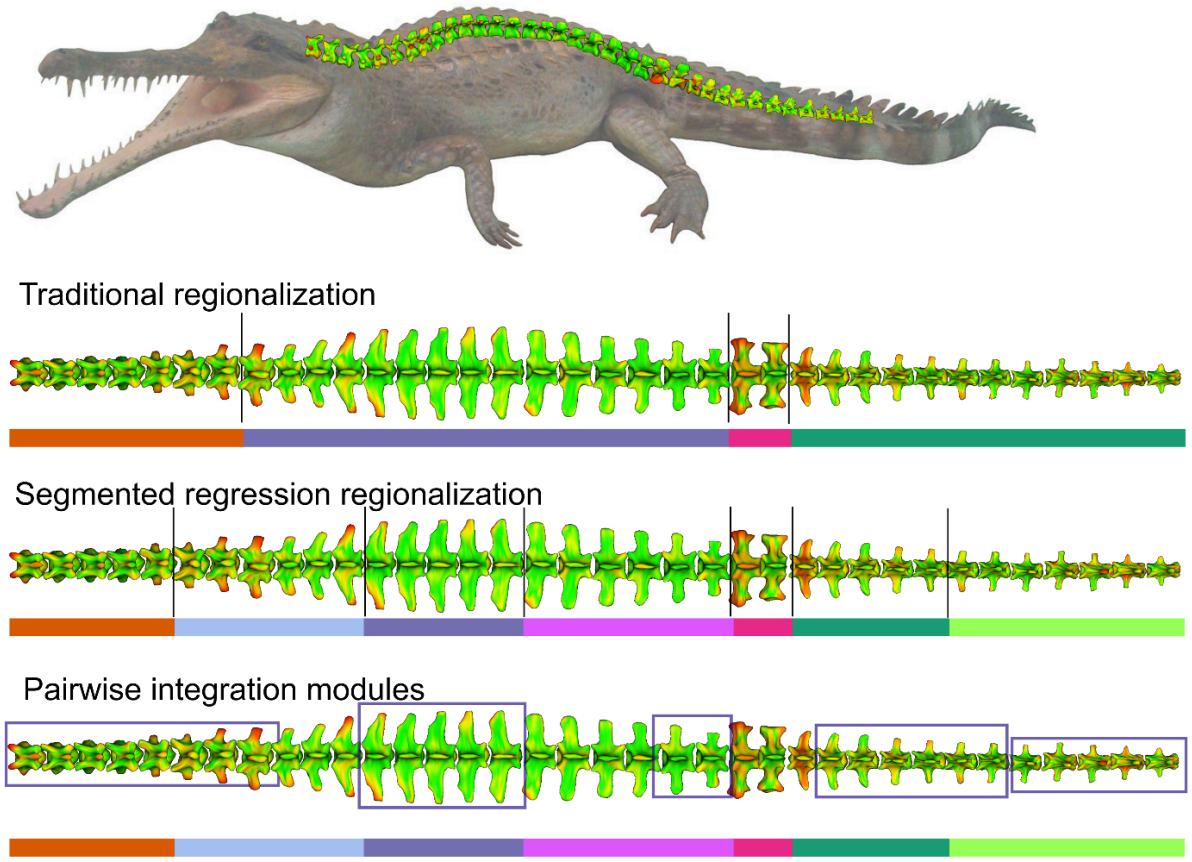

Figure 4.6. *Tomistoma schlegelii* axial variation, traditional regionalization, and calculated regionalization and modularity. Each vertebrae above is a representation of the Model-to-Model distance between itself and the vertebra anterior to it. For example, the anteriormost vertebra is the shape difference between the axis and cervical 3, with the differences between the vertebrae highlighted onto cervical 3. Photo taken at at the Natural History Museum of London used under Creative Commons Attribution-Share Alike 3.0 Unported license.

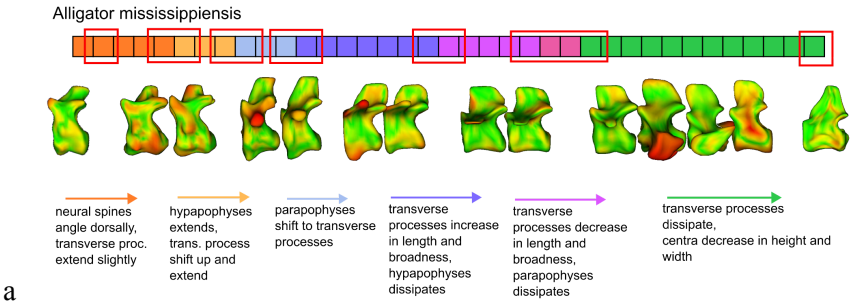
Alligator mississippiensis
neural spines angle dorsally, transverse proc. extend slightly
hypapophyses extends, trans. process shift up and extend
parapophyses shift to transverse processes
transverse processes increase in length and broadness, hypapophyses dissipates
transverse processes decrease in length and broadness, parapophyses dissipates
transverse processes dissipate, centra decrease in height and width

a

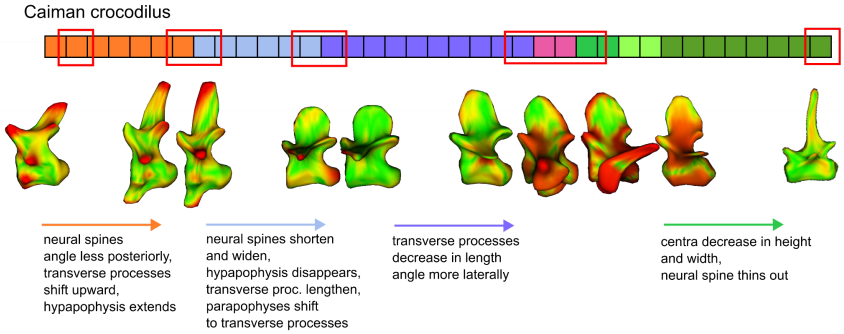
Caiman crocodilus
neural spines angle less posteriorly, transverse processes shift upward, hypapophysis extends
neural spines shorten and widen, hypapophysis disappears, transverse proc. lengthen, parapophyses shift to transverse processes
transverse processes decrease in length angle more laterally
centra decrease in height and width, neural spine thins out

b

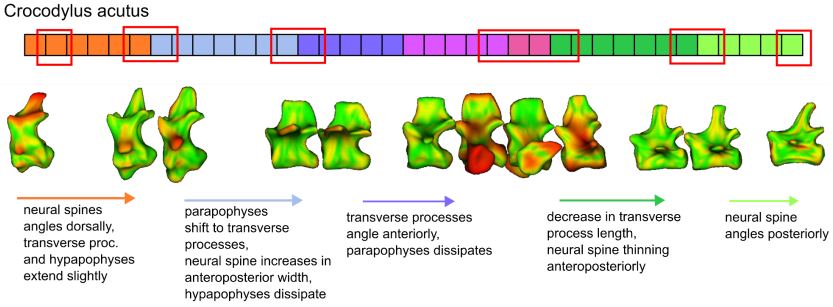
Crocodylus acutus
neural spines angles dorsally, transverse proc. and hypapophyses extend slightly
parapophyses shift to transverse processes, neural spine increases in anteroposterior width, hypapophyses dissipate
transverse processes angle anteriorly, parapophyses dissipates
decrease in transverse process length, neural spine thinning anteroposteriorly
neural spine angles posteriorly

c

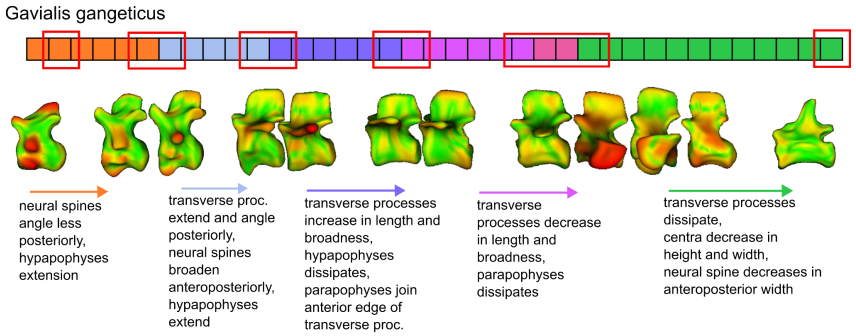

d

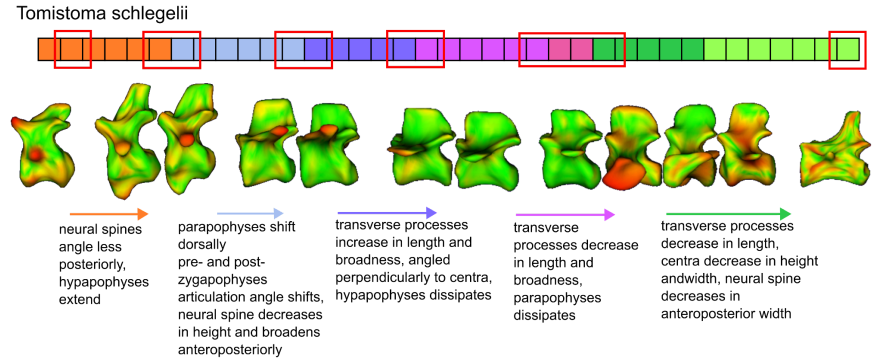

e

Figure 4.7. Transitional vertebra along each taxa's (a-e) vertebral column using SPHARM derived models. Variation is based on a Model-to-model absolute distance between preceding vertebrae. Rows of boxes represent our regionalization model, with groups of vertebrae represented by the outlined boxes, specifically those in transitional roles.

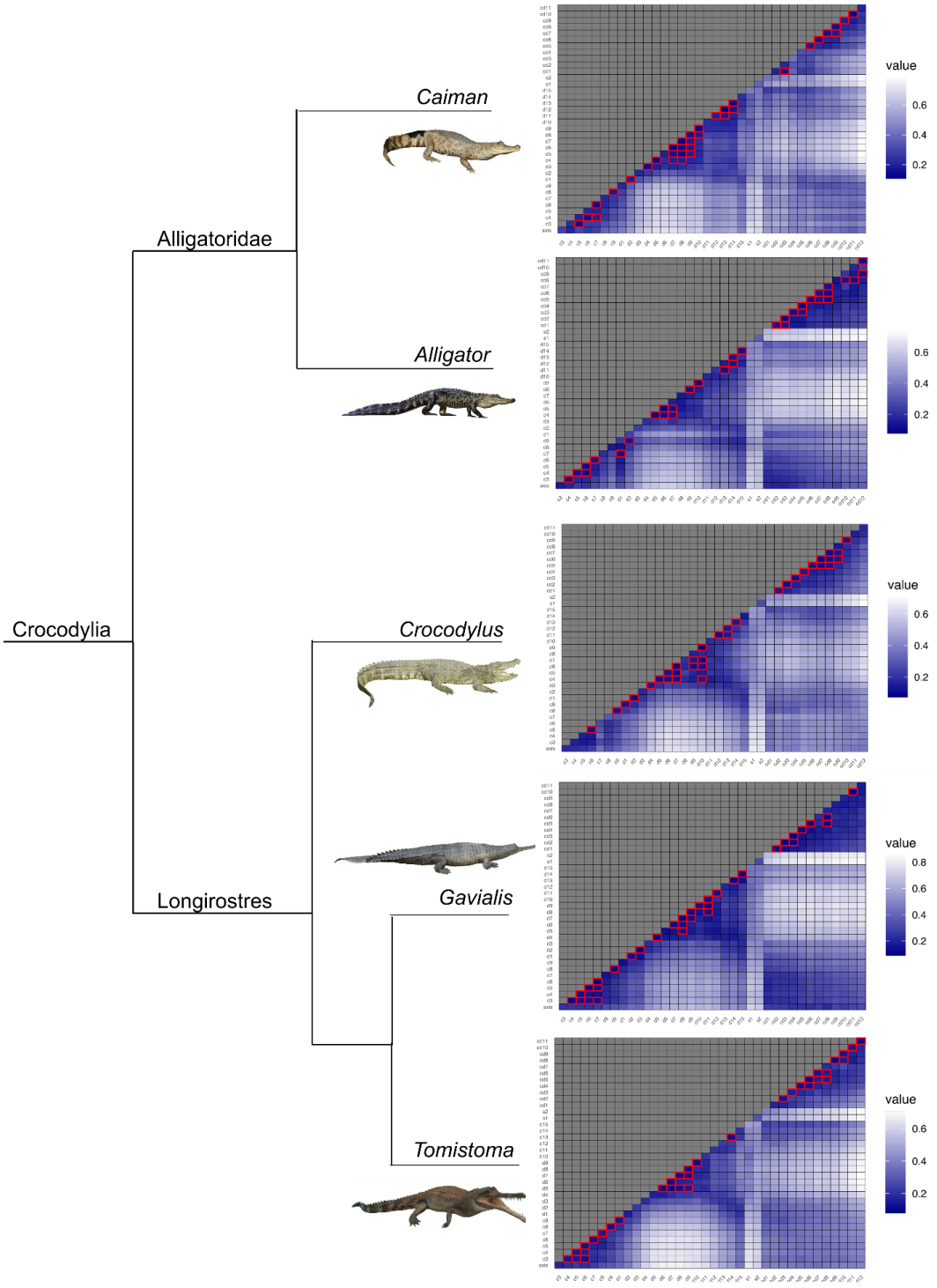

Figure 4.8. Simplified phylogeny displaying pairwise integration and modularity between taxa. The lowest fifth percentile of pairwise distance data (highest covariation) is highlighted in red.

References

Adams, D. C., Collyer, M. L., Kaliontzopoulou, A., & Sherratt, E. (2019). Geomorph: Software for geometric morphometric analyses. R package version 3.0. 5. In.

Arratia, G., Schultze, H. P., & Casciotta, J. (2001). Vertebral column and associated elements in dipnoans and comparison with other fishes: development and homology. *Journal of morphology, 250*(2), 101-172.

Benton, M. J., & Clark, J. (1988). Archosaur phylogeny and the relationships of the Crocodylia. *The phylogeny and classification of the tetrapods, 1*, 295-338.

Berio, F., Bayle, Y., Riley, C., Larouche, O., & Cloutier, R. (2022). Phenotypic regionalization of the vertebral column in the thorny skate Amblyraja radiata: Stability and variation. *Journal of Anatomy, 240*(2), 253-267.

Boas, J. E. V. (1929). Biologisch-anatomische Studien über den Hals der Vögel (Vol. 1): *AF Høst & søn.*

Böhmer, C., Rauhut, O. W., & Wörheide, G. (2015). New insights into the vertebral Hox code of archosaurs. *Evolution & development, 17*(5), 258-269.

Bolker, J. A. (2000). Modularity in development and why it matters to evo-devo. *American Zoologist, 40*(5), 770-776.

Brocklehurst, R. J., Moritz, S., Codd, J., Sellers, W. I., & Brainerd, E. L. (2017). Rib kinematics during lung ventilation in the American alligator (Alligator mississippiensis): an XROMM analysis. *Journal of Experimental Biology, 220*(17), 3181-3190.

Brocklehurst, R. J., Schachner, E. R., & Sellers, W. I. (2018). Vertebral morphometrics and lung structure in non-avian dinosaurs. *Royal Society Open Science, 5*(10), 180983.

Buchholtz, E. A. (1998). Implications of vertebral morphology for locomotor evolution in early Cetacea. In *The emergence of whales: evolutionary patterns in the origin of Cetacea* (pp. 325-351): Springer.

Buchholtz, E. A. (2001). Vertebral osteology and swimming style in living and fossil whales (Order: Cetacea). *Journal of Zoology, 253*(2), 175-190.

Buchholtz, E. A. (2007). Modular evolution of the cetacean vertebral column. *Evolution & development, 9*(3), 278-289.

Bui, H.-N. N., & Larsson, H. C. (2021). Development and evolution of regionalization within the avian axial column. *Zoological Journal of the Linnean Society, 191*(1), 302-321.

Burke, A. C., Nelson, C. E., Morgan, B. A., & Tabin, C. (1995). Hox genes and the evolution of vertebrate axial morphology. *Development, 121*(2), 333-346.

Chamero, B., Buscalioni, Á. D., Marugán‐Lobón, J., & Sarris, I. (2014). 3D geometry and quantitative variation of the cervico‐thoracic region in Crocodylia. *The Anatomical Record, 297*(7), 1278-1291.

Chen, X., Milne, N., & O'Higgins, P. (2005). Morphological variation of the thoracolumbar vertebrae in Macropodidae and its functional relevance. *Journal of morphology, 266*(2), 167-181.

Chevrinais, M., Johanson, Z., Trinajstic, K., Long, J., Morel, C., Renaud, C. B., & Cloutier, R. (2018). Evolution of vertebrate postcranial complexity: axial skeleton regionalization and paired appendages in a Devonian jawless fish. *Palaeontology, 61*(6), 949-961.

Christ, B., Huang, R., & Wilting, J. (2000). The development of the avian vertebral column. *Anatomy and embryology, 202*, 179-194.

Cleuren, J., De Vree, F., & Schwenk, K. (2000). Feeding in crocodilians. *Feeding: form, function, and evolution in tetrapod vertebrates*, 337-358.

Cobley, M. J., Rayfield, E. J., & Barrett, P. M. (2013). Inter-vertebral flexibility of the ostrich neck: implications for estimating sauropod neck flexibility. *PLoS On*e, 8(8), e72187.

Collyer, M. L., & Adams, D. C. (2018). RRPP: An r package for fitting linear models to high‐dimensional data using residual randomization. *Methods in ecology and evolution, 9*(7), 1772-1779.

Drumheller, S. K., Darlington, J., & Vliet, K. A. (2019). Surveying death roll behavior across Crocodylia. *Ethology Ecology & Evolution, 31*(4), 329-347.

Dzemski, G., & Christian, A. (2007). Flexibility along the neck of the ostrich (Struthio camelus) and consequences for the reconstruction of dinosaurs with extreme neck length. *Journal of morphology*, 268(8), 701-714.

Erickson, G. M., Gignac, P. M., Steppan, S. J., Lappin, A. K., Vliet, K. A., Brueggen, J. D., . . . Webb, G. J. (2012). Insights into the ecology and evolutionary success of crocodilians revealed through bite-force and tooth-pressure experimentation. *PLoS One, 7*(3), e31781.

Esteban, J. M., Martín-Serra, A., Pérez-Ramos, A., Mulot, B., Jones, K., & Figueirido, B. (2023). The impact of the land-to-sea transition on evolutionary integration and modularity of the pinniped backbone. *Communications Biology, 6*(1), 1141.

Fish, F. E., Bostic, S. A., Nicastro, A. J., & Beneski, J. T. (2007). Death roll of the alligator: mechanics of twist feeding in water. *Journal of Experimental Biology, 210*(16), 2811-2818.

Fronimos, J. A., & Wilson, J. A. (2017). Concavo-convex intercentral joints stabilize the vertebral column in sauropod dinosaurs and crocodylians. *Ameghiniana*, *54*(2), 151-176.

Head, J. J., & Polly, P. D. (2015). Evolution of the snake body form reveals homoplasy in amniote Hox gene function. *Nature, 520*(7545), 86-89.

Iijima, M., & Kubo, T. (2019). Comparative morphology of presacral vertebrae in extant crocodylians: taxonomic, functional and ecological implications. *Zoological Journal of the Linnean Society, 186*(4), 1006-1025.

Janvier, P. (1996). *Early vertebrates*: Oxford University Press.

Johanson, Z., Sutija, M., & Joss, J. (2005). Regionalization of axial skeleton in the lungfish Neoceratodus forsteri (Dipnoi). *Journal of Experimental Zoology Part B: Molecular and Developmental Evolution, 304*(3), 229-237.

Johnson, S. E., & Shapiro, L. J. (1998). Positional behavior and vertebral morphology in atelines and cebines. *American Journal of Physical Anthropology: The Official Publication of the American Association of Physical Anthropologists, 105*(3), 333-354.

Jones, K. E., Angielczyk, K. D., Polly, P. D., Head, J. J., Fernandez, V., Lungmus, J. K., . . . Pierce, S. E. (2018). Fossils reveal the complex evolutionary history of the mammalian regionalized spine. *Science, 361*(6408), 1249-1252.

Jones, K. E., & German, R. Z. (2014). Ontogenetic allometry in the thoracolumbar spine of mammal species with differing gait use. *Evolution & development, 16*(2), 110-120.

Jones, K. E., Gonzalez, S., Angielczyk, K. D., & Pierce, S. E. (2020). Regionalization of the axial skeleton predates functional adaptation in the forerunners of mammals. *Nature ecology & evolution, 4*(3), 470-478.

Jones, K. E., & Pierce, S. E. (2016). Axial allometry in a neutrally buoyant environment: effects of the terrestrial‐aquatic transition on vertebral scaling. *Journal of Evolutionary Biology, 29*(3), 594-601.

Kida, M., Johnson, D., McAndrew, T., & O'HIGGINS, P. (1999). Adaptation in the vertebral column: a comparative study of patterns of metameric variation in seven species of small mammals. *The Journal of Anatomy, 194*(2), 207-214.

Kikinis, R., Pieper, S. D., & Vosburgh, K. G. (2013). 3D Slicer: a platform for subject-specific image analysis, visualization, and clinical support. In *Intraoperative imaging and image-guided therapy* (pp. 277-289): Springer.

Krings, M., Nyakatura, J. A., Fischer, M. S., & Wagner, H. (2014). The cervical spine of the American barn owl (Tyto furcata pratincola): I. Anatomy of the vertebrae and regionalization in their S-shaped arrangement. *PLoS One, 9*(3), e91653.

M Woltering, J. (2012). From lizard to snake; behind the evolution of an extreme body plan. *Current genomics, 13*(4), 289-299.

Mallison, H., Pittman, M., & Schwarz, D. (2015). *Using crocodilian tails as models for dinosaur tails* (2167-9843). Retrieved from

Mallo, M., Wellik, D. M., & Deschamps, J. (2010). Hox genes and regional patterning of the vertebrate body plan. *Developmental biology, 344*(1), 7-15.

Mannion, P. D., Benson, R. B., Carrano, M. T., Tennant, J. P., Judd, J., & Butler, R. J. (2015). Climate constrains the evolutionary history and biodiversity of crocodylians. *Nature communications, 6*(1), 8438.

Mansfield, J. H., & Abzhanov, A. (2010). Hox expression in the American alligator and evolution of archosaurian axial patterning. *Journal of Experimental Zoology Part B: Molecular and Developmental Evolution, 314*(8), 629-644.

Marchesi, M. C., Mora, M. S., Dans, S. L., & González-José, R. (2021). Allometry and ontogeny in the vertebral column of southern hemisphere dolphins: a 3D morphofunctional approach. *Journal of Mammalian Evolution, 28*(1), 125-134.

Martín-Serra, A., Pérez-Ramos, A., Pastor, F. J., Velasco, D., & Figueirido, B. (2021). Phenotypic integration in the carnivoran backbone and the evolution of functional differentiation in metameric structures. *Evolution Letters, 5*(3), 251-264.

Molnar, J., & Watanabe, A. (2023). Morphological and functional regionalization of trunk vertebrae as an adaptation for arboreal locomotion in chameleons. *Royal Society Open Science, 10*(3), 221509.

Molnar, J. L., Pierce, S. E., Bhullar, B.-A. S., Turner, A. H., & Hutchinson, J. R. (2015). Morphological and functional changes in the vertebral column with increasing aquatic adaptation in crocodylomorphs. *Royal Society Open Science, 2*(11), 150439.

Molnar, J. L., Pierce, S. E., & Hutchinson, J. R. (2014). An experimental and morphometric test

of the relationship between vertebral morphology and joint stiffness in Nile crocodiles (Crocodylus niloticus). *Journal of Experimental Biology, 217*(5), 758-768.

Morin-Kensicki, E. M., Melancon, E., & Eisen, J. S. (2002). Segmental relationship between somites and vertebral column in zebrafish.

Pierce, S. E., Ahlberg, P. E., Hutchinson, J. R., Molnar, J. L., Sanchez, S., Tafforeau, P., & Clack, J. A. (2013). Vertebral architecture in the earliest stem tetrapods. *Nature, 494*(7436), 226-229.

Polly, P. D., Head, J. J., & Cohn, M. J. (2001). Testing modularity and dissociation: the evolution of regional proportions in snakes. *Beyond heterochrony: the evolution of development*, 307-335.

Preuschoft, H., & Klein, N. (2013). Torsion and bending in the neck and tail of sauropod dinosaurs and the function of cervical ribs: insights from functional morphology and biomechanics. *PLoS One, 8*(10), e78574.

Randau, M., & Goswami, A. (2017). Morphological modularity in the vertebral column of Felidae (Mammalia, Carnivora). *BMC Evolutionary Biology, 17*, 1-12.

Randau, M., & Goswami, A. (2018). Shape covariation (or the lack thereof) between vertebrae and other skeletal traits in felids: the whole is not always greater than the sum of parts. *Evolutionary biology, 45*(2), 196-210.

Randau, M., Goswami, A., Hutchinson, J. R., Cuff, A. R., & Pierce, S. E. (2016). Cryptic complexity in felid vertebral evolution: shape differentiation and allometry of the axial skeleton. *Zoological Journal of the Linnean Society, 178*(1), 183-202.

Renous, S., Gasc, J.-P., Bels, V., & Wicker, R. (2002). Asymmetrical gaits of juvenile Crocodylus johnstoni, galloping Australian crocodiles. *Journal of Zoology, 256*(3), 311-325.

Richardson, M. K. (1999). Vertebrate evolution: the developmental origins of adult variation. *BioEssays, 21*(7), 604-613.

Romer, A. S. (1923). Crocodilian pelvic muscles and their avian and reptilian homologues. Bulletin of the AMNH; v. 48, article 15.

Rose, K. A., Tickle, P. G., Elsey, R. M., Sellers, W. I., Crossley, D. A., & Codd, J. R. (2021). Scaling of axial muscle architecture in juvenile Alligator mississippiensis reveals an enhanced performance capacity of accessory breathing mechanisms. *Journal of Anatomy,*

239(6), 1273-1286.

Salisbury, S., & Frey, E. (2000). Crocodilian biology and evolution. *Surrey Beatty & Sons*, 85-134.

Sallan, L. C. (2012). Tetrapod-like axial regionalization in an early ray-finned fish. *Proceedings of the Royal Society B: Biological Sciences, 279*(1741), 3264-3271.

Seidel, M. R. (1978). *The somatic musculature of the cervical and occipital regions of Alligator mississippiensis*: City University of New York.

Shapiro, L. J. (2007). Morphological and functional differentiation in the lumbar spine of lorisids and galagids. *American Journal of Primatology: Official Journal of the American Society of Primatologists, 69*(1), 86-102.

Salisbury, S., & Frey, E. (2001). A biomechanical transformation model for the evolution of semi-spheroidal articulations between adjoining vertebral bodies in crocodilians.

Troxell, E. L. (1925). Thoracosaurus, a Cretaceous crocodile. *American Journal of Science, 10*(57), 219-233.

Tsuihiji, T. (2005). Homologies of the transversospinalis muscles in the anterior presacral region of Sauria (crown Diapsida). *Journal of morphology, 263*(2), 151-178.

Tsuihiji, T. (2007). Homologies of the longissimus, iliocostalis, and hypaxial muscles in the anterior presacral region of extant Diapsida. *Journal of morphology, 268*(11), 986-1020.

Vicory, J., Pascal, L., Hernandez, P., Fishbaugh, J., Prieto, J., Mostapha, M., . . . Liu, Z. (2018). *Slicersalt: Shape analysis toolbox.* Paper presented at the Shape in Medical Imaging: International Workshop, ShapeMI 2018, Held in Conjunction with MICCAI 2018, Granada, Spain, September 20, 2018, Proceedings.

Ward, A. B., & Mehta, R. S. (2014). Differential occupation of axial morphospace. *Zoology, 117*(1), 70-76.

Werneburg, I., Wilson, L. A., Parr, W. C., & Joyce, W. G. (2015). Evolution of neck vertebral shape and neck retraction at the transition to modern turtles: an integrated geometric morphometric approach. *Systematic biology, 64*(2), 187-204.

Wilhite, R. (2023). A detailed anatomical study of M. Caudofemoralis longus in Alligator mississippiensis. *Ruling reptiles: Crocodylian biology and archosaur paleobiology*, 80-99.

Zweers, G., JC, V. B., & Koppendraier, R. (1987). Avian cranio-cervical systems. Part I:

Anatomy of the cervical column in the chicken (Gallus gallus L.). *Acta Morphologica Neerlando-Scandinavica, 25*(3), 131-155.

Zweers, G. A., Van Der Leeuw, A. H., & Bout, R. G. (2001). Evolutionary morphology of the neck system in ratites, fowl and waterfowl. *Netherlands Journal of Zoology, 51*(2), 243-262.

Appendix C:

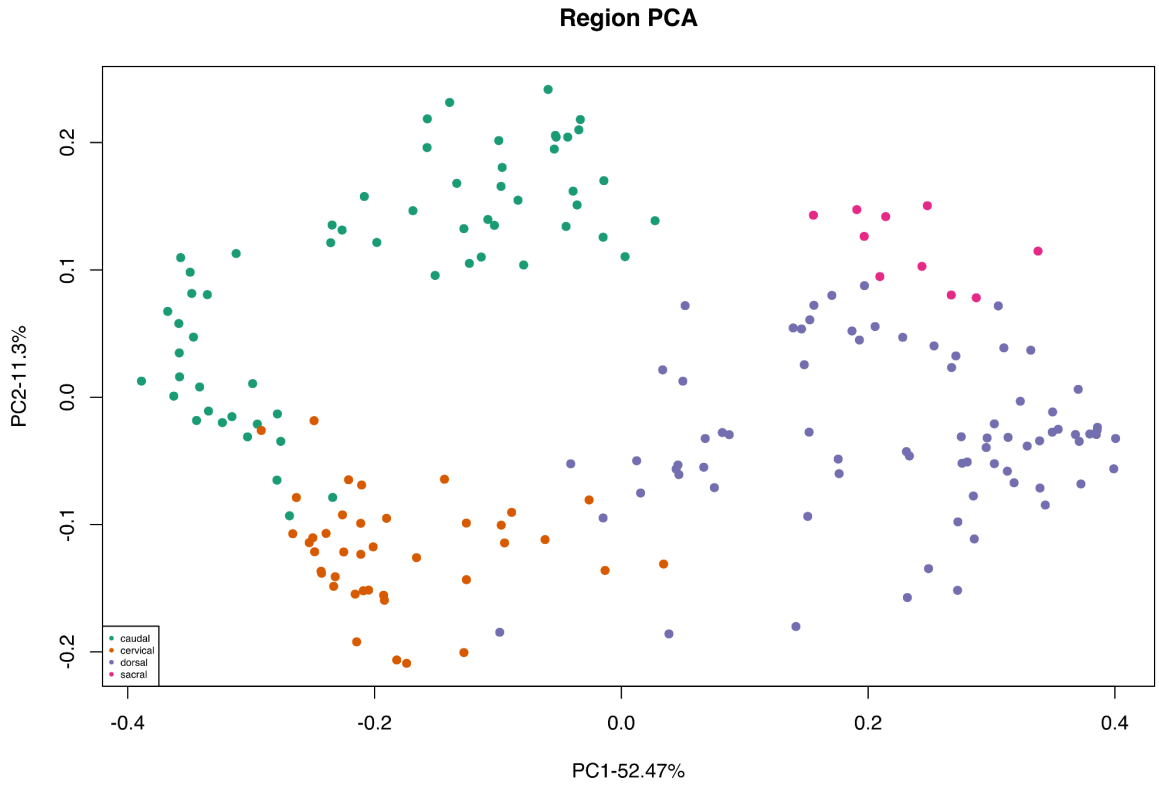

Appendix C1. PC1 and PC2 of all vertebrae of all taxa studied colored by region. Cervicals are coded in orange, dorsals in purple, sacrals in pink, and caudals in green.

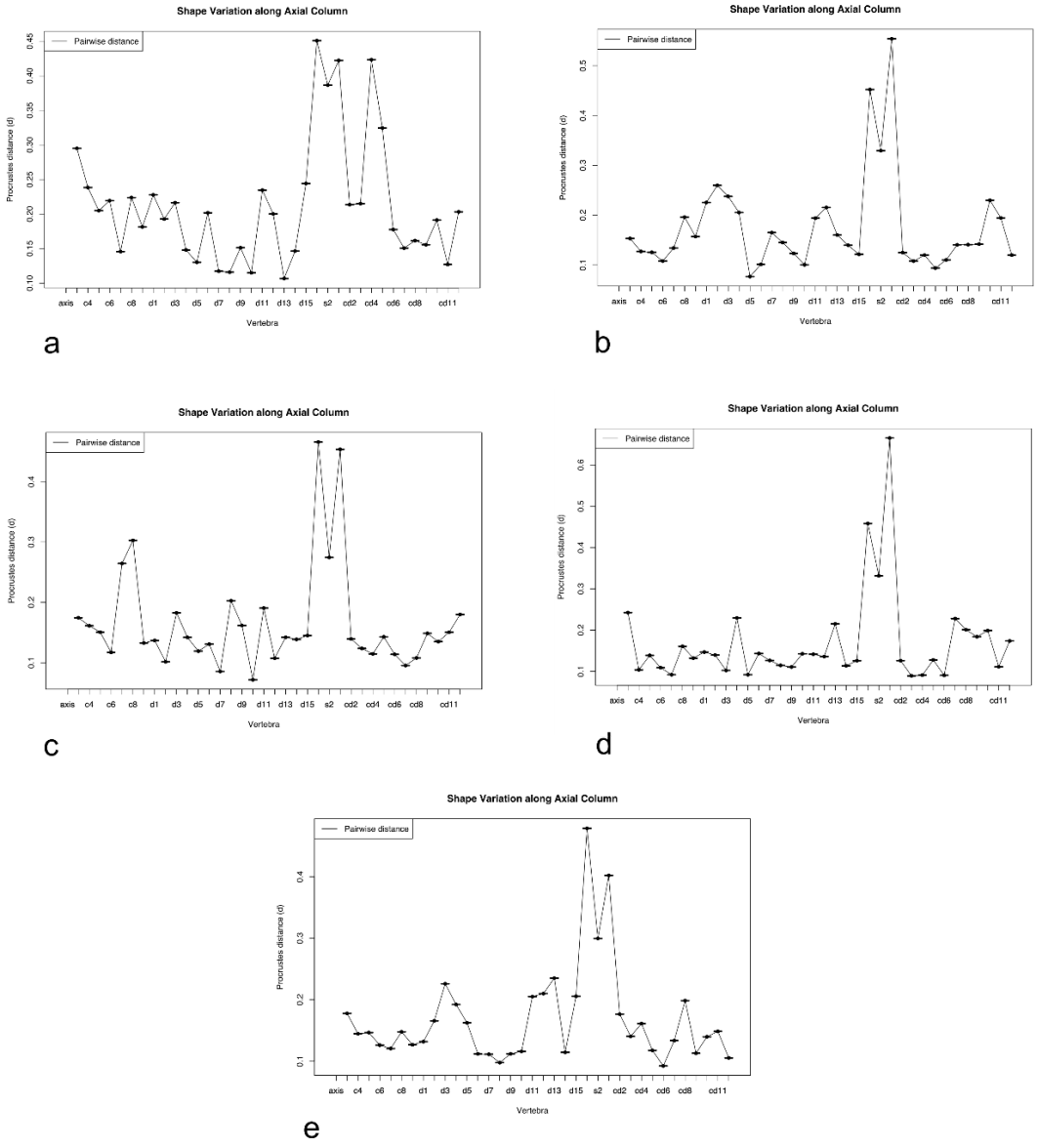

Appendix C2. Sequential pairwise Procrustes distance differences showing axial variation along the axial columns of *Caiman crocodilus* (a), *Alligator mississippiensis* (b), *Crocodylus acutus* (c), *Gavialis gangeticus* (d), *Tomistoma schlegelii* (e).

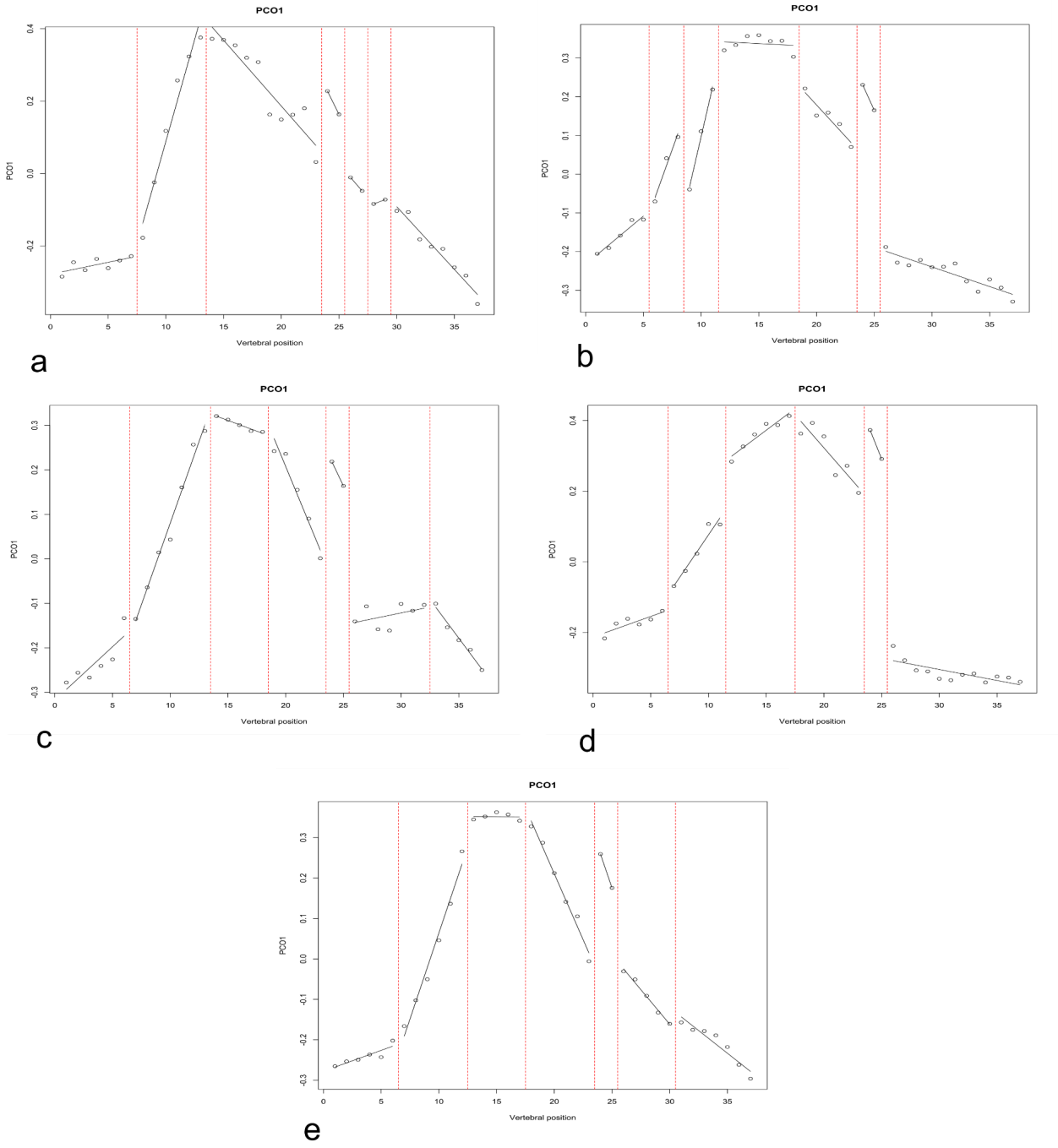

Appendix C3. Segmented regression analysis of axial columns of *Caiman crocodilus* (a), *Alligator mississippiensis* (b), *Crocodylus acutus* (c), *Gavialis gangeticus* (d), *Tomistoma schlegelii* (e).

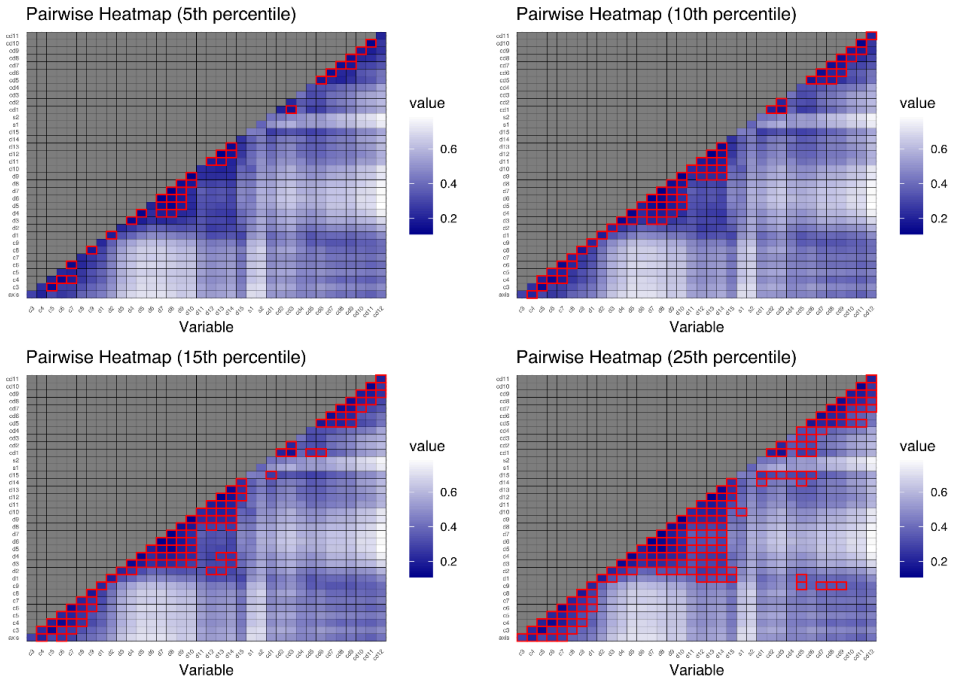
Pairwise Heatmap (5th percentile)
Pairwise Heatmap (10th percentile)
Pairwise Heatmap (15th percentile)
Pairwise Heatmap (25th percentile)
value
0.6
0.4
0.2
Variable

a

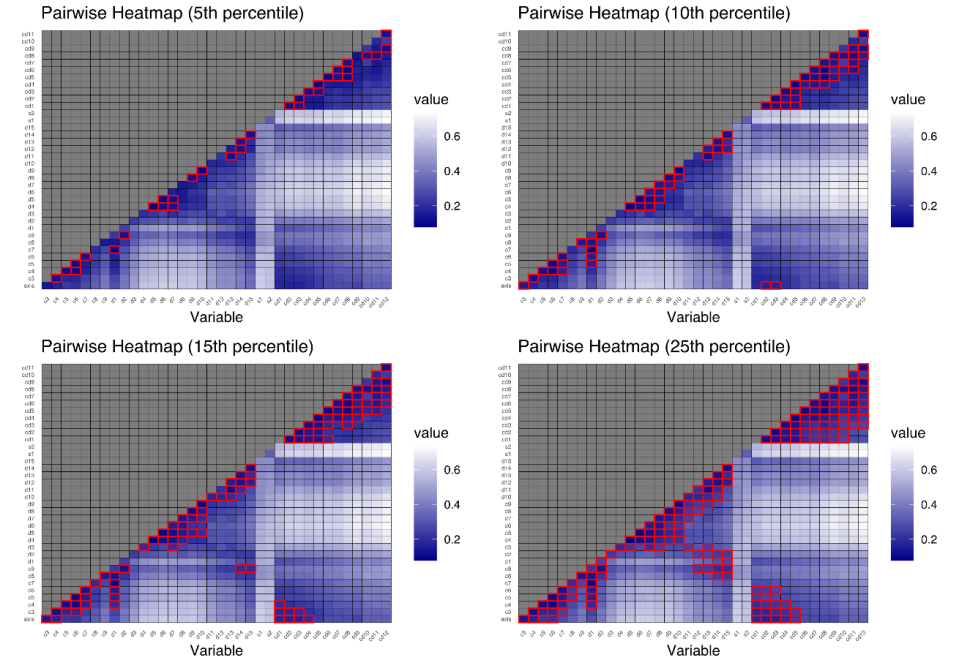
Pairwise Heatmap (5th percentile)
Pairwise Heatmap (10th percentile)
Pairwise Heatmap (15th percentile)
Pairwise Heatmap (25th percentile)
value
0.6
0.4
0.2
Variable

b

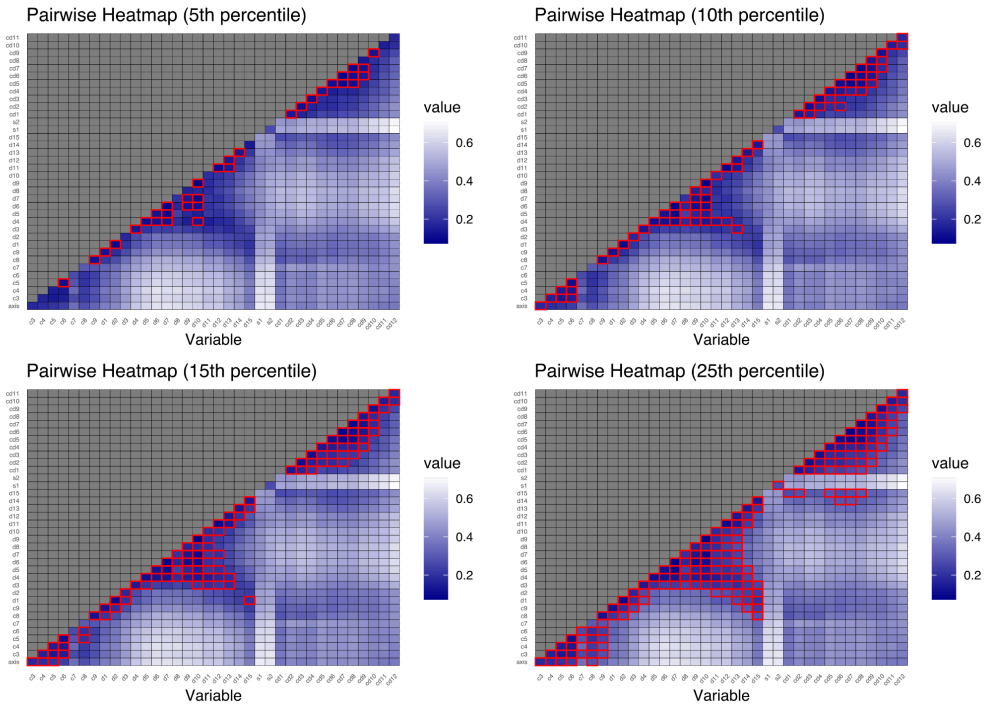
Pairwise Heatmap (5th percentile)
Pairwise Heatmap (10th percentile)
Pairwise Heatmap (15th percentile)
Pairwise Heatmap (25th percentile)
value
0.6
0.4
0.2
Variable

c

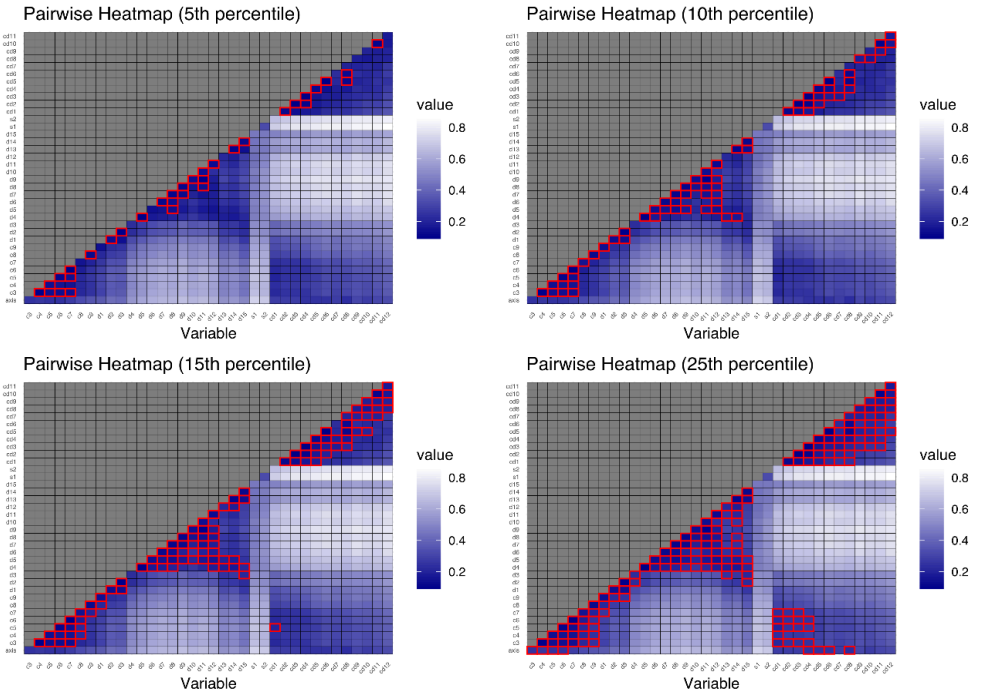
Pairwise Heatmap (5th percentile)
Pairwise Heatmap (10th percentile)
Pairwise Heatmap (15th percentile)
Pairwise Heatmap (25th percentile)
value
0.8
0.6
0.4
0.2
Variable

d

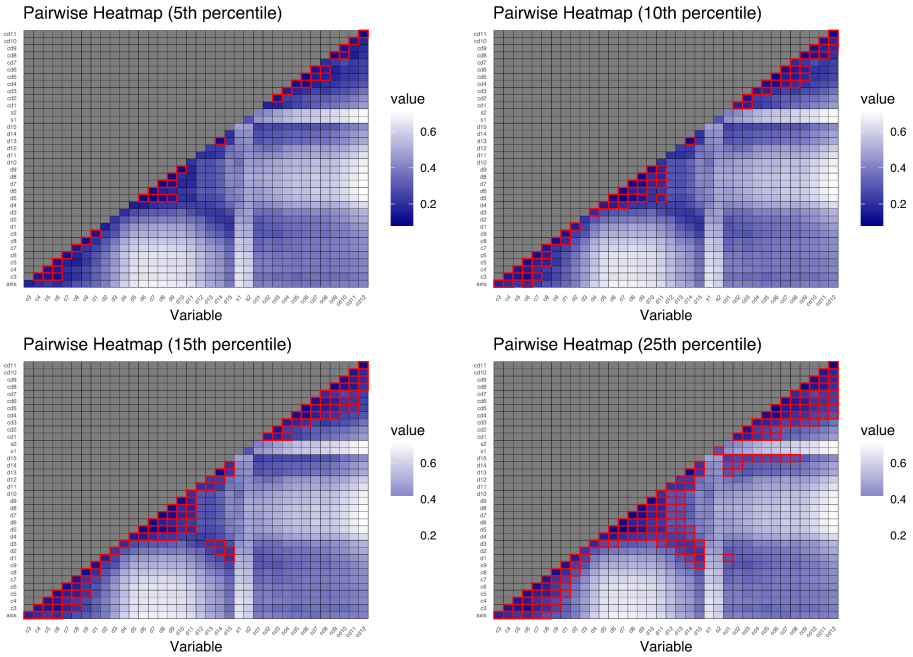

e

Appendix C4. Modularity and integration exploration heatmaps of *Caiman crocodilus* (a), *Alligator mississippiensis* (b), *Crocodylus acutus* (c), *Gavialis gangeticus* (d), *Tomistoma schlegelii* (e).

Chapter 5
Discussion and Final Conclusions

This thesis presents a comprehensive collection of work that underscores the intricate evolutionary and developmental processes underlying morphological diversity of the axial column in vertebrates, with a particular focus on Archosauria. All chapters of this thesis converge on the axial column as a key anatomical innovation in Vertebrates, leveraging its morphology, development, and evolutionary history to shed light on the mechanisms and drivers behind phenotypic variation and the origin of evolutionary novelty.

By examining the axial skeleton through various lenses– ranging from developmental biology to paleontology and biomechanics– we gain insights into how this structure has diversified across time and lineages. Through the utilization of new techniques, this work seeks to qualify and quantify morphology and morphological variation, addressing how specific processes may constrain or drive various evolutionary processes. In doing so, this research contributes to a broader understanding of the evolutionary processes that underpin the morphological complexity observed in vertebrate taxa, with an emphasis on the axial column.

Archosauria includes all living crocodilians and birds, as well as extinct dinosaurs, pterosaurs and basal ‘thecodontians’ (Benton & Clark, 1988). A diverse clade represented by large variations in form and function, archosaurs are broadly distributed and comprise numerous species and ecological habitats (Brusatte et al., 2010). Archosaurian vertebral columns, and their associated structures, therefore play a large number of roles in morphology, physiology, ecology, and organismal function, such as locomotion, posture, and food acquisition (Böhmer et al., 2015). Unlike their mammalian counterparts in which presacral count and regionalization is highly conservative with variable morphology (Bömer et al., 2015), Archosauria displays high

variability in vertebral count and regionalization, and relatively conserved vertebral morphologies within Aves and Crocodilia. Traditional anatomical markers delineate specific axial regions in extant birds and crocodilians, but regionalization and modularity remains quite variable with the presence of fusions and varying vertebral counts (Bui & Larsson, 2021).

The axial columns of Archosauria remain a complex and understudied structure. Conserved Hox gene expression patterns contribute to some patterns of regionalization but do not fully explain the observed morphological diversity (Bui & Larsson, 2021). Vertebral number is determined by somitogenesis, the sequential addition of somites cranially to caudally in pairs until the total species-specific number of embryonic segments is reached (Christ et al., 2000). The axial column is a serially homologous structure, and yet each individual unit has a specific role and specialized morphology within the structure itself. The sclerotomal component of each somite differentiate through resegmentation into vertebrae, leading to distinct morphologies according to their position and identity within vertebral regions along the anteroposterior axis (Böhmer et al., 2015).

In Chapter 2, we map the development of each vertebra throughout ontogeny, utilizing the timing of ossification to track morphological variation and the appearance of characters over time. Using clearing and staining to track endochondral ossification, the gradual process of the replacement of a cartilage model by bone (Mackie et al., 2007), we outline axial column development through high-resolution character mapping. We hoped to gain insight into the timing of development and the process of axial column development to shed light into the mechanisms behind morphological diversification and evolutionary transformations seen within the Archosaurian axial column. We find the ontogeny of axial regionalization to reveal patterns that are partially mirrored in evolutionary history, as well as more complex ossification patterns

compared to the anterior to posterior ossification expectation. With fusions occurring independently of regional boundaries, we note an increased complexity in axial organization, as well as modular organization that is not directly driven by gene expression. This study drove us towards questioning ways in which the axial column can be used to study complexity and organization, conceptualizing these ideas through the study of modularity and integration.

In Chapter 3, I turn my efforts to focus on a relatively simple axial column in an effort to quantify shape variation over entire surfaces. These efforts were conducted utilizing open-source medical software, co-opted to quantify surface variation in a relatively complex structure that is simple in organization. My goals for this chapter were to determine whether the utilization of discrete characters, previously used in Chapter 2, captures true variation seen within a single structure. Discrete anatomical characters have been paramount in taxonomic and phylogenetic research, as changes in presence of characters themselves are the foundation for the study of morphological variation (de Beer, 1954). I focus on a specific method of shape quantification of a complex surface to determine whether the discrete characters utilized in phylogenetic studies are truly reflective of variation.

This is followed by the expansion of the methods used in Chapter 3 to a larger study system. Chapter 4 utilizes the approach from Chapter 3, to expand on our ability to quantify shape variation in a complex structure across a phylogeny. My goals for this chapter were to utilize a complex analytical tool to quantify and compare shape variation across taxa and determine relationships between modularity, regionalization, and integration in more than one specimen. I focus on Crocodylia, as studies on axial column variation are limited to specific regions and regional transitions, and morphological characters mainly consist of those related to

the atlas-axis complex, the third cervical, and the state of the hypapophyses (Chamero et al., 2014).

With the transition from a simple, cryptically regionalized axial column in crocodilians to a highly complex structure bracing the origin of flight in avians, limited work has been conducted to deepen the understanding of this perceived increase in biological complexity. Most work has been conducted on specific regions such as the cervicals of birds (Boas, 1929; Cobley et al., 2013; Dzemski & Christian, 2007; Zweers et al., 1987), or the cervical-thoracics of crocodiles (Chamero et al., 2014). This work as a whole therefore, is an effort to describe the morphological variation in Crocodilia and the development of specialized axial columns.

Utilizing the concept of regionalization, modularity, and integration, we have been able to frame complexity in a hierarchical manner. This allowed for the study of a structure that is composed of repeating units, regulated by conserved genetic pathways, and evolved through multiple macroevolutionary transitions. The axial skeleton is a key characteristic to vertebrate anatomy, supporting both locomotion and protection of vital organs. Its evolution is intricately linked to genetic pathways that regulate segmental development, morphology, and functional specialization.

Specializations in the vertebral column are closely tied to the locomotor and behavioral kinematics of an animal (Johnson & Shapiro, 1998). The relationships the axial column holds to directly relate genetics, development, morphology, and function makes it an incredibly powerful tool to paint a larger picture in studying macroevolutionary transitions and the origins of evolutionary novelties. Through the identification of specific modules, the quantification of covariation and integration, and its relationship between taxa and development, we are able to

delve into a deeper understanding of functional constraints and flexibility within the development and evolution of the axial column.

Another question posed in this work is whether or not we are studying biological complexity and variation in a way that is effective and truly encompassing objective variation. Traditional methods in comparative morphology often rely on discrete anatomical characters, which have provided a baseline for determining morphological variation and the origins of novel structures (de Beer, 1954). However, these methods can be inherently subjective and biased, as they depend on the selection and description of specific landmarks or characters by the researcher. Semi-landmarks and curves along surfaces are often also used, but remain limited by the need for homology across structures, and typically cannot accommodate new characters.

This thesis proposes a new approach to address these limitations by utilizing whole surfaces and non-objective landmarks to study variation along a serially homologous structure, the axial column. By employing whole-surface analysis, I was able to track variation along the entire structure, highlighting areas of both high and low variation. This approach provided a more comprehensive and unbiased view of morphological diversity. This method allowed for an identification of specific regions exhibiting significant variation, inherently corresponding to functional adaptations or evolutionary changes. This is particularly valuable in understanding how these different regions may have evolved to support various locomotor and behavioral strategies across taxa.

Moreover, the application of spherical harmonics in this thesis has enabled a more holistic approach to studying morphological variation. Through high resolution 3D models of vertebrae, acquired through CT scanning and open-access files in Morphosource, I was able to objectively identify regions with high variability and regions of low variation between individual

vertebrae. I was able to identify groupings of vertebrae along the axial column in which shape was more conserved, as well as identify where gradual shifts in morphology created breaks into regions. This approach allowed us to determine various breaks along the entire axial column, whilst also highlighting regions of high variation along the individual surface. The ability to analyze the entire surface rather than discrete landmarks facilitates the identification of novel characters that may have been overlooked using traditional methods.

The selection of landmarks to be used in shape studies, or even linear measurements, is often met with time constraints, structural homology constraints, or even irregular shapes difficult to work with (Ege et al., 2020). The implications of this approach are profound, as they can be extended beyond the study of the axial column to other anatomical structures. By reevaluating character states and identifying important morphological characters through an objective, data driven approach, we can gain a deeper understanding of the relationships between genetics, development, morphology, and function in vertebrate evolution.

This thesis is the first of its kind to use high resolution development and surface morphology to approach variation and evolutionary interrogation related to the axial column. I provide a detailed examination of the development and regionalization of the avian axial column, revealing how ossification patterns and vertebral fusions contribute to morphological modularity, influenced by mechanisms beyond *Hox* gene expression. Higher resolution analysis of axial development shows complex patterns of regionalization, such as sub-regions developing within the lumbosacral area, highlighting the intricate evolutionary transformations that have occurred from non-avialian theropods to modern birds.

I use spherical harmonics analysis (SPHARM) to quantify and analyze shape variation in the axial column of *Caiman crocodilus*, offering a novel, objective method to study

morphological regionalization and integration. I ask if discrete characters used in coding phylogenies or landmark analyses are enough to describe total variation. I approach this question using an entire surface approach, highlighting areas of high variation and low variation that did and did not align with coded character states. This work reveals significant anatomical variation within a single taxon's axial column, highlighting regions of high variation, and providing a comprehensive basis for considering evolutionarily relevant anatomical characters. The approach using spherical harmonics, despite its challenges, complements traditional methods by objectively capturing the entirety of surface morphology and enabling detailed analysis with minimal subjectivity.

Extending this innovative methodology to Crocodylia, I focus on uncovering significant regional and morphological diversity across taxa, and highlighting the functional implications of vertebral modularity for functions such as locomotion and respiration. I note distinct regions and modules linked to costal ventilation, swimming ability, and feeding behaviors such as the death roll. I compare these patterns to expression data for *Alligator mississippiensis* (Böhmer et al. 2015; Mansfield & Abzhanov, 2010). Challenging the traditionally held view of basal archosaurs displaying 'simple' and 'cryptically regionalized' axial columns, our findings reveal significant regional and morphological diversity among taxa with varying levels of conservatism.

Our study remains limited, however, in both the breadth and number of sampled taxa to which these methods have been applied. While the utilization of spherical harmonics and high-resolution developmental data has provided unprecedented detail and objectivity in morphological character analyses, our sampling has been confined to a relatively narrow range and number of species. This limitation restricts our ability to make broader generalizations about the evolutionary and developmental processes influencing vertebral morphology across all of

Archosauria. Expanding the taxonomic breadth of our study to include a wider variety of species would provide a more comprehensive understanding of different trajectories within this clade. Furthermore, the analysis was also constrained by the sheer number of landmarks acquired, particularly in Chapters 3 and 4, where each vertebra was represented by 1,000 landmarks. While this high density of landmarks allows for a truly accurate representation of vertebral morphology, it also introduces significant challenges in data processing and statistical analysis.

The complexity of managing these extensive landmark numbers often results in 'watered down' test results, where the statistical power to detect significant differences was diminished. Our attempts to determine modularity and integration were therefore exploratory and based on user-determined cut-offs. The high dimensionality of the data made it challenging to apply traditional geometric morphometric statistics effectively. Our approach, while necessary given the current limitations, underscores the need for more robust and scalable analytical techniques.

My hope is to provide a foundational background for deeper analysis and the use of greater computational power for quantifying morphological variation. These approaches can be expanded towards ontogenetic trajectories, as the utilization of spherical harmonics was made to accommodate new and novel structures without the need for homology (Polly, 2008). Crocodilian ontogenetic trajectories may be compared to my work in Chapter 2 in order to fill out our understanding of Archosaurian axial column development in conjunction with published gene expression (Böhmer et al., 2015; Mansfield & Abzhanov, 2010). Avian axial columns may be quantified using a modified methodology from Chapters 2 and 3 in order to analyze discrete characters or modularity and integration. With the increased accessibility of high resolution imaging, open-source morphological data, high processing power, and a streamlined methodology acquiring 3D point clouds through SPHARM, our ability to map morphological

variation and anatomical change is unprecedented. This approach can be used to reevaluate character states and the identification of important morphological characters.

Together, these studies demonstrate the value of advanced analytical techniques in revealing the complexity and evolutionary significance of vertebral morphology, providing a deeper understanding of the processes driving the emergence of biological complexity, specifically within the realm of axial skeletons. Each chapter builds upon the other, as our findings in Chapter 2 drove our questioning for Chapters 3 and 4. An in-depth exploration of axial column development and morphology, this thesis acts as a window peering into the processes driving morphological variation. By integrating genetic, developmental, functional, and phylogenetic perspectives, we aimed to unravel these mechanisms giving rise to the diversity observed in vertebrate axial structures.

This work as a whole encompasses an interdisciplinary approach that is both novel and unique, paving the way for future research to integrate broader taxonomic ranges, molecular data, and ontogenetic perspectives, enhancing our understanding of the evolution of morphological complexity in vertebrates. I am able to demonstrate the value of advanced analytical techniques in shedding light on biological complexity, how it develops, and how we may quantify it. As advancements in imaging and technology continue to improve the accessibility and ease of acquiring high-resolution 3D data, these types of analyses will become increasingly valuable in enhancing our knowledge of vertebrate skeletal morphology and its evolutionary history.

References

Benton, M. J., & Clark, J. (1988). Archosaur phylogeny and the relationships of the Crocodylia. The phylogeny and classification of the tetrapods, 1, 295-338.

Boas, J. E. V. (1929). Biologisch-anatomische Studien über den Hals der Vögel (Vol. 1): AF Høst & søn.

Böhmer, C., Rauhut, O. W., & Wörheide, G. (2015). Correlation between Hox code and vertebral morphology in archosaurs. Proceedings of the Royal Society B: Biological Sciences, 282(1810), 20150077.

Böhmer, C., Rauhut, O. W., & Wörheide, G. (2015). New insights into the vertebral Hox code of archosaurs. Evolution & development, 17(5), 258-269.

Brusatte, S. L., Benton, M. J., Lloyd, G. T., Ruta, M., & Wang, S. C. (2010). Macroevolutionary patterns in the evolutionary radiation of archosaurs (Tetrapoda: Diapsida). Earth and Environmental Science Transactions of the Royal Society of Edinburgh, 101(3-4), 367-382.

Bui, H.-N. N., & Larsson, H. C. (2021). Development and evolution of regionalization within the avian axial column. Zoological Journal of the Linnean Society, 191(1), 302-321.

Chamero, B., Buscalioni, Á. D., Marugán‐Lobón, J., & Sarris, I. (2014). 3D geometry and quantitative variation of the cervico‐thoracic region in Crocodylia. The Anatomical Record, 297(7), 1278-1291.

Christ B, Huang R, Wilting J. 2000. The development of the avian vertebral column. *Anatomy and Embryology* 202: 179–194.

Cobley, M. J., Rayfield, E. J., & Barrett, P. M. (2013). Inter-vertebral flexibility of the ostrich neck: implications for estimating sauropod neck flexibility. PLoS One, 8(8), e72187.

De Beer, G. (1954). Archaeopteryx lithographica: A study based upon the British Museum specimen. (No Title).

Dzemski, G., & Christian, A. (2007). Flexibility along the neck of the ostrich (Struthio camelus) and consequences for the reconstruction of dinosaurs with extreme neck length. Journal of morphology, 268(8), 701-714.

Ege, Y. C., Foth, C., Baum, D., Wirkner, C. S., & Richter, S. (2020). Adapting spherical-harmonics-based geometric morphometrics (SPHARM) for 3D images containing large cavity openings using ambient occlusion: a study with hermit crab claw

shape variability. Zoomorphology, 139, 421-432.

Johnson, S. E., & Shapiro, L. J. (1998). Positional behavior and vertebral morphology in atelines and cebines. American Journal of Physical Anthropology: The Official Publication of the American Association of Physical Anthropologists, 105(3), 333-354.

Mackie, E., Ahmed, Y., Tatarczuch, L., Chen, K.-S., & Mirams, M. (2008). Endochondral ossification: how cartilage is converted into bone in the developing skeleton. *The international journal of biochemistry & cell biology*, 40(1), 46-62.

Mansfield, J. H., & Abzhanov, A. (2010). Hox expression in the American alligator and evolution of archosaurian axial patterning. Journal of Experimental Zoology Part B: Molecular and Developmental Evolution, 314(8), 629-644.

Polly, P. D. (2008). Adaptive zones and the pinniped ankle: a three-dimensional quantitative analysis of carnivoran tarsal evolution. In Mammalian evolutionary morphology: A tribute to Frederick S. Szalay (pp. 167-196): Springer.

Zweers, G., JC, V. B., & Koppendraier, R. (1987). Avian cranio-cervical systems. Part I: Anatomy of the cervical column in the chicken (Gallus gallus L.). Acta Morphologica Neerlando-Scandinavica, 25(3), 131-155.

Appendix D1: Python and R Code for Chapters 3 and 4

#Exporting landmarks of models from Slicer to be utilized in statistical analysis

In Slicer open python interactor (Ctrl+3)

```
import os
import numpy as np
import slicer

# Define the directory where you want to save the CSV files
output_directory = os.path.expanduser("~/Desktop/")

# Check if the specified directory exists, and create it if it doesn't
if not os.path.exists(output_directory):
    os.makedirs(output_directory)

# Define a list of node names you want to export
node_names = [
    "modelname_1",
    "modelname_2",
    "modelname_3",
    "modelname_4",
    "modelname_5",]

for node_name in node_names:
  # Obtain the MeshModelNode
   meshModelNode = slicer.util.getNode(node_name)

  # Check if the node exists
   if meshModelNode:
    # Obtain points from the model node
    points = slicer.util.arrayFromModelPoints(meshModelNode)

        if points is not None:
      # Convert the points to a NumPy array
        numpy_array = np.array(points)

      # Get the model node's name and use it as the filename
       filename = os.path.join(output_directory,
f"{meshModelNode.GetName()}.csv")

      # Save the NumPy array as a CSV file with the node's name as the filename
       np.savetxt(filename, numpy_array, delimiter=",")

     print(f"Points from node '{meshModelNode.GetName()}' have been
successfully exported to '{filename}' in the specified working
directory.")
       else:
```

```
        print(f"Node '{node_name}' does not contain valid points.")
    else:
        print(f"Node '{node_name}' not found in the scene.")
```

#Main analysis in R

Load required libraries

Define the structure of your data

```
p <- 1002  # Number of rows
k <- 3  # Number of columns
n <- 52  # Number of "sheets"
```

Create an empty array for your data

```
combined_array <- array(NA, dim = c(p,k,n))
```

List of file names

```
file_names <- c("0.csv", …,"51.csv")
```

Read and store the matrices into the array

```
for (i in 1:n) {
  data <- read.csv(file_names[i], header = FALSE, colClasses =
"character")
  data <- apply(data, 2, as.numeric)
  combined_array[, , i] <- data
}
```

##Procrustes alignment##

```
gp <- gpagen(combined_array, surfaces = NULL, PrinAxes = TRUE,
max.iter = NULL, ProcD = F, Proj = TRUE, print.progress = TRUE)
plotAllSpecimens(gp$coords, mean = TRUE)
```

##PCA##

```
pca<-gm.prcomp(gp$coords)
summary(pca)
```

Proportion of variance of principle components

```
proportionvariance <- function(x) {
  x.var <- x$sdev ^ 2
  x.pvar <- x.var/sum(x.var)
  print("proportions of variance:")
```

```
  print(x.pvar)
  par(mfrow=c(2,2))
  plot(x.pvar,xlab="Principal component", ylab="Proportion of
variance explained", ylim=c(0,1), type='b')
  plot(cumsum(x.pvar),xlab="Principal component", ylab="Cumulative
Proportion of variance explained", ylim=c(0,1), type='b')
  screeplot(x)
  screeplot(x,type="l")
  par(mfrow=c(1,1))
}
proportionvariance(pca)
```

Geomorph dataframe

```
classifiers<-read.csv(file="caimanclass.csv")
gdf<- geomorph.data.frame(gp, shape=gp$coords, size= gp$Csize,
region=classifiers$region, ID=classifiers$num, name=
classifiers$sample.id, position = classifiers$position)
gdf$region<- as.factor(gdf$region)
gdf$position<- as.factor(gdf$position)
```

####linear discriminant analysis###

```
library(MASS)
fit<- procD.lm(shape~region, SS.type = "I", data=gdf, print.progress
= F,iter=10000)
prep.lda(fit, inherent.groups = TRUE) #see groups available
fit.prep.lda<- prep.lda(fit, CV=TRUE, PC.no = 6)
lda.region<- lda(fit.prep.lda$x,fit.prep.lda$grouping)
lda.region
plda<- predict(lda.region, newdata= fit.prep.lda$x)
plda$posterior
boxplot(plda$x)
prop.lda<- lda.region$svd^2/sum(lda.region$svd^2)
prop.lda<- round(prop.lda*100)
Prop.lda
```

```
plda$class
ct<- table(fit.prep.lda$grouping, plda$class)
Ct
```

###pairwise tests###

region model

```
region<-procD.lm(shape~ region, SS.type = "I", data=gdf,
print.progress = F)
region.pw<- pairwise(region, groups = gdf$region, print.progress = F)
summary(region.pw, test.type = "dist", confidence = 0.95)
```

individual vertebrae model##

```
procd.lm <- procD.lm(shape ~ position, SS.type = "I", data = gdf,
print.progress = FALSE)
pairwise_tests <- pairwise(procd.lm, groups = gdf$position,
print.progress = FALSE)
summary(pairwise_tests, test.type = "dist", confidence = 0.95)
distances<- summary(pairwise_tests, confidence = 0.95, test.type =
"dist")
pairwise_table<-distances$summary.table
```

##integration and modularity###

```
# Get the Procrustes-aligned coordinates
aligned_coords <- gp$coords
# Initialize a list to store coordinates for each specimen
coordinates_per_specimen <- vector("list", length =
dim(aligned_coords)[3])
# Loop through each specimen's Procrustes-aligned coordinates
for (i in seq_along(coordinates_per_specimen)) {
  # Extract the aligned coordinates for the current specimen
   coordinates_per_specimen[[i]] <- aligned_coords[, , i]
   # Name the list element with the specimen number
   names(coordinates_per_specimen)[i] <- as.character(i)}
# Print or use coordinates_per_specimen as needed
```

```
print(coordinates_per_specimen)

# Create a function to run integration.test for a pair of specimens
run_integration_test <- function(coords1, coords2) {
  integration.test(
    A = coords1,
    A2 = coords2,
    partition.gp = NULL,  # You can adjust this if needed
    iter = 999,
    seed = NULL,
    print.progress = TRUE  )}
# Initialize a list to store integration.test results
integration_results <- list()
# Loop over all pairs of specimens and run the integration.test
num_specimens <- length(coordinates_per_specimen)
for (specimen1 in 1:(num_specimens - 1)) {
  for (specimen2 in (specimen1 + 1):num_specimens) {
    coords1 <- coordinates_per_specimen[[as.character(specimen1)]]
    coords2 <- coordinates_per_specimen[[as.character(specimen2)]]
    test_result <- run_integration_test(coords1, coords2)
    # Store the result in the list
    result_key <- paste("Specimen", specimen1, "and", specimen2)
    integration_results[[result_key]] <- test_result
    # Process the test result as needed
    print(paste("Integration test for specimens", specimen1, "and",
specimen2, "completed."))
    print(test_result)  }}

# Initialize a list to store the results for all pairwise comparisons
all_pairwise_results <- list()

# Loop over all pairs of specimens and extract the results
for (specimen1 in 1:(num_specimens - 1)) {
  for (specimen2 in (specimen1 + 1):num_specimens) {
```

```
    result_key <- paste("Specimen", specimen1, "and", specimen2)
    # Access and store the result in the all_pairwise_results list
    all_pairwise_results[[result_key]] <-
integration_results[[result_key]]  }}

# Extract r.pls, Z, and P.value for each specimen pair
result_table <- do.call(rbind, lapply(all_pairwise_results,
function(result) {
  data.frame(
    r.pls = result$r.pls,
    Z = result$Z,
    P.value = result$P.value )}))

### Allometry free: size corrected PCA, residuals ###
gp <- gpagen(combined_array, surfaces = NULL, PrinAxes = TRUE,
max.iter = NULL, ProcD = F, Proj = TRUE, print.progress = TRUE)
pca<-gm.prcomp(gp$coords)
gdf<- geomorph.data.frame(gp, shape=gp$coords, size= gp$Csize,
region=classifiers$region, ID=classifiers$num, name=
classifiers$sample.id, position = classifiers$position)
ANOVA<- procD.lm(shape ~ log(size), data = gdf, iter=9999)
shape.resid <- arrayspecs(ANOVA$residuals, p=dim(gp$coords)[1],
k=dim(gp$coords)[2])
adj.shape<- shape.resid + array(gp$consensus, dim(shape.resid))
allometryfree<- gm.prcomp(adj.shape)
plot(allometryfree)
summary(allometryfree)

## Calculate total surface variation##
landmark_list <- list()
for (landmark_num in 1:1002) {
  landmark_matrix <- matrix(, nrow = 52, ncol = 3)
  for (specimen in 1:52) {
    # Extract X, Y, Z coordinates for the current landmark of each specimen
```

```
    landmark <- gp$coords[, , specimen][landmark_num, , drop = FALSE]
    # Assign the current landmark to the matrix
    landmark_matrix[specimen, ] <- landmark}
  # add dimension and variable names
  dimnames(landmark_matrix) <- list(paste0("specimen", 1:52), c("X",
"Y", "Z"))
  # Add the current landmark matrix to the list
  landmark_list[[paste0("landmark", landmark_num)]] <-
landmark_matrix }
# create variables using assign function
for (landmark_num in 1:1002) {
  assign(paste0("landmark", landmark_num),
landmark_list[[paste0("landmark", landmark_num)]])}

##calculate Csize###
centroid_sizes_matrix <- matrix(, nrow = 1002, ncol = 1)
for (landmark_num in 1:1002) {
  current_landmark <- get(paste0("landmark", landmark_num))
  if (!is.null(current_landmark)) {
    centroid_current_landmark <- colMeans(current_landmark)
    centroid_size_current_landmark <-
sqrt(sum(centroid_current_landmark^2))
    centroid_sizes_matrix[landmark_num, 1] <-
centroid_size_current_landmark
  } else {
    print(paste("Warning: landmark", landmark_num, "is not defined"))
  }}
rownames(centroid_sizes_matrix) <- paste0("landmark", 1:1002)

# Create a matrix to store average landmark information
average_landmarks_matrix <- matrix(NA, nrow = 1002, ncol = 3,
dimnames = list(paste0("landmark", 1:1002), c("X", "Y", "Z")))
# Loop through all landmarks (from 1 to 1002)
for (landmark_num in 1:1002) {
```

```
  # Calculate the average landmark for the current landmark
   current_landmark <- get(paste0("landmark", landmark_num))
   average_landmarks_matrix[landmark_num, ] <-
colMeans(current_landmark, na.rm = TRUE)
}

avglandmarks_centroids <- cbind(average_landmarks_matrix, centroid =
centroid_sizes_matrix)
colnames(avglandmarks_centroids)[4] <- "centroid"
write.csv(avglandmarks_centroids, file = "totalsurface.csv",
row.names = FALSE)

# Create a function to map values to colors with hexadecimal color codes
map_to_color <- function(value) {
  if (value <= 0.02) {
    return("#00ff00")  # Green
  } else if (value <= 0.025) {
    return("#fff700")  # Yellow
  } else if (value <= 0.035) {
    return("#ffbf00")  # Orange
  } else {
    return("#ff2a00")  # Red
  }
}
# Apply the mapping function to the matrix values
color_column <- apply(centroid_sizes_matrix, 1, function(x)
map_to_color(x[1]))
# Create a new matrix with two columns: Centroid size and Color
centroid_sizes_colored_matrix <- cbind(centroid_sizes_matrix,
color_column)
# Merge the color information from centroid_sizes_colored_matrix
merged_matrix <- cbind(average_landmarks_matrix, color =
centroid_sizes_colored_matrix[, "color_column"])
# Open a new RGL window
```

```
open3d()
# Loop through all landmarks
for (landmark_num in rownames(merged_matrix)) {
  # Extract the average landmark for the current landmark
   average_current_landmark <- matrix(merged_matrix[landmark_num,
1:3], nrow = 1, dimnames = list(NULL, c("X", "Y", "Z")))
   # Get the corresponding color from the merged_matrix
   color <- merged_matrix[landmark_num, "color"]
  # Plot the average landmark in 3D with color coding based on centroid size
   points3d(average_current_landmark[, "X"],
average_current_landmark[, "Y"], average_current_landmark[, "Z"],
           col = color, size = 10)
}

##Regions and regression analysis##
# Regions functions available via Github (Jones et al. 2020 #

##Prepare data##

Xvar<- gdf$position #positional variable selected as independent
variable for analysis
nvert<-length(Xvar)
Xvar<- as.numeric(Xvar)
Xvar[1:5]

##Regression models##
noregions<-7 #Set the maximum number of regions which will be
calculated
regiondata<-compileregions(Xvar,pca$x[,1:10],noregions)
pander::pandoc.table(regiondata[1:5,1:5])

##Data reduction##
nopcos<-5
```

```
nopcos

#bootstrapped with 100 itterations
pco.boot<-PCOcutoff(pca$x,100, "euclidean")
nopcos<-pco.boot$sigpco#Select significant axes
nopcos

#plot bootstrapped eigenvalues
eigenplot(pco.boot$eigen.true, pco.boot$eigen.boot)

##Variance cutoff##
nopcos<-length(which(pca$x/sum(pca$x)>0.05))#more than 5% of variance
nopcos

###maximimize region scores##
nopcos<-PCOmax(regiondata, noregions, nvert)$pco.max
nopcos

##select best models##
models<-modelselect(regiondata,noregions,nopcos)
pander::pandoc.table(models)

###E. Compare hypotheses using AICc

#Regionalization score is the weighted average of region number,scaled by Akaike weight.
support<-model_support(models,nvert, nopcos)
pander::pandoc.table(support$Model_support)

#To check the fit of the model, you can calculate the multivariate r-squared using `multvarrsq`
rsq<-multvarrsq(Xvar,as.matrix(pca$x[,1:nopcos]),
support$Model_support)

####Plotting regionalization models
```

#Examine the fit of your model using `plotsegreg`

```
plotsegreg(Xvar,pcono=1, data=pca$x,
modelsupport=support$Model_support)
```

##Plot the region breaks using `regionmodel`

```
plot<-regionmodel(name="Alligator mississippiensis", Xvar=Xvar,
regiondata=support$Model_support)
print(plot)
```